STRUCTURAL DYNAMICS OF OLIGOPEPTIDES DETERMINED BY FLUORESCENCE QUENCHING OF ORGANIC DYES

Dissertation zur Erlangung des
naturwissenschaftlichen Doktorgrades
der Julius-Maximilians-Universität Würzburg

vorgelegt von
Stefan Bollmann
aus
Oelde.

Würzburg, 2013

Gutachter: Prof. Dr. Markus Sauer & Prof. Dr. Jens Pflaum
Universität Würzburg

ABSTRACT

For determination of structures and structural dynamics of proteins organic fluorophores are a standard instrument. Intra- and intermolecular contact of biomolecular structures are determined in time-resolved and stationary fluorescence microscopy experiments by quenching of organic fluorophores due to Photoinduced Electron Transfer (PET) and dimerization interactions. Using PET we show in this work that end-to-end contact dynamics of serine-glycine peptides are slowed down by glycosylation. This slow down is due to a change in reaction enthalpy for end-to-end contact and is partly compensated by entropic effects. In a second step we test how dimerization of MR121 fluorophore pairs reports on end-to-end contact dynamics. We show that in aqueous solutions containing strong denaturants MR121 dimerization reports advantageously on contact dynamics for glycine-serine oligopeptides compared to the previously used MR121/tryptophane PET reporters. Then we analyze dimer interactions and quenching properties of different commercially available fluorophores being standards in Förster Resonance Energy Transfer (FRET) measurements. Distances in biomolecules are determinable using FRET, but for very flexible biomolecules the analysis of masurement data can be distorted if contact of the two FRET fluorophores is likely. We quantify how strong the quenching of fluorophore pairs with two different or two identical fluorophores is. Dimer spectra and association constants are quantified to estimate if fluophores are applicable in various applications, e.g. in FRET measurements with unstructured peptides and proteins.

ZUSAMMENFASSUNG

Zur Charakterisierung von Proteinen werden in der fluoreszenzbasierten Mikroskopie organische Farbstoffe benutzt, um strukturelle Informationen bzw. Informationen über dynamische Prozesse zu gewinnen. In der zeitaufgelösten und stationären Fluoreszenzmikroskopie können hiermit Kontaktprozesse durch photoinduzierten Elektronentransfer und auch Dimerisierung der Fluorophore analysiert werden. In dieser Arbeit wird mittels photoinduziertem Elektronentransfer PET gezeigt, dass Glykosylierung End-zu-End Kontaktkinetiken verändert. Sehr flexible Serin-Glycin Peptide zeigen glykosyliert langsamere Kinetiken durch Veränderung der Reaktionsenthalpie der Kontaktreaktion beider Peptidenden verglichen zu unglykosylierten. Diese enthalpischen Beiträge werden zum Teil von entropischen Beiträgen kompensiert. Außerdem wird gezeigt, dass Glycin-Serin Peptiddynamiken auch mittels Farbstoffpaaren gemessen werden können, die auf Löschwechselwirkungen durch Dimerisierung beruhen. Die Stärke dieser Löschwechselwirkungen hängt vom Farbstoffpaar ab. In Lösungen mit Denaturierungsmitteln können Farbstoffpaare des Fluoreszenzfarbstoffes MR121 vorteilhaft für Messungen von Dynamiken von Glycin-Serin Peptiden genutzt werden. Die Dimerwechselwirkungen können bei sehr flexiblen Biomolekülen und möglichem Kontakt von Fluorophoren die konventionelle Analyse von Förster Resonanz Energie Transfer (FRET) Messungen erschweren. Wir untersuchen an Glycin-Serin Oligopeptiden das Dimerisierungsverhalten kommerziell erhältlicher Fluorophore, die in FRET Messungen verwendet werden. Für gleiche und verschiedene Fluorophore wird die Löschung durch Dimerwechselwirkungen quantifiziert. Dabei werden Dimerspektren und Assoziationskonstanten für Dimerisierungsreaktionen bestimmt. Letztere helfen bei der Abschätzung, ob Fluorophorpaare für verschiedene Anwendungen geeignet sind, zum Beispiel in FRET-Messungen in unstrukturierten Peptiden und Proteinen.

PUBLIKATIONSLISTE

[BBP+11] Stefan Bollmann, Anne Burgert, Carolin Plattner, Lilly Nagel, Norbert Sewald, Marc Löllmann, Markus Sauer, and Sören Doose. Conformational flexibility of glycosylated peptides. *ChemPhysChem*, 12(16):2907–2911, 2011.

[BLSD11] Stefan Bollmann, Marc Löllmann, Markus Sauer, and Sören Doose. Dimer formation of organic fluorophores reports on biomolecular dynamics under denaturing conditions. *Phys Chem Chem Phys*, 13(28):12874–12882, 2011.

[SBND13] Katrin Steger, Stefan Bollmann, Frank Noe, and Sören Doose. Systematic evaluation of fluorescence correlation spectroscopy data analysis on the nanosecond time scale. *Phys Chem Chem Phys*, 15(25):10435–10445, Jul 2013.

ACKNOWLEDGMENT

Many thanks to everybody who contributed in whatever way to this work!

I would like to thank my supervisor PD. Dr. Sören Doose for all the advice, help, and guidance through the labyrinth of biophysical science. I am very grateful for your encouragement and that your office door was always open for me.

Prof. Dr. Markus Sauer, many of these words also apply to you. Here I thank you for giving me the opportunity to work in your group and to share this tremendous working atmosphere first in Bielefeld and, after the move to Frankonia, in Würzburg.

I am grateful to Prof. Dr. Jens Pflaum for being the second assessor of this work.

A work like this is hardly possible without the input of good colleagues and collaborators.

I am happy for collaborating with Prof. Dr. Norbert Sewalds working group of Organic Chemistry 3 at Bielefeld University. Dr. Carolin Plattner established the protocol to synthesize glycosylated peptides and Dr. Lilly Nagel further enhanced the synthesis to give us enough samples to work with.

Without the help of Anne Burgert, glycosylation and heterodimerization results would not have such a basis. I hope you enjoyed working with me as well as I enjoyed it with you. Lisa Pließ, I learnt many things from you, too. It is always good to have someone who bothers about the HPLC and I know it in good hands. Katrin Steger, it is always, who bothered about Fluorescence Correlation Spectroscopy (FCS) analysis.

I thank my colleagues of the whole Sauer working group in Würzburg, including the former Heilemann subgroup now forming their own group in Frankfurt. Also thanks to the people I had the chance to work with starting this doctoral thesis in the workgroup of D3 in Bielefeld, that is now headed with Prof. Dr. Thomas Huser. Dr. Marc Löllmann introduced me into the field of FCS analysis and helped me with my first steps into peptide labeling and sample preparation. Dr. Ralph Brune helped me in using and understanding HPLC and Dr. Idir Yahiatene supported my fascination of single-molecule experiments.

Recently I had the chance to work in an office together with Sven Proppert, thanks for the buttermilk, and Dominik Pfaff. Steve Wolter, hacker of our working group in Bielefeld and Würzburg, thank you for the introduction into climbing. I thank the old office colleagues in Bielefeld for the great working atmosphere there.

Thanks to Antonia Göhler, Thorge Holm, Anne Burgert, Elvira Bollmann, and Marijke Viveen for corrections and for the tips regarding style you gave to me.

Last but not least, I am very grateful for my family for your love and support. You built the general basis for everything in my life and therefore for this work. Special thanks go to Marijke Viveen for bearing with me for the last couple of years.

CONTENTS

LIST OF FIGURES

LIST OF TABLES

ACRONYMS

A	acceptor
AA	amino acid
ACN	acetonitrile
APD	Avalanche Photo Diode
CW	continuos wave
CYS	cysteine
D	donor
DEO	Dimerization Estimation by oligopeptides Only
DMF	dimethylformamide. $(CH_3)_2N{-}CHO$
ET	Electron Transfer
FC	Franck-Condon
FCS	Fluorescence Correlation Spectroscopy
FRET	Förster Resonance Energy Transfer
FWHM	Full Width at Half Maximum
GDCL	guanidinium mono-hydrochloride
GLY	glycine
GS	glycine-serine
HOMO	Highest Occupied Molecular Orbital
HPLC	High Precision Liquid Chromatography
IC	Internal Conversion
IRF	Intensity Response Function
ISC	Inter-System-Crossing
LUMO	Lowest Unoccupied Molecular Orbital
LYS	lysine
NHS	N-hydrosuccinimide
OD	Optical Density
PBS	Phosphate Buffered Saline
PBST	Phosphate Buffered Saline with 0.05 % Tween
PET	Photoinduced Electron Transfer
PFP	pentafluorophenyl
QYDYN	dynamical quantum yield
QYSS	steady-state quantum yield
QYST	static quantum yield
RNA	ribonucleic acid
SER	serine
TCSPC	Time Correlated Single Photon Counting
TRP	tryptophane
TTET	Triplet-Triplet Energy Transfer

1 INTRODUCTION

At the end of the last millenium it was a paradigma that the function of a protein is fully determined by its three dimensional structure. Proteins perform directed tasks in all living species. The picture was that many proteins can fold into three dimensional structures to accomplish their function or interact specifically with other molecules.[39] And mostly based on X-ray crystallography a large variety of different folds were identified. Eventually a different class of proteins were reported to be important for the understanding of certain functional processes.[108] This new protein class was named by different terms including pliable, floppy, rhomorphic, mobile, vulnerable, chameleon, malleable, dancing proteins, protein clouds, and 3^2 protein.[108] Nowadays these molecules are often called intrinsically disordered proteins. They not only are a big part of the whole protein family, they are also central to normal function and stability of protein-protein networks in any organism.[108] Besides, there are many proteins containing both rigid structure and intrinsically disordered regions. These regions can serve as flexible linkers between functional domains of the proteins.[108] Furthermore the dynamic behaviour of flexible parts of proteins can be important for binding interactions. Flexible linkers add structural plasticity and enable a relatively unhindered spatial search. Often, structure formation is induced upon binding with significant functional consequences.[31]

The characterization of these intrinsically disordered proteins is not easy as fast dynamic processes govern structural changes. One common technique to get structural informations of proteins is X-ray cristallography. For this technique protein cristalls are formed and static structures are determined by scattering and diffraction of incoming light. Cristallization often fails due to the strong flexibility of disordered proteins. Therefore, solution based NMR[36], ESR, and X-ray[13] spectroscopy has been applied to characterize intrinsically disordered proteins.

One of the most striking features of highly disordered proteins is their high content of charged residues.[108] The high net charge is crucial for extended conformations to occur, since sequences that are rich in uncharged polar amino acids usually form heterogeneous ensembles of collapsed structures in aqueous solutions.[108] Comparison of structured and unstructured protein sequences revealed disorder- and order promoting amino acids (AAs).[108] Among others, glycine (Gly) and serine (Ser) are rather disorder promoting.[108] Gly is the smallest AA commonly found in proteins. Ser is a polar amino acid and therefore well-soluble in polar media like water. Both can be connected via peptide bonds to form GS polypeptides with repeating units of these two AA.

These GS polypeptides, among others, were extensively examined.[14, 61, 73, 74] It was pointed out[61] that long GS polypeptide chains with over 10-30 AAs behave like random chains with excluded volume. When the blueprint for polypeptides and proteins, messenger ribonucleic acid (RNA), is available for translation into amino-acid sequences, modifications are possible during (co-) or after (post-translational) translation. A detailed understanding of the implications of these modifications could help to construct artificially designed proteins.

Often amino-acid side chains of proteins are chemically modified after or during expression by so-called co- or post-translational modifications. The AA-chain-modifications in cells change the behaviour of polypeptide chains strongly. The formation of disulfide bonds is the most common post-translation modification. It can happen spontaneously or it can be assisted by enzymes.[106] Due to the tendency of disulfide bonds to form spontaneous and thus stabilize proteins, intrinsically disordered proteins have a low level of cysteines.[106] Phosphorylation of Ser, tyrosine, and threonine is catalized by kinases and can be reversed by phosphatases. This modification often causes changes in function and is thus often used for regulatory purposes. Adding a ubiquitin protein is sometimes called the "kiss of death" for proteins.[106] Glycosilation of proteins may occur at amino or hydroxyl groups. It means that single or multiple branched carbohydrates are added to the polypeptide chain. This process increases solubility, lenghtens the biological lifetime of the protein, or modifies its interactions with other constituents of the cell.[106] Glycosylated proteins are often involved in highly specific cell-cell contacts or interactions between the cell and extracellular matrix.[106]

For several years now posttranslational modifications of proteins and of simple polypeptide systems have been examined, but it is still not fully understood what single or multiple posttranslational modifications of polypeptides change with regard to structure and structural dynamics.[82] Therefore, the first part of this work describes our results of exploring the dynamical differences between unglycosylated and glycosylated glycine-serine peptides.

In the other part of this work we investigated and optimized methods based on fluorescence quenching for the monitoring of peptide conformational dynamics. Water is the main component of living cells. Therefore, when examining biomolecules in the life sciences using optical methods one has to deal with the optical properties of water. In water (cf. fig. 1) the visible spectrum from 390 nm to 700 nm is tranmitted nearly without loss. Here detection of fluorophore emission is not hindered by high solvent absorption and radiation damages of biologic samples are very small.

Microscopes operated with visible light can achieve a minimal resolution of about 200 nm, because of the Abbe-limit which states that resolution is the half wavelength divided by the numerical aperture of the

optical instrument.[98] Since the size of biomolecules is in the nanometer range, different techniques are established to improve the resolution in optical microscopy. There are super-resolution[53, 54, 126] imaging techniques based on single-molecule localization that use blinking of attached fluorophores to distinguish different fluorophore locations by forcing the majority of them into an "off"-state. Single fluorophores can be localized with high precision down to 5-20 nm depending on the size of the point-spread-function and the number of photons detected from the single molecule.[83] To tune the duration of "off"-states often stable and non-fluorescent radical states are promoted by redox reactions between fluorophores and reducing compounds like thiols.[114] With this technique reconstruction of super-resolved images of cells have become possible visualizing protein agglomerations or sceletal structure at unprecedented detail. Even some kinetic measurements of structural reorganization are possible, but they are limited by the switching processes and camera frame rates to rather slow processes beyong second time scales.[7]

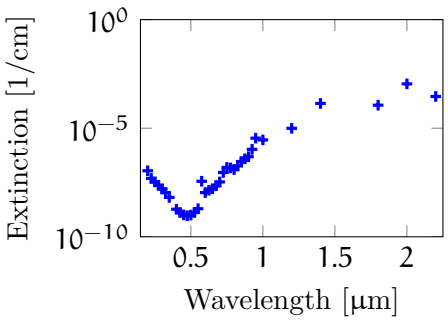

Figure 1: Absorption of water from 200 nm to 2.2 µm. In the optical range water absorption is at minimum for a wide range.[52]

Due to the limited time resolution of modern cameras, other techniques have to be used for the analysis of biomolecular dynamics that happen much faster than 1 ms. Confocal measurements are often made with 1 femtolitre focal volume. Together with contact induced quenching interactions like Triplet-Triplet Energy Transfer (TTET)[87], PET[29], and H-dimerization[BLSD11] high temporal resolution of contact-measurements in biomolecules are achievable. Modern Avalanche Photo Diodes (APDs) offer together with the electronics hardware time resolutions down to picoseconds. Therefore structural changes that happen in the nanosecond range can be analyzed.

In this work, we used PET as one possible quenching mechanism to resolve the dynamical behaviour of short non- and glycosylated oligopeptides. We attached the amino acid tryptophan and an organic fluorophore at opposite ends of the flexible oligopeptides. At contact of the ends of the peptide the fluorophore does not fluoresce due to formation of a ground-state complex between fluorophore and tryptophan. For several measurement techniques it is essential to have the right complex stability as it determines the ratio between the time of fluorescence emission (on-time) and the time in which fluorophores are non-fluorescent (off-time).[7, 119] For different biomolecules and different solvents the PET quenching may not be the best choice of contact

reporter system due to an unfavorable on- to off-time ratio. Therefore, other quenching mechanisms may be a better choice.

We tested what differences in contact kinetics a change of the contact reporter system brings about. We compared a PET reporter pair consisting of MR121 and tryptophane and a contact reporter system consisting of two MR121 fluorophores attached to GS-peptides at both ends that can form non-fluorescent dimers. Dimerization was already used for biomolecular investigations with other organic fluorophores.[79] We found that in solutions with high concentrations of the denturing reagent GdCl, a salt that weakens hydrogen bonding, a contact reporter with two MR121 fluorophores is advantageous to the PET contact reporter system.

Dimerization occurs for many organic fluorophores due their planar aromatic structures. The equilibrium binding constant of MR121 is rather high compared to dimerization constants of fluorophores typically used in live cell imaging.[59, 68] As there are plenty of fluorophore pairs that can be tested we further concentrated on studying fluorophores that are often used in single-molecule measurements of structural changes in biomolecules. For this task FRET is often monitored. FRET is based on an interaction between two molecules, in which the spectrum of the emission of one fluorophore, an energy donor, overlaps with the absorption spectrum of an acceptor fluorophore.[42] If the donor fluorophore is excited and both fluorophores are near to each other compared to a characteristic distance of this fluorophore pair R_0, energy from the donor is transfered to the acceptor. FRET is sensitive around this characteristic distance R_0, which is between 2 nm and 10 nm. It is possible to use the same fluorophores for so called homo-FRET and different fluorophores for hetero-FRET.

Using hetero-FRET, different fluorophores are attached at specific positions in peptides[101], proteins[63, 93], or DNA.[26] Even in the first theoretical treatment of FRET[42] small distance effects were described limiting FRET measurements. At van der Waals contact the same quenching interactions occur between the FRET fluorophores that can be used used as end-to-end contact reporter for FCS: electron transfer and dimerization effects due to overlap of electronic orbitals of the fluorophore molecules. Recent publications[26] indicate this for a selected number of FRET fluorophores.

In this work we tested several FRET reporters typically used in single-molecule fluorescence detection. Using ensemble spectroscopy methods, we characterize the various quenching contributions in different fluorophore pairs and identify the pair with the the least amount of quenching interactions. These fluorophore pairs qualify to be the best choice for FRET measurements from our fluorophore collection. We also tested dimerization of fluorophore pairs consisting of the same species providing comparative data to the analyzed MR121 dimer end-to-end reporter pair regarding dimerization.

2

THEORY

Optical spectroscopy is a main tool to measure in vivo biological structures and dynamics [64, 71, 111]. As long as excitation powers are kept low, biological samples do not get radiation damages as in x-ray or electron spectroscopy.

Biomolecules like proteins and polypeptides can be described as chains of amino acids. The essential organic amino acid tryptophan is often incorporated in the amino acid code and fluoresces in the ultraviolet range. Wagenknecht et al. [115] showed that tryptophane (Trp) is in electron transfer reactions an electron donor. This was exploited to probe molecular contact[28] with organic dyes quenched by photo-induced electron transfer from Trp to the excited dye.

The use of UV/Vis light in classical microscopy has the drawback that the wavelength of the used light limits the achievable resolution. Abbe formulated this in his diffraction limit d as $d = \frac{\lambda}{2n\sin(\theta)} = \frac{\lambda}{2NA}$.[9] The numerical aperture NA depends on refractive index n of the sample and the angle θ, describing how fast light diverges after a focus. However, the highest numerical aperture achievable with oil immersion objectives is 1.57, giving a resolution of about $\frac{\lambda}{3}$. Using red emitting lasers, resolution is approximately 200 nm.

Coarse structures of cells are still resolvable with standard optics using visible light. Other techniques are needed to get insight into behaviour of proteins and smaller amino acid chains like polypeptides. The dimensions of these molecules in aqueous environment are down do the subnanometer scale. Using the quenching of fluorescent organic dyes, molecular structures and kinetic information can be revealed using UV/Vis light microscopy. Therefore reporter systems are needed helping to be able to resolve biomolecular interactions. In this work I will focus on samples using fluorescent probes. Here dyes are quenched, if intra- or intermolecular contact or distance changes happen.

In a first section of this chapter a classification of examined peptides of this work is given. The second section introduces the characteristics, properties, and their underlying physical principles of the dyes used in the studies presented here. A brief overview of physical principles of modern fluorescent experiments is given in the third section. The fourth section describes diffusional properties of particles and their relation to experimentally accessible parameters. This is followed in the fifth section by a description of FCS, one technique with which these parameter are experimentally available for fluorescent probes. For the presented biomolecules here, structural intramolecular dynamics and

diffusional properties of the whole molecule can be connected. The concepts are presented in the sixth section.

2.1 ELECTRODYNAMICS

All samples in this work were probed via optical spectroscopy. For an overview of the used approximations and for the sake of completeness the most important relations of this are derived from basic physical principles. Using the International System of Units, maxwell's equations are[57, 84]

$$\begin{aligned}\vec{\nabla}\cdot\vec{D} &= \rho\\ \vec{\nabla}\cdot\vec{B} &= 0\\ \vec{\nabla}\times\vec{H} &= \frac{\partial\vec{D}}{\partial t}+\vec{J}\\ \vec{\nabla}\times\vec{E} &= -\frac{\partial\vec{B}}{\partial t}.\end{aligned} \tag{1}$$

with

$$\vec{D} = \epsilon_0\vec{E}+\vec{P}, \qquad \vec{B} = \mu_0\vec{H}+\mu_0\vec{M} \tag{2}$$

$\vec{E},\vec{B}$ are macroscopic electric and magnetic fields and $\vec{D},\vec{H}$ are corresponding fields given by a change of the fields by polarization $\vec{P}$ and magnetization $\vec{M}$ of media in the electromagnetic field. ρ and $\vec{J}$ are charge and current densities that may exist.

In this work the corresponding field $\vec{D}$ and $\vec{H}$ are connected linearly to the free electric and magnetic fields $\vec{E}$ and $\vec{B}$ via

$$\vec{D} = \epsilon_0\epsilon\vec{E}, \qquad \vec{B} = \mu_0\mu\vec{H}, \qquad \vec{J} = \sigma\vec{E} \tag{3}$$

Magnetization $\vec{M}$, free charges, and free currents of the samples are negligible. For the third maxwell's equation of eq. (1), when using eq. (3) and eq. (2) one gets then

$$\begin{aligned}\vec{\nabla}\times(\vec{\nabla}\times\vec{E}) &= -\frac{\partial}{\partial t}\vec{\nabla}\times\vec{B}\\ &= -\mu_0\frac{\partial}{\partial t}(\vec{\nabla}\times\vec{H})\\ &= -\mu_0\frac{\partial\vec{J}}{\partial t}-\mu_0\epsilon_0\frac{\partial^2\vec{E}}{\partial t^2}-\mu_0\frac{\partial^2 P}{\partial t^2}\\ &= \vec{\nabla}\cdot(\vec{\nabla}\vec{E})-\Delta\vec{E}\end{aligned} \tag{4}$$

In this work the polarization effects in the tested samples are in a macroscopic view homogeneously distributed. Therefore the local derivative of $\vec{P}$ is zero. Then one gets a wave equation for electromagnetic fields

$$\Delta\vec{E}-\frac{1}{c_0^2}\frac{\partial^2}{\partial t^2}\epsilon\vec{E} = 0 \tag{5}$$

with the speed of light in vacuum $c_0 = \sqrt{\mu_0\epsilon_0}^{-1}$

2.1.1 *Polarizability*

POLARIZATION OF AN ENSEMBLE OF IDEAL MOLECULES. Using the expressions for electrical fields of eq. (2) and eq. (3) one gets an expression for the polarization $\vec{P}$ of a sample in an external field $\vec{E}$

$$\vec{P} = \epsilon_0(\epsilon - 1)\vec{E} \tag{6}$$

$$= \iota\vec{E}. \tag{7}$$

ϵ itself is for asymmetric molecules a diagonal 3×3 matrix. One may then define the polarizability matrix ι as pointed out above.

The size of organic molecules is on the nm-scale (s. sec. 2.3.2.3). As it will be explained in sec. 2.3,, they have a core consisting of polymethines or -benzenes with multiple pi-sigma bonds. In these bond systems electrons are quasi free. Therefore electromagnetic radiation induces oscillations of the electrons. In a multipole expansion of the electric field one can define (s. sec. 9.1) dipole moments of the molecules. In a lorentz model one can describe these (sec. 9.2) polarizabilities of singly dipole emitters. Summation over all these emitters gives the Polarization $\vec{P}$ of the whole ensemble (s. sec. 9.3) and eq. (7) holds also for an ensemble of molecules. In the part of this chapter, where we deal with time dependent anisotropy sec. 2.1.2.2, we will see, that with selective excitation of molecules, we can get an anisotropic excited medium that changes over time reaching equilibrium. Knowing this, examination of its time dependence gives information about rotational diffusion of dye molecules.

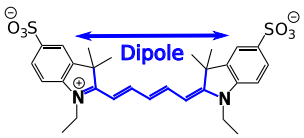

Figure 3: Polymethine dyes like Cy5 can be approximated as a dipole.

2.1.2 *Absorption and refraction*

As depicted in sec. 9.2, ι and therefore ϵ are in general complex tensors. Let $\vec{k}$ be parallel to x. Because of the homogeneous distribution of molecules in the solution, ϵ is diagonal with the same values in x- and y-direction. Therefore they can be treated as scalars in a one dimensional notation. We skip longitudinal contributions in x here, because the particles are low concentrated and have high mass. The wave equation for the electrical field $\vec{E}$ eq. (5) is solved by plane waves having the form of eq. (8).

$$\vec{E}(x,t) = \vec{E}_{0,x}\exp(i(kx - \omega_0 t)) \times \vec{E}_{y,z} \tag{8}$$

$$k^2 = \frac{\omega_0^2 n}{c_0^2}$$

$$n = \sqrt{\epsilon - \frac{ic_0^2\mu\sigma}{\omega_0}}$$

As long as there are free charges in the medium, the refractive index is complex. Especially organic dyes have very mobile electrons in their

conjugated chromophore systems (compare fig. 3). A complex refractive index of a sample means absorption. Introducing $n = \tilde{n} + i\tilde{\kappa}$ with a real part $\tilde{n}$ and imaginary part $\tilde{\kappa}$, one sees in eq. (10) that the electrical field decays exponentially.

$$k = \frac{\omega}{c_0}(n + i\tilde{\kappa}). \tag{9}$$

$$\Rightarrow \vec{E} = \vec{E}_0 \exp(i[\frac{\omega n}{c_0}x - \omega t]) \exp(-\tilde{\kappa}x). \tag{10}$$

2.1.2.1 *Lambert-Beer law*

The intensity I of an electromagnetic wave is proportional to its poynting vector $\vec{S} = \vec{E} \times \vec{H}$. For transversal electromagnetic waves the pointing vector is proportional to the squared magnitude of the electric field vector $\vec{E}$.[57] Then from eq. (10) follows $I \propto |E_0^2| \times \exp(-2\kappa x)$. In the following the connection to values we get from photometer experiments is made.

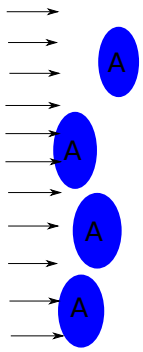

Figure 4: The cross section of dyes in diluted solution is the sum over all cross sections every dye has in the light path. $N\sigma(\omega) = \sum_{n=1}^{\text{Nr.ofdyes}} A_n(\omega)$.

Every dye has a wavelength dependent cross-section $\sigma(\omega)$ (s. fig. 4). For a strong diluted sample, absorption of light by molecules can be linearly approximated. Then the decrease in transmitted intensity is proportional to the cross-section of all molecules in the light path. The cross-section of all molecules depends on the concentration c of the sample, a molecule dependent, wavelength dependent cross-section $\sigma(\lambda)$, and the length of the light path d in the sample.

$$\frac{dI(\omega)}{I(\omega)} = -N\sigma(\omega)dx \tag{11}$$

$$\Rightarrow I(\omega) = I_0 \exp(-Nd\sigma(\omega))$$

$$OD(\omega) = \log\left(\frac{I_0(\omega)}{I(\omega)}\right)$$

$$= \log(e) \cdot Nd\sigma(\omega) \tag{12}$$

$$= cd\epsilon(\omega).^1 \tag{13}$$

The value $\epsilon(\omega) = N_A \log(e)\sigma(\omega)$ is the molar extinction coefficient. Cross-section is usually used in particle physics whereas in chemistry and molecular biology molar extinction coefficients are the common used terms.

2.1.2.2 *Time dependent anisotropy*

In ensemble experiments often the molecules of interest are distributed isotropically in the solution. In fig. 3 was shown, that dyes act as dipoles. The probability to absorb light is maximal for parallel orientation of dipoles to the polarization of light. So, exciting the dyes with polarized light induces an anisotropic distribution of excited dyes. The

1 An elegant derivation using particle summation is in Valeur [111].

emission of fluorescence in our measurements of anisotropy happens stochastical with a mean fluorescence time τ_{fl}. In the time between absorption and emission the dyes move in the solution, they rotate and translate. The rotational diffusion of one dye causes a change in its polarization from absorption to emission of fluorescence. We will connect here the polarization P of a sample with the anisotropy r, that we measure in our anisotropy experiments and give a description of the underlying concepts that we need later to understand the results of anisotropy measurements.

Having the geometry fig. 6 in mind, the polarization is defined as the fraction of light that is linearly polarized (s. eq. (14)).[64] Polarized light can be divided into a natural[2] n and a polarized p component.

The detected polarization of emitted light p one gets by calculation of the difference between detected parallel and perpendicular $I_{\parallel/\perp}$ intensities, where parallel and perpendicular is relative to the incoming excitation light polarization. Because intensities are proportional to the squared norm of the electric field, (compare fig. 6) $I(\phi,\theta)_{\parallel} \propto \cos^2\theta$ and $I(\phi,\theta)_{\perp} \propto \sin^2\phi\sin^2\theta$. The polarizer in the detection light path to detect only parallel and perpendicular polarization effects only θ, therefore detected intensities are ϕ independent and detected intensities are the integral of $I_{\perp/\parallel}(\phi,\theta)$ over ϕ giving $I_{\perp}\theta \propto \cos^2\theta$ and $I_{\parallel} \propto \frac{1}{2}\sin^2\theta$. Even in an isotropical medium with molecules randomly orientated the total number of molecules with angle θ_1 is only in a special case equal to the total number of molecules with a different angle θ_2 due to photoselection. To get the full emission of $I_{\parallel}$ and $I_{\perp}$ one integrates $I_{\parallel}(\theta)$ and $I_{\perp}(\theta)$ weighted with a function $f(\theta)$ giving the weight of the photoselection.[64] This yields the detected intensities in eq. (16).

In anisotropy measurements it is common to use the anisotropy value r in eq. (17), where p is divided by the total intensity of the emitted light.[64] P and r are directly connected. Therefore it is a matter of opinion which one to use for a description of anisotropy phenomena. With this definition and the derivations of the foregone paragraph, one can see that r is expressible via $<\cos^2\theta>$ as done in eq. (18).

With this definition time dependent anisotropy r(t), that can be measured via TCSPC, is given by the rotational correlation time of the sphere θ and the fundamental anisotropy $r_0 = r(t=0)$.

2 non-polarized

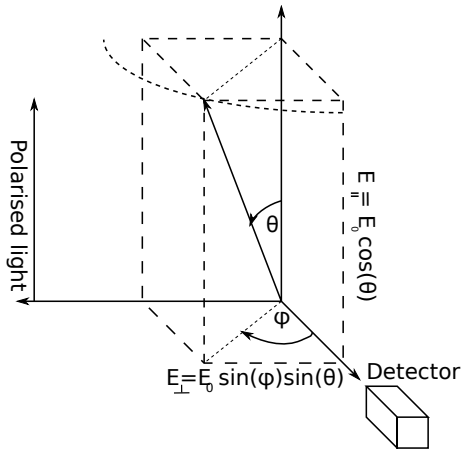

Figure 6: Connection of polarization parameters and the geometry of fluorescence experiments.

$$P = \frac{p}{p+n} \tag{14}$$

$$= \frac{I_{\parallel} - I_{\perp}}{I_{\parallel} + I_{\perp}} \tag{15}$$

$$I_{\parallel} \propto < \cos^2\theta > \qquad I_{\perp} \propto \frac{1}{2} < \sin^2\theta > \tag{16}$$

$$r(t) = \frac{I(t)_{\parallel} - I(t)_{\perp}}{I(t)_{\parallel} + 2I(t)_{\perp}} \tag{17}$$

$$= \frac{3 < \cos^2\theta > -1}{2} \tag{18}$$

$$r(t) = r_0 \exp(-\frac{t}{\vartheta}) \tag{19}$$

MAGIC ANGLE If not corrected otherwise, absorption and emission of light by biomolecules has in the experiment polarization effects, e.g. because of the polarization of excitation light and different rotation time scales of biomolecules. If one wants to exclude these effects, magic angle θ_m conditions, which give no anisotropy effects in the detected intensities ($r(t) = 0$), are chosen. This condition is fulfilled for all θ, if $\cos(\theta_m) = \sqrt{(\frac{1}{3})}$ - resulting in $\theta_m = 54.7°$.

2.2 DIFFUSIONAL PROPERTIES OF PARTICLES

The diffusional behaviour of molecules depends on their own characteristics and on properties of their environment. This was shown in statistical treatments derived by Einstein[33] and Stokes formulated in the Stokes-Einstein equation eq. (21).

$$D = \frac{k_B T}{\gamma} \tag{20}$$

$$\gamma = 6\pi\eta R_h. \tag{21}$$

The mean particle velocity is proportional to the temperature T of the sample and decreases with higher viscosities η. The factor of the proportionality is given by the Boltzmann-constant k_B. The hydrodynamic radius R_h is an estimate for the dimensions of a particle in a solvent that depends on the dimensions of the molecular structure itself and on the interaction with the solvent.

2.3 FLUORESCENT MOLECULES

Dyes are important for our everyday life. Absorbing pigments are present where ever colouring is needed. Fluorescence is often present, when active signaling with emission of light is accomplished. Pigments have high absorption in the pigment specific wavelength range giving it its colorant property and have to be attached to a substrate by means of additional compounds to give e.g. a car its color. Dyes are soluble molecules. If they are used for coloring, they possess in contrast to pigments a specific affinity to the substrate.[127] Luminescent dyes are soluble molecules that absorb light and convert the energy they get by absorption into emitted light. These luminescence can be divided into fluorescence, being fast emission of light happening in nanoseconds, and phosphorescence, here the emission of light happens in microseconds to longer timescales.

This section gives the basic theoretical for description of molecular properties of fluorescing molecules. With the Franck-Condon description of transitions for excitation of molecules, molecular properties like the Stokes shift, differences in fluorescent and phosphorescent lifetimes, and similarities of spectral shapes of absorption and emission of fluorescent molecules can be explained in a quantum mechanical theory. In a section about organic dyes the dipole behaviour will be connected to the quantum mechanical considerations in this chapter.

Organic dyes always consist of delocalized electrons. The simplest configuration achieving delocalized electrons are carbon-carbon $\pi - \sigma$ bonds aligned in a polymethine chain. This is depicted in fig. 8, where $R_{1,2}$ are remainder groups attached to the dye and the polymethine chain length is given by n.

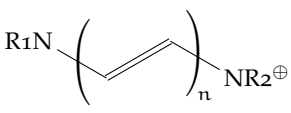

Figure 8: Typical structure of polymethine dyes consisting of n methines and rest groups $R_{1,2}$.

2.3.1 *Quantum mechanical considerations*

While the electromagnetic waves discussed in sec. 2.1 are the wavefunctions of the photons, the quantum mechanical description of matter gives insight into the interactions between light and matter by treating

protons and electrons also as waves. This is done by assuming that their state is described by wave functions Ψ. In the wave equation for electromagnetic fields eq. (5) the mathematical operation of derivation to time and space applied on the electric field gives a trivial solution. In more general cases than homogeneously distributed polarization in our experiments, the right side of the equation can be linearly dependent on the electric field. Then this wave equation is an eigenwert equation and one could set the complicated mathematical operator $B = \Delta - \mu_0\sigma\frac{\partial}{\partial t} - \frac{1}{c_0}\frac{\partial^2}{\partial t^2}\epsilon$. Then eq. (5) reduces to $B\vec{E} = 0$

The non-relativistic quantum mechanical state of a particle and its energies can be calculated by solving the Schrödinger equation eq. (22). This is an eigenwert equation with an operator H for the energy in the system. One needs to know the potential V (and kinetic energy operator H_{kinetic}) with which the particle interacts to formulate the Hamilton operator $H = H_{\text{kinetic}} + V$. The Hamilton operator is the sum of kinetic and potential energy operators and applied on the wave-function of a particle it yields the possible energies of the particle - the eigenenergies E of the eigenstates $\Psi(\vec{r}, t)$.

2.3.2 *Franck-Condon principle*

Molecules consist of several atoms. The positively charged core of an atom has about thousand times higher mass m_{core} than its electrons $m_e \ll m_{\text{core}}$. Therefore distances between atomic cores follow changes in electronic states slow. Then the approximation eq. (24) is possible. Using again $m_e \ll m_{\text{core}}$ the schrödinger-equation eq. (22) the hamiltonian of the molecule can be split into an electronic part H^{el}, kinetic and potential energy $H^{\text{nuc}}_{\text{kin}}, V^{\text{nuc}}_{\text{kin}}$ of the core eq. (23). Therefore H separates into an electronic and a part describing atom motion.[35, 51]

$$H|\Psi(\vec{r}, t)> = E|\Psi(\vec{r}, t)> \tag{22}$$

$$H = H^{\text{el}} + H^{\text{nuc}}_{\text{kin}} + V^{\text{nuc}}_{\text{kin}} \tag{23}$$

$$|\Psi(r; R_n)> = |\Upsilon(r; R_n)> |\Phi R_n> \tag{24}$$

$$< \Phi'| < \Upsilon'|\vec{\mu}|\Phi > |\Upsilon > =< \vec{\mu} > FC_{\Phi\to\Phi'} \tag{25}$$

$$FC_{\Phi\to\Phi'} =< \Phi(r; R)|\Phi'(r'; R) > \tag{26}$$

The quantum-state $\Psi(\vec{r}, t)$ of a molecule then depends mainly on electronic excitation, vibration of the cores in the molecule, and rotational motions. Because of the attractive forces between nuclear cores and electrons, the electrons are held in a specific volume around the cores. Waves held in a confined space can only exist in quantized states. The molecular states are characterized by quantum numbers n for electronic states, ν vibrational states, and the rotational quantum number J that yield for every quantum number combination quantized states with quantized energies. Protons and electrons are both fermions giv-

ing an additional quantum number for the spin state $\mathfrak{s}$ of spin up or spin down.

As stated above, organic dyes can be approximated as dipoles. The part of the hamiltonian responsible for transition calculations is then mainly the dipole part, the electronic dipole operator $\vec{\mu}$. The probability of electronic transitions is calculated by eq. (25). Transitions have some initial vibrational state Φ of the electronic ground-state Υ and an excited vibrational state Φ' in the excited electronic state Υ'. In eq. (25), the principal allowance of a transition is calculated via $< \vec{\mu} >=< \Upsilon|\mu|\Upsilon' >$ yielding rules for possible transitions of molecules with quantum number triples $\mathfrak{n}$, ν,J, and in ground state into excited states with $\mathfrak{n}'$, ν', J$'$. The probabilities of the allowed transitions from Φ to excited states Φ' are given by their Franck-Condon factors $\mathsf{FC}_{\Phi\Phi'}$ (s. eq. (26)). To describe de-excitation of molecules by emission of photons, the above formulas hold by exchanging stroked variables with non-stroked.

The lowest energies possible to excite molecular electronic transitions are the excitations of electrons that have the lowest binding energies. Electrons of atoms shared in binding are the electrons with lowest binding energies of the atoms. Bonds resulting from this binding can be separated into σ- and π-bonds.[90] Electrons in σ bonds are shared by both atom cores and are distributed uniformly in a rotational ellipsoid with the rotation axis along the bond.[90] π-bonds are distributed parallel to the bonding direction.[90] Electrons participating in π-bonds have the lowest molecular binding energies - called Highest Occupied Molecular Orbital (HOMO). This is usually equal to the singlet state S_0 and the first excited state S_1 is called Lowest Unoccupied Molecular Orbital (LUMO).

This is illustrated in fig. 9 for transitions usually occurring in fluorescent molecules. Electronic transitions from the HOMO into LUMO, happen on a femtosecond, relaxation of vibrational and rotational transitions on a picosecond, and fluorescent transitions on the nanosecond timescale. Therefore eq. (24) is valid. Excitation and emission in fig. 9 are then vertical lines, the most probable transitions are the ones, where Franck-Condon factors of eq. (26) are maximal.

Having fig. 9 in mind, depending on Franck-Condon factors, several de-excitation processes are possible. This is depicted in a Jablonski-diagram fig. 10. Excitation of electromagnetic waves excites electrons from the ground state S_0 into singlet states $\mathsf{S}_\mathfrak{n}$ with n referring the n-th excited state. Then several processes are possible and compete with each other. First, there are non-luminescent transitions like Internal Conversion (IC) and Inter-System-Crossing (ISC). ICs are processes where vibrational and rotational modes of molecules equilibrate by interaction with the environment. When the spin of the electron flips, this is called ISC and the electron changes from a singlet to a triplet state. The de-excitation happens then via ICs in the triplet state and

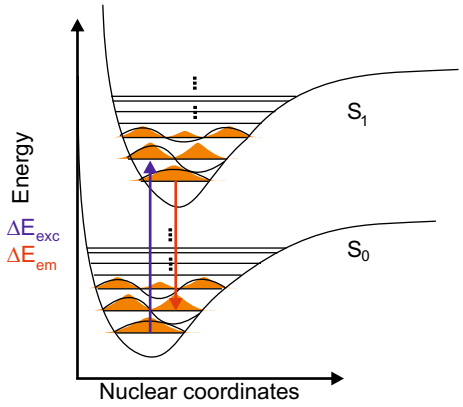

Figure 9: Electronic transitions in a excitation de-excitation process to illustrate the Franck-Condon principle. Absorption and emission of photons are vertical processes, because nuclear motion are thousandfold slower due to mass differences. Most probable transitions are transitions from and into states, where the integral over probability densities of electrons in these states are maximal. Vibrational and rotational de-excitation are processes changing core positions. In molecules with harmonic electronic potentials, excitation from base vibration of HOMO into n-th vibrational mode in LUMO has a de-excitation path the one from base vibration of LUMO to n-th vibrational mode in HOMO. The more the potential is deformed, the less this mirror-rule is valid.

somehow there has to be again a ISC or the molecule shows phosphorescence (P). Fluorescence is a transition usually occurring from S_1 to some vibrational mode of S_0.

Knowing that there exist non-fluorescing ICs it is straightforward, that fluorescent molecules emit at longer wavelengths than their excitation. This phenomenon is called the Stokes shift. The wavelength difference of the exciting to the emitting light is released by other kinds of energy than fluorescent light packages. The fluorescent processes with rates k_r and non-radiative processes with rates k_{nr} compete. How much of the excitation energy is converted into fluorescence is expressed in the steady-state quantum yield. We come back to this in sec. 2.4.1.

2.3.2.1 *Absorption and fluorescence emission by organic dyes*

In a semiclassical model of organic dyes a wavelength dependence for the extinction coefficient ϵ and for the fluorescence spectrum $I(\lambda)$ can be derived.[17] These semiclassical formulas eq. (27) and eq. (28) are valid for weak coupling. This means, that in the case of complexation of molecules these formulas are not valid. In the rotating wave approximation one gets for the absorption of a molecule with a ground state in eq. (27) a dependence of the cross section σ proportional to ω weighted by Franck-Condon factors and the allowance of transitions for dipoles of eq. (25).

The rules for allowance of transitions have the same structure for absorption and spontaneous emission of photons of the ground states of

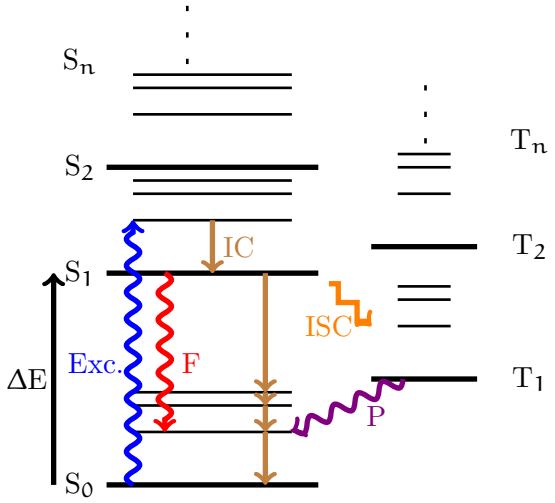

Figure 10: Jablonski representation of competing molecular transitions. Transition Exc. is excitation by absorption of a photon into a singlet state $S_n, n > 1$. The molecule de-excites via non fluorescent internal conversion IC by interactions with the environment to the ground state of the LUMO. Several de-excitation paths are now possible: again IC, inter-system-crossing ISC by spin flip of the excited electron with phosphorescence P or IC again as last step, or Fluorescence F.

the HOMO and LUMO. Therefore the formula for emission of photons by fluorophores is similar to eq. (27).

$$\sigma(\omega) = \frac{4\pi^2\omega n}{3c}|d_{eg}|^2\mathfrak{D}(\omega) \tag{27}$$

$$I(\omega') = \frac{4\omega'^3}{3c^3}|d_{eg}|^2\mathfrak{D}(\omega') \tag{28}$$

with

$$\omega^2\sigma(\omega) \propto I(\omega - \omega') \tag{29}$$

In an absorption process the incoming photon itself induces the transition of an electron from the HOMO into the LUMO of the absorbing molecule. In contradiction to stimulated emission, the definition of spontaneous transition of the electron in the LUMO of an excited fluorophore into the HOMO is that it is not induced by external photons. The electron couples to the vacuum state of the radiation state. This coupling introduces an additional ω^2 factor.[70]

2.3.2.2 *Mirror rule*

If transitions from HOMO to LUMO happen in the harmonic shaped part of the HOMO- and LUMO-potentials, then excitation- and emission lineshape functions show a mirror symmetry, because the Franck-Condon (FC)-factors of emission and excitation are in this special case

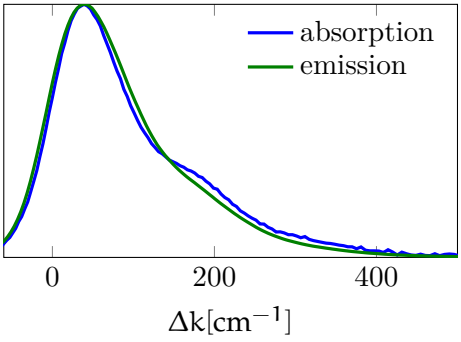

Figure 11: Lineshape functions $\mathfrak{D}(\Delta k)$ of absorption and emission of ATTO 488. The lineshape of absorption and emission were shifted to the center of mass of both lineshape functions. The lineshape function of the emission was mirrored at the center of mass.

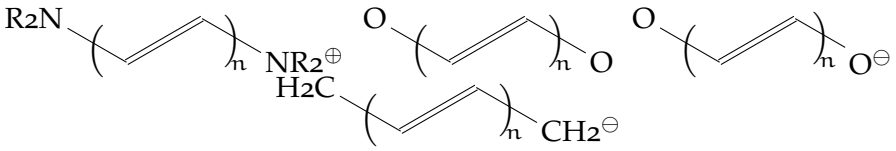

Figure 12: Basic polymethines: Streptopolymethine-cyanine cation, streptopolymethine-oxonol anion, natural streptopolymethine-merocyanine, and carboanions.[105]

equal for transitions into the same vibrational and rotational modes. An exemplary plot is shown in fig. 11. If spectra are corrected for $\omega = ck$ proportionality and Stokes-Shift, then a mirroring of the spectra at the center-of-mass of this corrected emission and absorption shows identical line shape for organic fluorophores. In fig. 11 this is exemplified with measurement data of the fluorophore species ATTO488.

2.3.2.3 *Organic dyes*

Inorganic dyes are usually non fluorescing dyes and are pigments for coloring. Organic dyes can be divided into polymethine and aromatic polybenzene dyes. They differ with regard to attached groups for solubility and changing optical properties. I will use in this work a differentiation between chromophoral part and attached groups of dyes. The chromophoral part of the dye is responsible for luminescence.[30]

In organic dyes these are methine groups having $\pi - \sigma$-bonds, where one of the electrons of every methine is quasi free (compare fig. 12). Polybenzene dyes consist of three methine groups in a ring structure. Benzene, naphtalene, anthracene, tetrazene, and pentazene are the basic structures of benzene dyes depicted in fig. 13.[19]

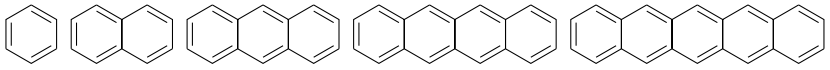

Figure 13: Benzene, naphta-, anthra-, tetra-, and pentacene.[19]

Following an argumentation of Kuhn[62] one can estimate roughly the transition energy E_n of polymethines using the particle-in-a-box model of quantum mechanics.[21] The length of the chromophoral part of the polymethine is the number N of methines plus one bond length representing the ends of the chromophore. The mean bond length of carbon bonds is 139 pm in methines. Then one obtains for the polymethine Cy5 in fig. 3 with eq. (31) for its wavelength $\lambda = 580$ nm. The longest excitation wavelength is the difference between energies of HOMO and LUMO. A molecule with N π-electrons has, because of spin pairing, $n_{HOMO} = N/2$ low levels filled. The first excited level is then $n_{LUMO} = N/2 + 1$. Cy5 has four carbon π electrons and three nitrogen π electrons, every carbon-carbon distance is 0.139 nm and about 8 bonds constitute the chromophoral part. Then $L = 1.12$ nm and $N = 7$.[62] Using this, Kuhn derived a model where the

$$E_n = \frac{n^2 h^2}{8 m_e L^2} \tag{30}$$

$$\lambda_{HOMO/LUMO} = \frac{8 m_e c}{h} \frac{L^2}{N+1} \tag{31}$$

2.4 QUENCHING MECHANISMS OF FLUORESCENT ORGANIC DYES

Theories of dye quenching interactions consider different length and time scales. Fluorescent organic dyes have a size of several Angstrom and the size of their longest molecular axis differs typically 3-5 times compared to the other two. We have previously used that this shape induces a dipolar behaviour in sec. 2.1.1.

2.4.1 *Kinetic aspects of bimolecular processes*

For quenching processes, where external molecules enhance non-radiative transitions, QYss can be separated in a dynamical quantum yield (QYdyn) and a static quantum yield (QYst) owing to the time behaviour of the intermolecular quenching processes.[17, 64, 111]

$$QYss = \frac{k_r}{k_r + k_{nr}} \tag{32}$$

$$= QYst \cdot QYdyn \tag{33}$$

By definition static quenching processes are processes, where the time the fluorophore is fully quenched lasts longer than several of its fluorescent lifetimes τ_{fl}. This is the case for complexation of fluorophore and quencher in excimers and exciplexes. Reactions, where no complexes are built show also a static contribution to quenching of fluorescence due to quenching that happens in a sphere of action around

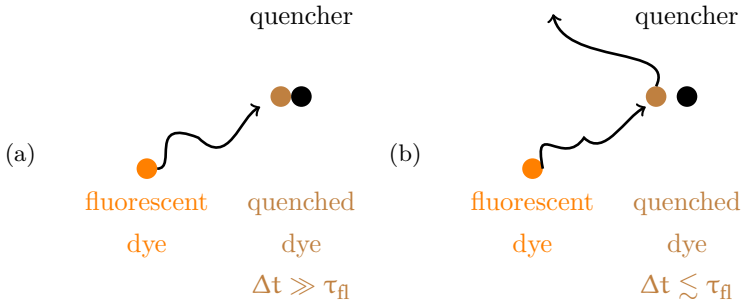

Figure 14: Static and dynamic quenching mechanisms. If a fluorescent molecule enters a sphere of a molecule that quenches it, static quenching happens, if the fluorophore stays in this quenching significantly longer than a excitation-emission cycle of the free dye. If the duration of molecular contact is as long or shorter than the fluorescence lifetime of the fluorophore, the quenching mechanism is called dynamical.[64, 111]

the quencher. In this sphere the quenching mechanism that governs the quenching interaction is still strong enough even without molecular contact. If both effects are present this last quenching process gets an extra term in eq. (33) and is called sphere-of-action quenching.[64]

The term dynamical quenching is used for quenching processes where the molecular contact is fast compared to an excitation-emission cycle of the used fluorophore (compare fig. 14). Fluorophores diffusing through a medium undergo excitation-emission cycles and are only quenched at collision with the quencher molecule.

In bimolecular quenching always both, static and dynamic, mechanisms exist, but only dynamic quenching influences fluorescence lifetime τ_{fl} in measurements[3]. To the non-radiative rates k_{nr} of eq. (32) a non-radiative de-excitation term k_q due to dynamic quenching $k_q[Q]$[4] is added, if a quencher Q with the concentration [Q] is given to a solution containing the fluorophore (compare eq. (34)). A comparison of the fluorescence lifetime of free dye with eq. (34) yields the Stern-Volmer equation for dynamical quenching eq. (35).[17, 111]

$$\tau_{fl} = \frac{1}{k_r + k_{nr}} \tag{34}$$

$$\tau = \frac{1}{k_r + k_{nr} + k_q[Q]} \tag{35}$$

Complexed molecules DQ, consisting of fluorophores D and quencher species Q, that are fully quenched, reduce the overall fluorescence in-

3 Static quenching is only obversable due to decrease of the overall detected intensity of the TCSPC instrumentation. Fluorescence lifetimes are not detectable for bimolecular complexes discussed here.

4 Here it is tacitly assumed, that the dynamical quenching rate is not time dependent. However, this can only be tested with ideal $\delta(t)$ laser pulses being infinitely sharp. The broader the excitation light to test the fluorescence lifetime with quenching τ is in time, the more eq. (35) holds.[111]

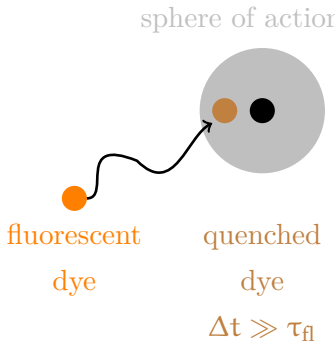

Figure 15: Sphere of action contribution to quenching. Whether a molecular contact happens with a complex of fluorophore and quencher or not, quenching interactions can be that strong, that the fluorophore is quenched in a sphere-of-action.[64]

tensity of a sample (see eq. (36)). With the equilibrium constant of the complexation reaction eq. (37) the decrease of fluorescence due to static quenching can be calculated using both formulas yielding eq. (39).

$$I = I_0 \left(1 - \frac{[DQ]}{[Q]}\right) \tag{36}$$

$$K_{St} = \frac{[DQ]}{[D][Q]} \tag{37}$$

$$\Rightarrow \frac{I}{I_0} = QYst \tag{38}$$

$$= 1 - K_{St}[Q]. \tag{39}$$

Quenching interactions are possible without molecular contact. For strong fluorophore quenching interactions the fluorophore can be fully quenched in a Volume V_q around the quencher (see fig. 15). Assuming a poisson distribution with n quenchers residing in V_q with a mean number of quenchers there of $< n >= V_q N_{Av}[Q]$, a decrease in quantum yield due to sphere-of-action can be connected to experimental available quantities in eq. (41).[64, 111]

$$P_n = \frac{< n >}{n!} \exp\left(- < n >\right) \tag{40}$$

$$QY_{Sphere} = \exp\left(-V_q N_{Av}[Q]\right) \tag{41}$$

By changing the quencher concentration [Q] of a solution and measuring intensities I, V_q is determined.

2.4.2 *Energy- and Electron Transfer*

Depending on the distance R_{DQ} of excited fluorophores D^* to quenching molecules Q there are several possible kinds of interactions (cf. fig.

16). On the one hand at distances $r_{DQ} \gg 100nm$ a classical description of the interactions is sufficient. In fig. 16 this is the area II. At these distances, fluorophore and quencher without any bridging medium between them, interact solely via energetic transfer by statistically emitted photons of the fluorophore.

Decreasing the distance between D^* and Q, the situation changes dramatically at distances under 20 nm, depending on fluorescence emission spectra of D and absorption spectra of Q. At least for shorter distances than 20 nm the classic particle picture of photons breaks down, if one considers the time-energy uncertainty formula $\Delta E \cdot \delta t \leqslant \frac{\hbar}{2}$ alone with $\Delta E = \hbar\omega$ being the energy of optical photons and Δt their mean time of flight for distances under 20 nm. Here the near field of the fluorophore and quencher give a sharp transition in the quenching rates by the FRET interaction.[42] Here it is still possible to describe FRET donor and acceptor as separated molecules. The less distant they are, the more they can be regarded as one molecular complex. So, depending on the interacting fluorophores and their environment, at distances comparable to their FRET radius the molecules can be in area III of fig. 16.

At least under 2 nm, other interactions are becoming important, where electron transfer happens. The simultaneous exchange of electrons of D^* and Q was first described in a quantum-mechanical theory that unified this electron transfer with FRET.[25] A more general applicable theory for calculating the possibility for strong quenching of D^* by Q by electron transfer was given by Marcus.[67] For D and Q molecules having strong attractive forces, molecular contact can lead to an overlap of molecular orbitals leading to molecular DQ complexes. These supramolecular complexes show splitting of energy levels that can lead to quenching. In this case a differentiation between electron and excitation energy transfer is hardly possible. Generally, from large to short distances the effects overlap and depending on molecular properties of D and Q different interactions have a general role in quenching.

2.4.2.1 *Photon mediated transfer*

In the derivation of the Lambert-Beer law in sec. 2.1.2.1 it was already used, that in a classical model, the photon absorption of a molecule Q is proportional to the effective area $\sigma_Q = \frac{A}{N_{Av}}$ with which Q absorbs (compare fig. 4). The fluorophore MR121 has an extinction coefficient of $\epsilon_{MR121} = 105000\ M^{-1}cm^{-1}$. Its single-molecular cross-section is $\sigma_{MR121} = 400\ pm^2$. To derive the probability of absorption of photons that are emitted by a isotropical[5] emitting point emitter at a distance of $R = 100$ nm, the fraction of σ_{MR121} to the area of a sphere with radius d is $f = \frac{4}{3} \times 10^{-8}$. If this point emitter is a fluorophore with

5 If one respects anisotropic emission of single dipole emitters, then the orientation of D and Q is also important, as it was pointed out in the section about time dependent anisotropy (sec. 2.1.2.2).

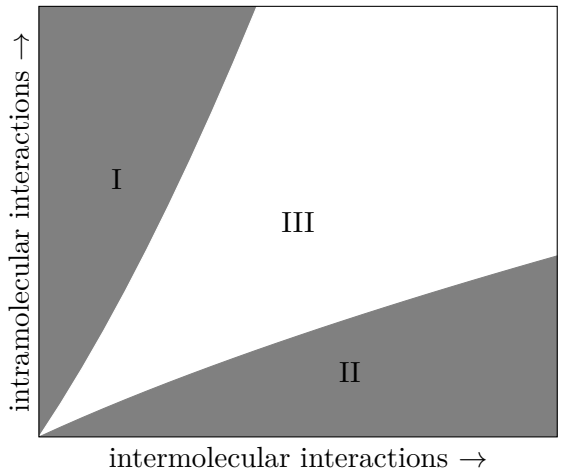

Figure 16: Different ranges of interaction strengths. The stronger the intramolecular interactions compared to intermolecular interactions, the more electron orbitals couple and the more a supramolecular picture of the complex is enhanced. The stronger intermolecular interactions are, the more properties of each molecule itself influences energy transfer.[70]

an emission rate of $k_{fl} = 10^9 s^{-1}$, the rate of energy transfer from the emitter to MR121 is about $k_{DQ} = f \cdot k_{fl} \approx 10\ s^{-1}$. We will see, that this is a low value compared to other transfer mechanisms at distances in the 10 nm range.

In this example the rate for photon mediated energy transfer from D to Q depends on R^2. In quantum electrodynamics it can be shown that this is the long range limit of a general equation for dipole-dipole energy transfer rates (eq. (42) in brown).[10, 70] In this equation κ_{DQ} ($\bar{\kappa}_{DQ}$) are (mean) orientation factors and $\mathfrak{D}$ is a line shape function which inherits the information of absorption and emission spectra of D and Q.

$$k_{DQ}^{pm} = \frac{2\pi}{\hbar}|d_D d_Q|^2 \left(\frac{\kappa_{DQ}^2}{R_{DQ}^6} + \frac{K_0^2 \kappa_{DQ}(\kappa_{DQ} - 2\kappa_{\bar{D}Q})}{R_{DQ}^4} + \frac{K_0^4 \bar{\kappa}^2}{R_{DQ}^2} \right) \mathfrak{D} \tag{42}$$

The blue part of this formula is important on short distances under 20 nm. This is the range of FRET and has a strong R^{-6} dependence. In this theory the transfer in the short distance range is still no classic transfer, but it is referred to as a *virtual photon exchange*.[11] The R^{-4} term here is the connecting domain between FRET and classical photon mediated energy transfer.

2.4.2.2 *Förster Resonance Energy Transfer*

The Förster Resonance Energy Transfer, also called fluorescence resonance energy transfer is an excitation energy transfer with weak coupling of the participating molecules. In this model, donor and quencher

molecules are still independent regarding motion of molecular coordinates on time scales for excitation and the equilibration of nuclear coordinates after excitation. Therefore in an ansatz using pertubation theory eq. (43), the potential V_{DQ} describing the interaction between fluorophore (energy donor) and quencher (energy acceptor) and the δ-function giving the selection rules for transitions between molecular orbitals can be separated into its molecular factors of fluorophore D and quencher Q. Then eq. (44) follows, giving now a factor J_{DQ} (eq. (45)) describing the alignment of participating molecules and two factors giving the franck-condon factors of each molecule.

$$\begin{aligned} k_{FRET} = \frac{2\pi}{\hbar} \sum_{M_D,N_D} \sum_{M_A,N_A} & f_D^* f_Q \dots \\ & \times | < \Psi_D^* \Psi_Q | V_{DQ} | \Psi_Q^* \Psi_D > |^2 \\ & \times \delta(E_D^* + E_Q - E_Q^* - E_D) \end{aligned} \tag{43}$$

$$< \Psi_D^* \Psi_Q | V_{DQ} | \Psi_Q^* \Psi_D >= J_{DQ} < \chi_D^* | \chi_D > \times < \chi_Q | \chi_Q^* > \tag{44}$$

$$J_{DQ} = \kappa_{DQ} \frac{|d_D||d_Q|}{|R_{DQ}|^3} \tag{45}$$

The terms $f_D^* < \chi_D^* | \chi_D >$ and $f_Q < \chi_Q | \chi_Q^* >$ are the emission lineshape of the fluorophore and the absorption lineshape function of the quencher. Therefore the FRET rate k_{FRET} depends on the spectral properties of FRET energy donor and energy acceptor molecules and a dipolar alignment factor as in eq. (46). Using the connection between absorption and emission to their lineshapes in eq. (27) and eq. (28), the rate for FRET can be directly computed (eq. (47)) by emission and absorption spectra $I(\omega)$, $\epsilon(\omega)$ in eq. (47) that are accessible by spectrometers. Introducing the Förster radius R_F in eq. (48), the distance of energy donor and acceptor, where the FRET rate equals the fluorescence emission rate $k_{FRET}(R_{FRET}) = k_D = \tau_0^{D^{-1}}$ one obtains for k_{FRET} eq. (48). If one has therefore already determined the R_{FRET} and knows τ_0^D, then distance information between fluorophore and quencher are determinable.

$$k_{FRET} = 2\pi |J_{DQ}|^2 \int_0^\infty d\omega \mathfrak{D}_D^{em}(\omega)\mathfrak{D}_Q^{abs}(\omega) \tag{46}$$

$$= \frac{9\hbar c^4 \kappa^2}{16\pi^2 n |R_{DQ}|^6} \int_0^\infty \frac{d\omega}{\omega^4} I_D(\omega)\epsilon(\omega) \tag{47}$$

$$\Rightarrow k_{FRET} = \frac{1}{\tau_0^D}\left(\frac{R_F}{R_{DQ}}\right)^6 \tag{48}$$

$$E \equiv \frac{k_{FRET}}{k_r + k_{nr} + k_{FRET}} \tag{49}$$

$$= \frac{1}{1 + \left(\frac{R_{DQ}}{R_F}\right)^6} \tag{50}$$

Usually the quencher molecule is itself a dye. Both molecules are then called donor and acceptor. With the definition of the FRET-efficiency E, the fraction of donor de-excitation by the quencher one can see, that FRET is sensitive for differences in distance between fluorophore and quencher at about R_{FRET}.

2.4.2.3 *Electron transfer reactions*

Electron Transfer is one of the basic types of chemical processes. It represents the initial step of a number of reactions like the making and breaking of chemical bonds or the change of molecular conformations.[70]

ET is a spontaneous charge redistribution between an initially prepared reactant state and a well-defined product state. In this work the important preparation of the reactant state is a metastable initial state of fluorophores by photoabsorption. Unlike systems where special charge carriers transport electrons over large spatial distances, electron transfer means here, that because of non-ionizing electronic molecular excitation an electron is transferred into a different region of the molecular complex in a tunneling process from one electron donor molecule to the electron acceptor molecule. This definition given in[70] excludes processes in biological systems where enzymes act as charge carriers - this work focusses more on bimolecular processes and therefore this definition is appropriate.

In ET reactions the whole electron wave function of the ET-complex changes by a transfer reaction. The steps discussed in sec. 2.3.2 can for pure ET reactions be described by changes of the electronic charge densities. These changes are induced by the changes of the states of single electrons of the molecules as depicted in fig. 17.[70]

In fluorescence quenching by ET, the fluorophore is excited by absorption of a photon meaning an electron is transferred by the excitation from the HOMO to the LUMO of the fluorophore. In a second

step an electron is transferred from the electron donor of the reaction to the electron acceptor. Depending on the potentials, the quencher molecule can be the electron donor. Then its electron is transferred from its LUMO to the LUMO of the fluorophore. If the fluorophore is the electron donor, its electron is transferred from its HOMO into an excited state of the quencher molecule. After this electron transfer several de-excitation paths are possible.

If the ET proceeds directly from the donor to the acceptor, the process is called through space transfer. This transfer is only possible for DA distances of less than 20 Angstrom.[70]The electron transfer can be described by thermodynamic energy parameters of reorganization energy E_λ, temperature T, and the standard free energy change of the complexation of fluorophore and quencher ΔG^0. E_λ contributes to the rate, because the solvent has dipolar properties, too, and the shell of solvent molecules around the complex changes changes energetic behaviour. The standard free energy is the sum of oxidation and reduction energies of electron donor and acceptor, the transition energy of the transition between the S_0 and S_1 state in the fluorophore, and a Coulomb potential of the charge separated state.[17, 65, 70] $|V_{DQ}|$ is a term relating to electronic coupling, that decreases exponentially with increasing distance R_{DQ}. Finally the distance dependence depends on an exponential attenuation factor β^{el} that is in the range 2-5 $Å^{-1}$.[17]

$$k_{ET} = |V_{DQ}|^2 \sqrt{\frac{\pi}{\hbar^2 k_B T E_\lambda}} \exp\left\{-\frac{(\Delta G^0 - E_\lambda)^2}{4\lambda k_B T}\right\} \tag{51}$$

$$\propto \exp\left(-\beta^{el} R_{DQ}\right) \tag{52}$$

DEXTER MECHANISM If fluorophore and quencher get for a short time in contact with overlap of molecular orbitals, it is possible that electrons are exchanged simultaneously. This is a special case of PET that was first described by Dexter[25] in a theory unifying FRET and this PET interaction. Here the assumptions that led from the quantum mechanical ansatz for transitions in eq. (43) to the separation of the excitation and de-excitation terms of energy donor and acceptor molecules in eq. (46) are not possible. In molecular contact it is also possible, that both electrons change simultaneously their quantum mechanical state.

2.4.2.4 *Dimerization*

At molecular contact with strong overlap of these molecular orbitals, splitting of molecular orbitals leads to J- and H-dimerization (compare fig. 18). J-bands were discovered by Jelley and Scheibe[58, 91, 92] for aggregation of dye monomers into loosely bound polymers that exhibit a sharp peak red-shifted to the maximal monomer peak.[34, 92] Scheibe

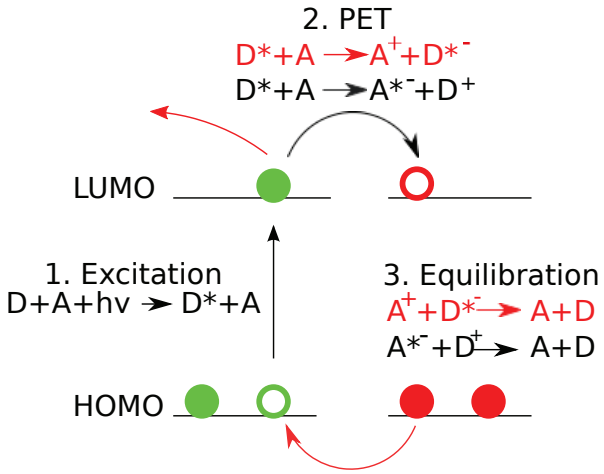

Figure 17: PET pathways. Excitation of the fluorophore leads to transition of an electron from the LUMO of the electron donor to the electron acceptor. After electron transfer equilibration of both molecules happens via different pathways. The electron donor can be the fluorophore or the quenching molecule. In the case of MR121 quenching by Trp, Trp is the electron donor.

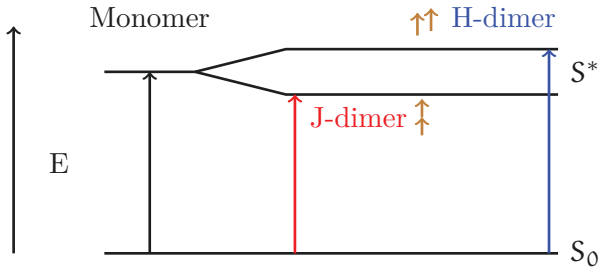

Figure 18: Energy level diagram of H- and J-dimers compared to monomeric energy level. By complexation of monomers, energy bands of the monomer split and depending on the angle theta of the point dipole center of both molecules, only excitation to the higher energy level (H-dimers) or lower energy level (J-dimer) are allowed.

also discovered dyes exhibiting blue-shifted absorption maxima and called them hypsochromical shift aggregates - H-Dimers.

J-Aggregates often show fluorescence at the red-shifted peak, while H-dimers do not.[121] Therefore H-dimerization represents another quenching mechanism for reporting contact of two molecules. In contrast to J-aggregates, H-dimers have a complicated vibrational structure. Therefore there exist only a few theoretical articles addressing the lineshape of H-aggregates.[35]

In an energetic view of the dimerization coupling of different molecules, the energy band of H-dimer complexes is the monomeric single molecules of the dimer still couple with their vibronic energy modes. In this case several vibronic modes of the monomers are excited. Therefore absorption spectra of H-dimers compared to J-dimers show a broad spectrum.

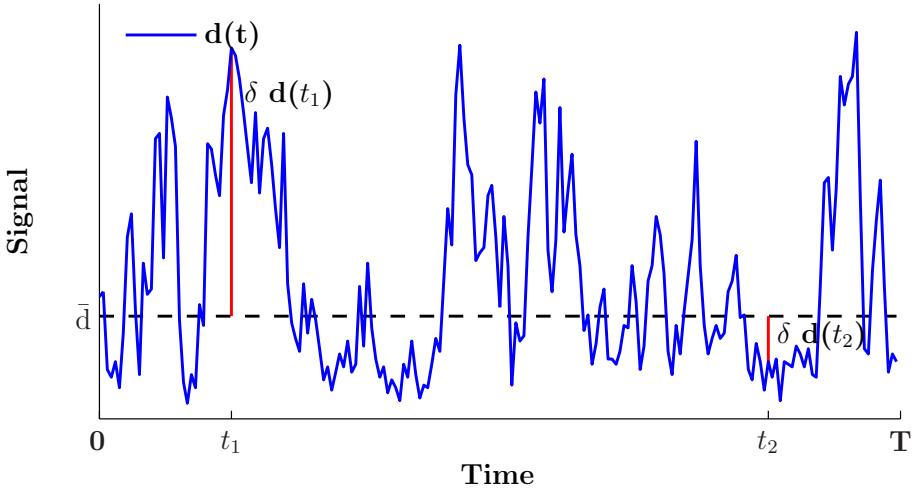

Figure 19: Typical 1 ms binned time trace of the APD signal of a FCS measurement. The signal $d(t)$ has a mean value $\bar{d}$ giving fluctuations $\delta d(t)$ depicted here for two different times t_1 and t_2.

2.5 THE SECOND ORDER CORRELATION FUNCTION OF FCS

Correlating is a powerful technique to find similar structures in noisy data. The dimensions of oligopeptides in solutions are far beyond 200 nm and structural or dynamical information on oligopeptides is therefore not achievable with visible light without any tricks. Fluorescence Correlation Spectroscopy is a technique, where specific interactions and diffusional properties of biomolecules are obtainable.

In confocal FCS signals of two detectors are correlated via the second order correlation function $G(\tau)$. In this section following the article of Krichevsky et al.[60] principles and formulae are derived that are needed to analyze the data of a confocal FCS setup.

On a FCS setup like in fig. 23 emission $d(t)$ of a sample illuminated by a excitation beam is detected. As depicted in fig. 19 a signal $d(t)$, measured over a time T, has a mean strength $\bar{d}(t)$ and fluctuates with $\delta d(t) = d(t) - \bar{d}(t)$ around $d(t)$. Using a setup with one detector, similarities of $d(t)$ in time can be analyzed by using autocorrelation, where $d(t)$ is compared with its copy. With a two detector setup both signals $d_1(t)$ and $d_2(t)$ of detector 1 and 2 are cross-correlated excluding dead time effects of detectors that are in the microsecond range.

The second order autocorrelation $G(\tau)$ is the average of the products of fluctuations normed to the average signal. In in ergodic systems one can write that as time or ensemble average.

$$G(\tau) = \frac{1}{\bar{d}^2 T} \int_0^T dt \delta d(\tau) \delta d(\tau + t) \tag{53}$$

$$= \frac{1}{\bar{d}^2} < \delta d(\tau) \delta d(\tau + t) > \tag{54}$$

Consider an ideal solution in equilibrium with two isomers having the same diffusion constant D, one fluorescent (open) the other not (closed). Rates k_o and k_c depict rates into fluorescent and non fluorescent state, respectively. They follow the reaction scheme

$$\text{open} \underset{k_o}{\overset{k_c}{\rightleftharpoons}} \text{closed},$$

having local opened species $C_o(\vec{r},t)$ and closed species $C_c(\vec{r},t)$ concentrations. One can establish a system of differential equations eq. (55) with a diffusional and a isomerization part that describe deviation $\delta C(\vec{r},t)$ of $C(\vec{r},t)$ from its mean. The differential equation system is solvable (s. sec. 9.4). Focussing on the fluorescent species with quantum yield QY, calculation of the detected emission signal $d(t)$ per sample time Δt yields eq. (56). If one has a gaussian excitation profile $I(\vec{r})$ (s. eq. (57)) that we can assume as two dimensional with diameter ω_{xy}, he gets a nice expression eq. (59) for $G(\tau)$. It depends only on experimental parameters: Mean particle number N in the excitation profile, mean diffusion time $\tau_D = \frac{\omega_{xy}^2}{4D}$ of particles passing through the focal volume, relaxation amplitude $K = \frac{k_c}{k_o}$, and relaxation time $\tau_K = (k_o + k_c)^{-1}$. The correlation function can be separated into a diffusional part $G_{\text{Diffusion}}(\tau)$ and one for blinking effects that can be described via eq. (55). Detailed deviations are in the appendix sec. 9.4.

$$\begin{aligned} \tfrac{\partial}{\partial t}\delta C_o(\vec{r},t) &= D\nabla^2\delta C_o(\vec{r},t) - k_c\delta C_o(\vec{r},t) + k_o\delta C_c(\vec{r},t) \\ \tfrac{\partial}{\partial t}\delta C_c(\vec{r},t) &= D\nabla^2\delta C_c(\vec{r},t) + k_c\delta C_o(\vec{r},t) - k_o\delta C_c(\vec{r},t) \end{aligned} \tag{55}$$

$$d(t) = \Delta t \int d^3\vec{r}\; I(\vec{r}) \cdot QY \cdot C_o(\vec{r},t) \tag{56}$$

$$I(\vec{r}) = I_0 exp\left(-\frac{2\left(x^2+y^2\right)}{\omega_{xy}^2}\right) \tag{57}$$

$$G(\tau)_{2D-\text{diffusion}} = \frac{1}{N}\left(1+\frac{\tau}{\tau_D}\right)^{-1} \tag{58}$$

$$G(\tau)_{2D,\text{kin.}} = \frac{1}{N}\left(1+\frac{\tau}{\tau_D}\right)^{-1}\left(1+K\exp\left[-\frac{\tau}{\tau_K}\right]\right) \tag{59}$$

$$\begin{aligned} G(\tau)_{2D,\text{tripl.+kin.}} = \frac{1}{N}&\left(1+\frac{\tau}{\tau_D}\right)^{-1} \cdot \\ &\left(1+T\exp\left[-\frac{\tau}{\tau_T}\right]+K\exp\left[-\frac{\tau}{\tau_K}\right]\right) \end{aligned} \tag{60}$$

with

$$\tau_D = \frac{\omega_{xy}^2}{4D} \tag{61}$$

$$K = \frac{k_c}{k_o} = \frac{c_c}{c_o} = K_{eq} \tag{62}$$

$$\frac{I_{FCS}}{N} = \frac{I_{APD1} + I_{APD2}}{N} \tag{63}$$

Several groups do not use the 2 dimensional approximation that accounts for a large ratio of z- against xy-width of the focal volume.[117, 118] Considering also z-direction of the gaussian beam, the diffusional correlation function is $G_{Diffusion}(\tau) = \frac{1}{N}\left(1+\frac{\tau}{\tau_D}\right)^{-1}\left(1+\kappa\frac{\tau}{\tau_D}\right)^{-\frac{1}{2}}$. Here a factor κ is introduced, that expresses the z to x,y diameter ratio.

Using the values τ_D, τ_K, K, N, and the overall detector intensity I_{FCS} the following parameters can be derived:

1. The mean particle intensity of particles that are detected via crossing the confocal volume of FCS $\frac{I_{FCS}}{N}$ can be directly compared to QYss measurements of ensemble measurements. It gives hints to subspecies of the sample that are in a non-fluorescent state on a timescale longer than the diffusion time τ_D. Also, $\frac{I_{FCS}}{N}$ can be used for characterization of FCS setups. For a dye standard dye this value shows how efficient photon detection is.

2. The diffusion time τ_D is via the focal volume V_{focal} and viscosity of the solvent directly connected by the Stokes-Einstein equation eq. (21) to the diffusion constant D of the inspected molecule.

3. With the equilibrium constant of blinking fluorescent species in the confocal detection volume of FCS K and its relaxation time τ_K rates of opening k_o and closing k_c processes can be derived via eq. (64). K gives also an estimate for the static quantum yield (eq. (65)).

$$\begin{aligned} k_c &= \frac{K}{\tau_K(1+K)} \\ k_o &= \frac{1}{\tau_K(1+K)} \end{aligned} \tag{64}$$

$$QYst^{FCS} = \frac{1}{1+K} \tag{65}$$

So the FCS signal gives informations about concentration, diffusional, photophysical and kinetic properties of molecules.

2.6 UNSTRUCTURED POLYPEPTIDES

Peptides and proteins are chains consisting of different sequences of AAs. The AA-sequence defines all these structures in a given environment. These structures must be experimentally determined to this day

and only structures of very small proteins can be simulated. There are 21 AAs that any organism uses in cells to encode proteins and most known proteins have 100-350[1] AAs. Therefore there are infinitely many possible protein configurations. This is the reason why finding rules how different AAs change and influence known configurations is a common task.

The AA-sequence is called primary structure and is the most basic element of peptide structure. Due to electrostatic interaction between these AAs, a secondary structure can be determined for every specific protein primary structure consisting of β-sheets, β-strands, α-helices, random coil and non-regular structure. The big picture of all these parts of a protein or polypeptide including interactions between all parts of the protein or polypeptide that cross-link the subunits of it is called tertiary structure. And if several proteins build a supramolecular complex, this is a quaternary structure.

The AAs isoleucine, leucine, valine, Trp, tyrosine, phenylalanine, cysteine (Cys), and aspargine are order promoting, rather disorder-promoting are alanine, arginine, Gly, glutamine, Ser, glutamic acid, lysine (Lys), and proline.[108] For this work we used short peptides containing glycine and serine residues with five to eight repeating units of glycine-serine building blocks. This peptide is known for its flexibility.[14]

2.6.1 *Rates of polymer dynamics*

When analyzing the kinetic behaviour of very flexible polypeptides in solution, one approximation is to neglect any interactions between the constituents of the peptide other than that their are connected loosely together in a chain. This is the random coil model that was extensively studied by Flory and Tanford for proteins in GdCl.[2, 40, 103] They found out, that in 6 M GdCl all their studied proteins "appear to be structureless, random chains." This random coil model is a basic descripton for very flexible proteins and peptides. In reality even very flexible peptides have electrostatic interactions between their constituents. The ideal chain model can still be used by dividing the peptide into s 'effective' segments with effective lengths $l_{\text{effective}}$ of its chain compartments.[2] Brownian motion of the angles of the segments in solution gives an estimate for the radius of gyration R_G for long freely jointed chains (eq. (67)). Determination of R_G is in our experiments in solution hardly possible, but it is proportional to the hydrodynamic radius R_H that was introduced in the Stokes-Einstein equation eq. (21).[104] Szabo, Szabo, and Schulten connected relaxation times for end-to-end contact τ to the root mean square of end-to-end distance r yielding a distance dependence for ideal chains beiing proportional to $|r|^{\frac{3}{2}}$.[2] For real chains one must note that compartments

of the polymers occupy volume that other chain segments are excluded from. Experimental data reveals that distance dependences of $|r|^{1.7}$[74].

$$s = \frac{L}{l_{effective}} \tag{66}$$

$$< R_G^2 > = \frac{< r^2 >}{6} \qquad \text{for } s \to \infty \tag{67}$$

$$\tau \propto \frac{\sqrt{< r^2 >}^3}{D} \tag{68}$$

2.6.2 *Modification of biomolecules*

Modification of biomolecules is on the one hand a process on purpose to utilize it e.g. for labeling fluorophores to specific areas at biomolecules for detection, or it is a naturally occurring process that we try to understand. In this study oligopeptides were labeled via N-hydrosuccinimide (NHS) ester labeling procedure. This is one of the most common activation chemistry for labeling of dyes to proteins.

2.6.2.1 *NHS Esters*

All proteins have the amino terminal end of the last AA in common. N-hydrosuccinimide ester are perhaps the most common activation chemistry for creating reactive acylating agents. Today the great majority of amine-reactive cross-linking or modification reagents commercially available utilize NHS esters. In protein molecules, NHS ester cross-linking reagents couple principally with the α-amines N-terminal and at the ϵ-amines of lysine side chains.[55]

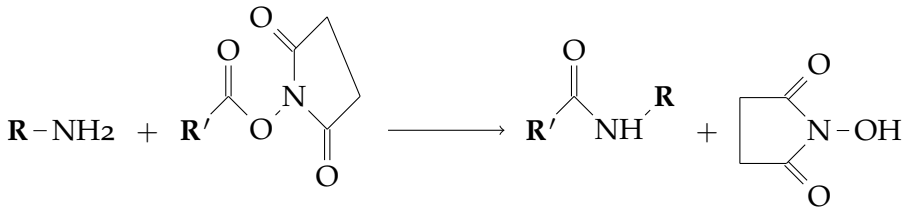

Amine Compound	NHS Ester Derivative	Amide Bond	NHS Leaving Group

NHS ester-containing reagents react with nucleophiles with release of the NHS leaving group to form an acylated product. The resulting esther linkages hydrolyze in aqueous solutions or exchange with neighbouring amines and form amide bonds. In protein molecules, NHS ester cross-linking reagents couple principally with the α-amines at the N-terminals and the ϵ-amines of lysine side chains. Literature data gives estimations for the half-life of NHS-esters under physiological pH conditions of several hours. [55]

2.6.3 *Glycine-Serine peptides*

Glycine serine peptides used in this study here are unstructured and fully flexible. Therefore end-to-end kinetics are only limited by the viscosity of the solvent[61, 65, 76]. Neuweiler et al.[76] measured for GS peptides of different lengths activation enthalpies of $(18 \pm 3)\ \frac{\mathrm{KJ}}{\mathrm{mol}}$. The activation enthalpy barrier for diffusional transport in water is 17 $\frac{\mathrm{KJ}}{\mathrm{mol}}$[6]. Therefore they conclude, that there are negligible intrachain interactions that give enthalpic contributions.

O-GLYCOSYLATION O-glycosylation is a post-translational modification occurring in living cells in the golgi apparatus. It is known that the first monosaccharide N-acetylgalactosamine (GalNAc) residue in a glycosylation process is attached to Ser or threonine. O-linked structures are often further connected with additional saccharides, but they are usually less branched than N-glycosylidic structures.[41].

O-glycans affect the rate either way depending on factors such as position and orientation.[72] The limited data available for the specific effect of glycosylation makes it difficult to generalize about the relation between the type of protein glycosylation and the thermodynamics of glycoproteins. Several studies of the folding and stability of glycoproteins in their glycosylated and non-glycosylated forms show that the sugars have diverse effects on folding kinetics.[97] It has yet to be determined whether there is any correlation among the sites of glycosylation and the ensuing effect in multiply glycosylated proteins. It is also not apparent whether there is a common pattern in the conservation of glycans in a related family of glycoproteins, but it is evident that glycosylation is a multifaceted post-translational modification.[72]

2.6.4 *Rates of chemical reactions*

Two state processes with an energy barrier given by the activation enthalpy ΔG^* at a temperature T of two reacting species in solution can be described by the arrhenius equation eq. (69).[94] In physical derivations the potential energy surfaces of the reaction have to be considered. For quadratic energy surfaces, the term A of eq. (69) can be calculated and is dependent on the curvature of the potential and of frictional forces of the system.[94] In general the constant A is dependent on the energy surface between reaction coordinates O and C.

$$\ln(k) = \ln A + \frac{\Delta G^*}{RT} \tag{69}$$

$$= \ln A + \frac{\Delta S}{R}\frac{\Delta H^*}{RT} \tag{70}$$

3

MATERIALS AND METHODS

3.1 ENSEMBLE SPECTROMETER

PHOTOMETER AND FLUORESCENCE SPECTROMETER Absorbance spectra were recorded with a UV/Vis spectrometer (V650; Jasco; Gross-Umstadt, Germany) at 293 K. Before measurements, the spectrometer had to warm up for 30 minutes to give fluctuations of Optical Density (OD) of about 10^{-4} with 10 mm light-path Hellma cuvettes or 10^{-3} using the nanocuvette. This was tested by repeated measurement of the sample that was used for offset estimation before each measurement. Spectra were always recorded with a scanning speed of 200 nm/min with fast integration and spectral bandwidths of 1 nm in excitation and emission paths.

Excitation and emission spectra were taken via a fluorescence spectrometer (FP-6500; Jasco; Gross-Umstadt, Germany) at 293 K. For MR121 dimerization measurements, the data are uncorrected for instrumental wavelength dependencies, while the data for dimerization measurements of all other samples is corrected.

Experimental determination of QYss Due to preparation of the samples, the concentration of measured samples is usually not known before doing ensemble experiments. Therefore QYss was always determined by measuring absorption $OD(\lambda)$ and emission spectra $I(\lambda)$ and calculating QYss via eq. (71) using the same cuvettes and the same spectrometer settings.

$$QYss = \frac{I(\lambda_{max})}{OD_{max}} \tag{71}$$

Time Correlated Single Photon Counting The FluoTime 200 TCSPC setup by PicoQuant (Germany) used for lifetime and time dependent anisotropy measurements is shown in fig. 22. As excitation source a blue pulsed laser with 482 nm (LDH-P-C-485) and a red pulsed laser with 637 nm (LDH-P-C-640B) emission wavelength were used with repetition rates up to 80 MHz for the red laser and 40 MHz for the blue laser. Repetition rates were always adjusted such that the time period between pulses was about 5-10 times longer than the fluorescence lifetime of the probe. Therefore the fluorescence of the sample is decayed until the next pulse excites the sample. Lasers were always operated just above laser threshold to get a pulse length with Full Width at Half Maximum (FWHM) of 90 ps. Using neutral grey nonselective filters excitation intensities were adjusted that at maximum 0.1 % of detector

counting rate was registered compared to laser repetition rate. Fluorescence lifetime measurements were always done with polarizers (P) in magic angle configuration to exclude polarization effects.[64] Attention was paid to get no backscattered light in the light pathway.

For each anisotropy measurement

1. Intensity Response Function (IRF) and a lifetime measurement with polarizers in magic angle position were made,

2. then vertical-horizontal and vertical-vertical polarizer positions of excitation-emission polarizers were chosen for VH and VV measurements.

The lifetime and anisotropy data were fitted with deconvolution fit-functions eq. (72), eq. (73) to get lifetimes τ_i with amplitudes A_i of the fluorescence lifetime decays and the fundamental anistropy r_0 as well as the lifetime of the anisotropy decay θ. Dependent on the fluorophore and on wheter it is free or coupled, the number of fitted fluorescence decays n varies between one and three. We always started fitting with mono-exponential decays and decided with the aid of χ^2 and the residual distribution of the fitted function if further exponents are needed. It is possible to fit magic angle measurements of MR121 using picosecond pulsed lasers with a monoexponential fit, the TCSPC was always tested with MR121. Therefore it is a good standard to check the setup. Because the detection system has different sensitivities for vertically and horizontally polarized light, we fitted in anisotropy measurements also the G-factor to our data. For anisotropy fits the starting fit parameters τ_i were determined by magic angle lifetime measurements and comparison of anisotropy decays at decay times, e.g. for MR121 samples of this work at 8.4 ns, where there is surely no anisotropy effect any more.

$$I(t) = \int_{-\inf}^{t} IRF(t') \sum_{i=1}^{n} A_i e^{\frac{t-t'}{\tau_i}} dt' \tag{72}$$

$$\begin{aligned} I_{VV} &= G \int_{-\inf}^{t} IRF(t') \frac{1}{3} \sum_{i=1}^{n} A_i e^{\frac{t'-t}{\tau_i}} \left[1 + 2r_0 e^{\frac{t'-t}{\Phi}}\right] dt' \\ I_{VH} &= \int_{-\inf}^{t} IRF(t') \frac{1}{3} \sum_{i=1}^{n} A_i e^{\frac{t'-t}{\tau_i}} \left[1 - r_0 e^{\frac{t'-t}{\Phi}}\right] dt' \end{aligned} \tag{73}$$

The monochromator (M, ScienceTech Model 9030) of this FluoTime 200 has a grating $N_{gr} = 1200 mm^{-1}$ at a width of 32 mm and was always used with 0.5 mm slits providing 4 nm spectral bandwidth. With the second diffraction order $m = 1$, one gets a maximal time delay i.e. for an erythrosin B TCSPC measurement at 560 nm with an IRF taken

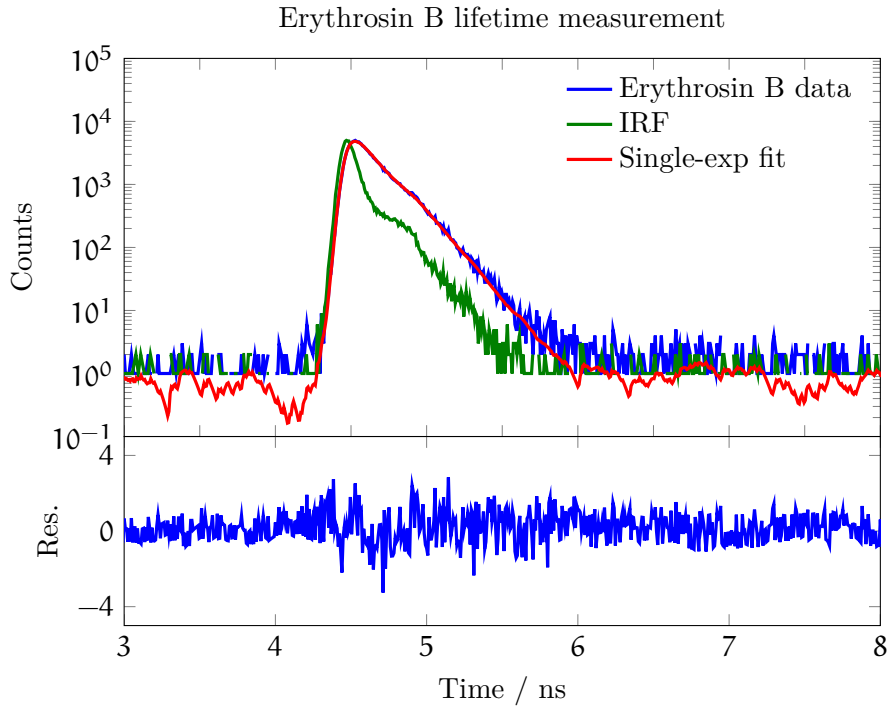

Figure 20: Top: IRF, measurement data and monoexponential reconvolution fit of Erythrosin B in degassed water. Bottom: Residuals of fit.

at 482 nm of $t_d = \frac{N m \lambda}{c} \approx 10ps$. Even if a shift between IRF and decay data was always fitted, systematic effects might effect the results. The fit shown in fig. 20 gives a lifetime of Erythrosin B $\tau_{ErythrosinB} = (89 \pm 1)ps$. With the systematic deviation due to t_d, this is in excellent agreement to Boens et al. [15].

3.2 FLUORESCENCE CORRELATION SPECTROSCOPY SETUP

The FCS setup used in this work (s. fig. 23) is a standard home-built setup.[4] Object slides are placed on a microscope (Axiovert 100; Zeiss, Germany) and are excited by a 637 nm continuos wave (cw) laser (CUBE; Coherent; Dieburg, Germany) with 200 µW power measured at the back aperture of the objective for quantification of diffusion and particle properties of the sample. When interested in conformational dynamics laser power was adjusted to 1 mW. Photobleaching of MR121 was not detectable at 200 µW.

This collimated laser beam was coupled into an oil-immersion objective (L_1, 63×, 1.4 NA; Zeiss; Germany) by a dichroic beam splitter (D, 645DLRP; Omega Optics, Brattleboro, VT, USA). The fluorescence signal was collected by the same objective, filtered by a band-pass filter (700DF75; Omega Optics; Brattleboro, VT, USA) and imaged via a cubic beam splitter onto the active area of two APDs (SPCM-AQR-14; EG&G, Canada) via multimode optical fibers (F_1, F_2) with a core

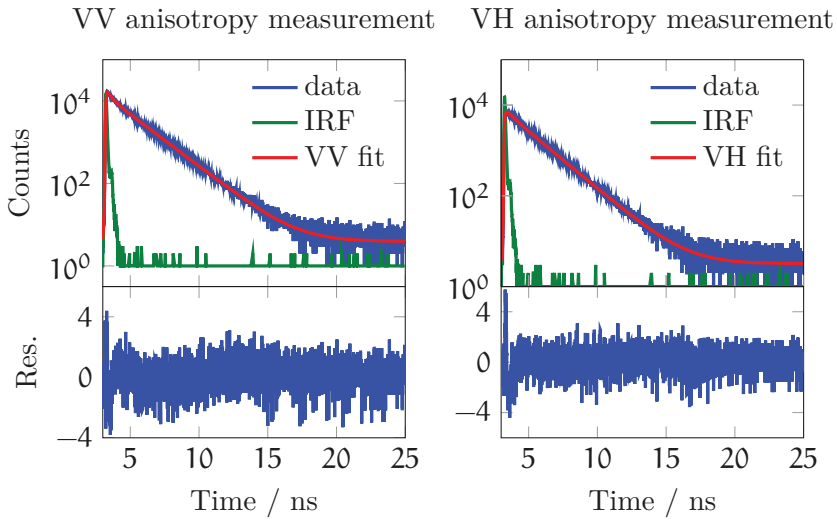

Figure 21: VV (left) and VH (right) anisotropy fluorescence lifetime data of MR121-$(GS)_5$K-MR121 with anisotropy fits using eq. (73). First, the fluorescence lifetimes τ_{fli} of the sample was determined via measurement and fitting of data in magical angle conditions. Then anisotropy fits according to eq. (73) with τ_{fli} as starting parameter yield fundamental anisotropy r_0 and anisotropy decay ϕ.

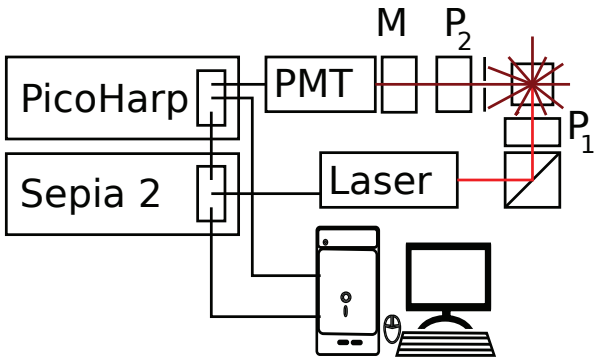

Figure 22: TCSPC setup consisting of P_1, P_2 polarizers, **M** monochromator, PMT and 480 nm or 640 nm pulsed lasers. For 4 ps precise timing a PicoHarp is used and a Sepia 2 can control up to eight pulsed lasers.

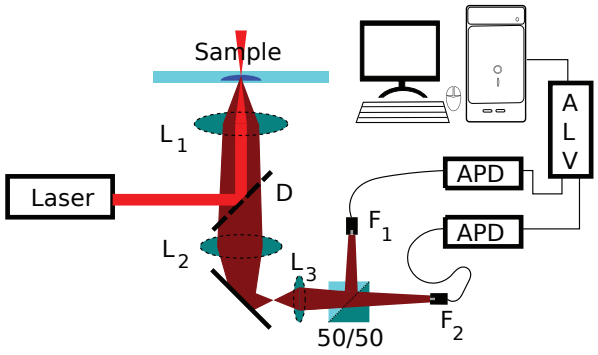

Figure 23: FCS setup. L_1-L_3 are lenses, D is a dichroic mirror, F_1 and F_2 are glass fibres and 50/50 means 50 % beam splitter.

diameter of 100 µm. The signals of the two APDs were recorded for 5 to 30 minutes using one of two signal processing modules.

1. The hardware correlator device (ALV-6010; ALV-GmbH; Langen, Germany) yields a maximum time resolution of 6.25 ns and its output is the correlated signal.

2. The standalone TCSPC module (PicoHarp 300; Picoquant GmbH; Berlin, Germany) yields a maximal time resolution of 4 ps. After each measurement the recorded time traces were correlated using SymphoTime Software (Picoquant GmbH; Berlin, Germany).

Cross-correlation circumvents dead time and afterpulsing effects.[37] A custom made objective-water-cooling device controlled temperature at 293 K, if not stated otherwise. All measurements were performed at nanomolar sample concentrations to circumvent intermolecular interactions and to decrease noise on correlation curves at small correlation times.

To calculate diffusional behaviour of molecules the following procedure was used. Diffusion constants are (compare eq. (21)) inverse proportional to the radius of particles. The known diffusion constant of ATTO655[24] $D_{298K}^{ATTO655} = 4.26 \cdot 10^{-6} \frac{cm^2}{s}$ in 298 K was used to determine via

$$\frac{D_x}{D_{298K}^{ATTO655}} = \frac{\tau_D^{298K}}{\tau_D^x} \tag{74}$$

and eq. (61) the diameter ω_{xy} of the focal volume at 200 µW with x being in this case 293 K. For measurements of diffusion constants the diameter of the focal volume was determined. The mean of 30 measurements with 200 µW at 293 K over 2 years is (860 ± 30) nm.

3.3 SAMPLE PREPARATION

PEPTIDES $(GS)_5K$ and $(GS)_5W$ were bought from IBA GmbH (Göttingen, Germany). Glycosylated peptides $(SGalG)_8W$ were synthesized by Lilly Nagel and Carolin Plattner in the organical chemistry 3 group of Prof. Norbert Sewald. This was done by solid-phase synthesis with glycosylated dipeptides as building blocks. Using HBTU and HOBt, dipeptides were prepared by coupling of Fmoc−Ser−OH and H−Gly−OtBu · HCl to get Fmoc-Ser-Gly-OtBu. The hydroxyl group in the side chain of the serine residue was then glycosylated with penta-O-acetyl-b-d-galactose. The peptide synthesis was accomplished by fragment condensation using Fmoc-Ser(b-Ac4Gal)-Gly-OH as building blocks and finally tryptophan.[BLSD11]

FLUOROPHORES Despite MR121 by courtesy of Prof. Dr. Drexhage (Siegen), all fluorophores in this work are commercially available and were purchased with NHS functional group.

ATTO488, ATTO 520, ATTO532, ATTO565, ATTO655 and ATTO647N were purchased from ATTO-Tec (Siegen, Germany). Cy3, Cy3B and Cy5 were purchased from GE-Healthcare (Freiburg, Germany). At arrival the fluorophore powder was dissolved in dimethylformamide (DMF) (puriss, Sigma-Aldrich, Germany) aliquoted in 0.1 mg portions and dried. The dry aliquots were stored at -253 K.

HIGH PRECISION LIQUID CHROMATOGRAPHY A Jasco-HPLC LC2000 (Gross-Umstadt, Germany, s. fig. 24) was used for sample preparation with linear gradients of H_2O/acetonitrile (ACN). In this configuration both solvents (LM A: H_2O, LM B: ACN) are pumped after passing the deaerator (DG-2080-53, D) with 1 ml/min. They are mixed by a high pressure dynamic mixer (MX-2080-32). The sample is injected by an autosampler (X-LC 3159 AS, AS) and separated by PFP- or C18-columns (Kinetex 2.6 µ, 100A, 150× 4.6 mm; Phenomenex; Aschaffenburg; Germany, C) tempered at 298 K. Samples are detected by a UV-Vis multiwavelength diode array detection (MD-2015, MWD) and by a fluorescence cell (X-LC FP3120, FD)

SAMPLE PREPARATION. Samples were modified via standard NHS coupling chemistry.[55] Therefore all peptide aliquots (0.1 mg) were dissolved in phosphate buffer (pH 7.7 at 298 K, 100 mM), fluorophore aliquots were dissolved in DMF (puriss, Sigma-Aldrich, Germany). Before starting the purification process via HPLC, mixtures of sample and fluorophore were filtered with sterile syringe filters.

Glycine-serine peptides with Trp. MR121-NHS solution was added in a 5:1 molar fluorophore:peptide ratio for labeling MR121 at the N-terminus of GS-peptides with Trp at the carboxyl end. A blanking sam-

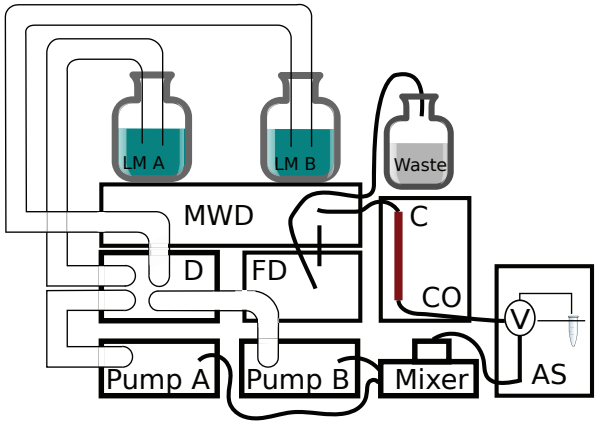

Figure 24: The HPLC setup consists of solvents A and B, deaerator D, pumps A and B, high pressure dynamic mixer, autosampler AS, column oven CO, columns C, a fluorescence detector FD and multiwavelength UV/Vis diode array absorption detector MWD.

ple containing about five times less MR121-NHS solution in the same amount of phosphate buffer was prepared at the same time. Mixtures containing $(SGalG)_8W$ were incubated over night, whereas $(GS)_xW$ samples were incubated several (>2) hours before purification.

Singly and doubly labeled glycine-serine peptides using one fluorophore. Preparation of $(GS)_5K$-MR121 was done analogue to the preparation of $(GS)_xW$ peptides using a 1:3 molar fluorophore:peptide ratio having an incubation time of several hours. Above all the ratio is important when dealing with ATTO647N-, MR121, ATTO565, and ATTO520. The more reactive fluorophore is in the incubating solution, the more the reaction tends to form $Fl{-}(GS)_5K{-}Fl$ samples. Cy-fluorophores do not form that much $Fl{-}(GS)_5K{-}Fl$ samples, therefore here a higher fluorophore:peptide ratio can be chosen for very short incubation times down to some minutes. $Fl{-}(GS)_5K{-}Fl$ samples were prepared with a 1:1 molar fluorophore:peptide ratio. For Cy-fluorophores a higher fluorophore:peptide ratio up to 5:1 with long incubation time of minimum one night was again used to get more doubly labeled peptides. It is possible to use dried $(GS)_5K$-MR121 sample that was used for $Fl_1{-}(GS)_5K{-}Fl_2$ production to dissolve it again in phosphate buffer with addition of reactive fluorophore solution to produce more $Fl{-}(GS)_5K{-}Fl$ sample.

Labeling glycine-serine peptides with two different fluorophores. To purify $Fl_1{-}(GS)_5K{-}Fl_2$ sample via HPLC, previously dried $(GS)_5K{-}Fl$ powder is dissolved in phosphate buffer. We used $(GS)_5K{-}Fl$ with the fluorophores Fl being Cy5 or ATTO532. This is due to a high yield of $(GS)_5K{-}Fl$ while getting low percentage of $Fl{-}(GS)_5K{-}Fl$ in a first purification step. The gain of $Fl_1{-}(GS)_5K{-}Fl_2$ in a second purification step depends on the combination of first fluorophore Fl_1 and secondary

Fl_2. Purification of $Fl_1{-}(GS)_5K{-}Fl_2$ with Cy3-NHS and Cy3B-NHS attached to $(GS)_5$K-Cy5 had to be repeated at least twice, the gain of Cy5-$(GS)_5$K-ATTO488 was that low, that several purification steps were needed. Therefore $(GS)_5$K-Cy5 sample could be reused. The exact ratio of fluorophore:$(GS)_5$K–Fl ratio is not given here, but because of the low gain of $Fl_1{-}(GS)_5K{-}Fl_2$ sample with ATTO532/ATTO647N, and ATTO532/ATTO565 high ratios up to about 10:1 were taken. Cy5/ATTO488 incubation achieved low $Fl_1{-}(GS)_5K{-}Fl_2$ concentrations. Because the PFP column of the HPLC seemed to be overloaded by less ATTO488-NHS concentration than with the other fluorophores yielding time shifts in sample retention times, ATTO488-NHS: $(GS)_5$K-Cy5 ratio was chosen lower than 1:1 ratio. Attachment of Cy3B and Cy3 for Cy5/Cy3, Cy5/Cy3B samples yielded good $Fl_1{-}(GS)_5K{-}Fl_2$ gains.

In fig. 25 absorption chromatograms of the purification of $Fl{-}(GS)_5K{-}Fl$ samples are shown. Because we used high fluorophore content, attention was given on segregation of $Fl_1{-}(GS)_5K{-}Fl_2$, $(GS)_5$K–Fl sample and free fluorophore. Picking the peaks indicated by the arrows in fig. 25(A-E), purity of samples is over 99%.

The samples were dried using a vacuum centrifuge (SPD111V, Thermo Electron LED GmbH, Langenseibold, Germany). First experiments were done the same or next day. To get statistical evidence fresh purified samples were used for a week for every sample to do all the ensemble measurements. For every series of measurements solutions were prepared by diluting a millimolar solution of the sample in GdCl or phosphate buffer.

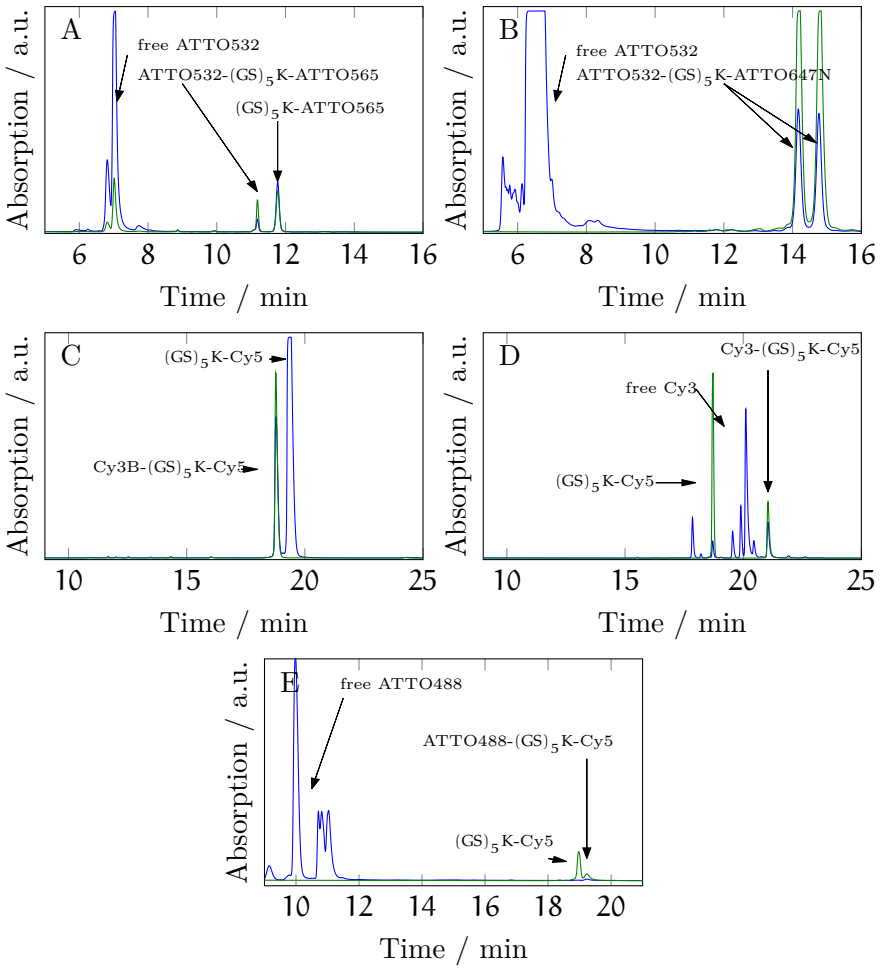

Figure 25: Absorption chromatograms of $Fl_1-(GS)_5K-Fl_2$ samples with A: ATTO532/ATTO565 (blue: 530 nm, green: 565 nm), B: ATTO532/ATTO647N (blue: 530 nm, green: 670 nm) 650 nm), E: Cy3B/Cy5 (blue: 550 nm, green: 650 nm), D: Cy3/Cy5 (blue: 550 nm, green: 650 nm), and E: ATTO488/Cy5 (blue: 485 nm, green.

4

REVEALING KINETICS OF OLIGOPEPTIDES USING FCS

Confocal Fluorescence Correlation Spectroscopy in solution is a powerful technique requiring only low sample concentrations to reveal kinetic information and information regarding interactions of molecules and solvent of fluorescing solutes.

Hydrodynamic radii of molecules describe their mean expansion in a solvent. These hydrodynamic radii vary due to inherent properties of the molecules like different masses and due to interactions with different solvents. The definition of denaturants is that they disrupt molecular conformations[3] yielding high hydrodynamic radii compared to water as solute. Molecules differing about 10 % in hydrodynamic radii can be easily distinguished from each other via measurements in about ten minutes.

While structural information is applicable by FCS, it is outstanding to get kinetic information of molecule inherent kinetics and of binding reactions of fluorescent molecules. There are several groups using quenching of dyes for measuring binding reactions of biomolecules.[18, 45, 86, 107, 124] Here we investigate intramolecular structural dynamics of oligopeptides.

In sec. 5 and sec. 6 the oxazine dye MR121 is first used as a reporter for end to end contact formation of non- and glycosylated GS-peptides. Then we establish a new reporter system consisting of two MR121 dyes to report end to end contact formation of GS-oligopeptides. Therefore this chapter gives the explanations for the experimental parameters we chose for FCS measurements using MR121 as fluorophore.

QUENCHING OF ORGANIC DYES REVEALS END-TO-END CONTACT FORMATION IN FCS Correlation curves of $(GS)_5$K-MR121 consist of a diffusional decay at 1 ms and a flat part between 100 µs and 6 ns. The value of the last one gives the inverse particle number. Shapes of correlation curves of MR121-$(GS)_5$K-MR121 are besides an exponential part of the curve at 10 ns like $(GS)_5$K-MR121 correlation curves.

DIFFUSION PROPERTIES OF GS OLIGOPEPTIDES ARE TESTED WITH LOW LASER POWER. When evaluating FCS curves, eq. (59) is fitted to the measurement data. An assumption made in sec. 2.5 relating to the setup for the derivation of eq. (59) was that the excitation profile is a Gauss profile. Power dependent measurements of MR121 done in Phosphate Buffered Saline with 0.05 % Tween (PBSt) at 293 K reveal power dependence of translational diffusion time (s. fig. 27).

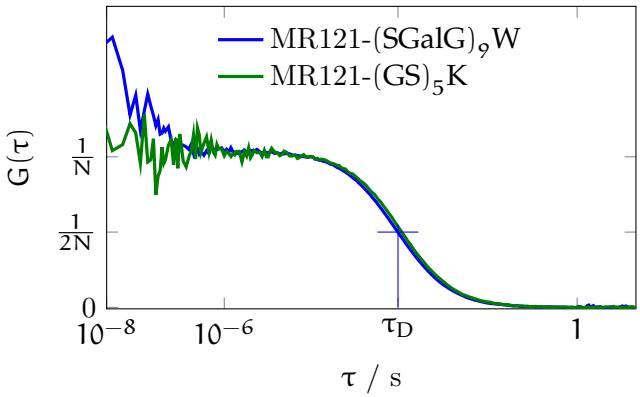

Figure 26: FCS curves of MR121-$(SGalG)_9W$ (blue) and MR121-$(GS)_5K$ (green) . Fluctuations of the detector signals have different causes: diffusion of fluorescent molecules in and out of the detection volume with a characteristic mean diffusion time τ_D being between 0.4 and 2 ms in the studies of this work. Fluctuations of the fluorescence signal can be caused by transition of the fluorescent molecule into its triplet state (here: $\approx 1\mu s$). From 10 ns to 100 ns an exponential decay is seen here in the correlation of MR121-$(SGalG)_9W$ not existent in the control MR121-$(GS)_5K$. This is due to the interaction between MR121 and Trp due to fluorescence fluctuations caused by quenching of MR121 by Trp.

For the fits in the 0 mW to 0.2 mW range the two dimensional correlation function $G_{diffusion}$ of eq. (58) is sufficient. With higher power at $\tau_T = (3 \pm 1.6)\mu s$ an exponential term can be fitted to the data yielding amplitudes lower than 0.05. In fig. 27 it can be seen, that diffusion measurements are stable for measurements with ł0.2 mW. Higher excitation power increases usually the excitation profile and therefore the diffusion time of dyes should be proportional to excitation power. But fig. 27 shows inversely proportional behavior. An explanation is possible photobleaching of fluorophores. Therefore measurements focusing on diffusional properties of samples are always done with $200\mu W$ in sec. 5 or $100\mu W$ in sec. 6.

STATISTICAL CONSIDERATIONS The background signal detected on our setup with 200 µW excitation power is about 1 kHz. This noise consists of detector shot noise of about 100 Hz and scattered or reflected laser light. To get FCS curves with low background regarding shot noise high sample concentrations are preferable. Contrarily, the amplitude of the correlation itself scales with 1/N. So the data to fit has a smaller amplitude at small concentrations where the laser light represents a noise contribution on the FCS curve.[60] On the setup used for this work the best particle number with MR121 samples is 10 and we did all measurements with 5-20 particles in the focal volume.

END-TO-END KINETICS ARE TESTED USING MW-LASER POWER When the rotational diffusion time of fluorescing species

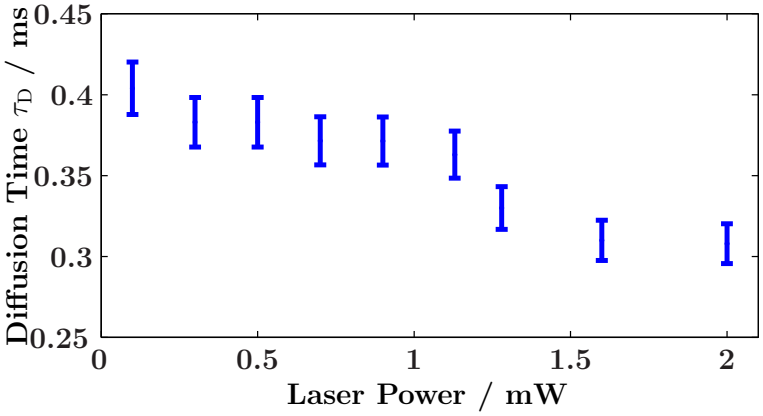

Figure 27: Dependence of FCS diffusion time τ_D on power of excitation light measured at the objective back aperture. Errorbars indicate the relative standard deviation of 4 % that was tested by several series of measurements.

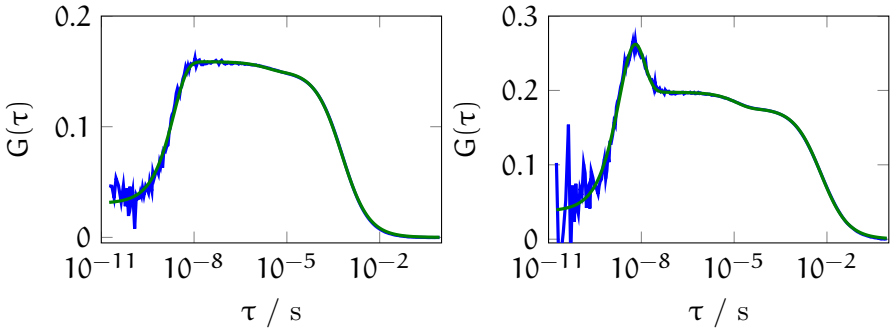

Figure 28: Fluorescence correlation curves of singly labeled GS-peptide at 293 K in 0 % and 52 % sucrose concentration at a pH 7.4.

in solution gets larger than the fluorescence lifetime, that is responsible for the antibunching term, then fluorescence fluctuations due to rotation of the excitation dipole are detected. The dipole axis of the fluorescent molecule then rotates into or out of the polarization plane of the detector.[66] This gives a new exponential term on the correlation function eq. (59). On our setup this effect can clearly be seen. In fig. 28 FCS curves of the same singly labeled peptide in 0 % and 53 % at 293 K with 1 mW laser power sucrose yielding viscosities of 0.9 mPas and 20.9 mPas respectively are shown.

5 DYNAMICS OF GLYCOPEPTIDES

Modifications of GS-peptides by glycosylation induce changes in their dynamic behaviour. There is also much research on glycosylated biomolecules. Available data are limited. This makes it difficult to generalize the relation between the type of glycosylation and the structural properties of glycoproteins.[97] So here we look into conformational dynamics of glycosilated peptides.

While N-glycosylated samples are thoroughly studied right now, O-glycosylation is not investigated that often. This is, because N-linked glycosylation is the most common type of glycosidic bond.[8, 97] However, O-linked glycans are typically found in proline, threonine, and serine-rich regions of membrane proteins[75]. An example is given by antifreeze glycoproteins, in which glycans are coupled to the protein via O-glycosidic bonds. These antifreeze proteins and peptides protect fish in the polar seas from death by damage of cells due to ice crystals. They might be applied to store food, organic tissues, or organs at low temperatures.[16, 47, 113]

5.1 SAMPLE CHARACTERIZATION

We investigated GS-peptides with and without O-glycosylation of serines. After labeling of the non- and glycosylated samples by NHS linker chemistry with MR121 and purification with HPLC, concentrated stocks were made to reduce possible oxidation processes of Trp induced by the attached dye[76] for expanding measurement time of these samples.

First QYss and QYdyn are studied to validate the dynamic and static quenching behaviour of the glycosylated peptides. On the one hand these measurements should verify FCS measurements on peptide kinetics and on the other hand they should give first insights into the dynamics of the oligopeptides.

The following two control experiments were designed to compare our data with already published data and to reveal molecular properties in this study. The free dye MR121 was measured in solution in ensemble and later FCS measurements to get information about setup stability. Singly labeled GS-peptides without the quencher Trp were measured to exclude quenching of the dye due to interactions with the oligopeptide itself. Further investigations via FCS were accomplished to get more details about the diffusional dynamics of the peptides. Fluorescence anisotropy measurements were done to test for dye-glycan or dye-backbone interactions.

Sample	QYss = $\frac{I}{I_0}$	QYdyn = $\frac{\tau}{\tau_0}$	QYst = $\frac{1}{1+K}$	QYst
	%	%	%	%
MR121	91 ± 1	93 ± 1	1	91 ± 1
$(GS)_8W$	44 ± 5	88.5 ± 1	50 ± 3	50 ± 5
$(SGalG)_8W$	59 ± 4	96 ± 1	62 ± 1	61 ± 1

Table 1: QYss, QYdyn and QYst of MR121 itself, glycosylated and non-glycosylated peptides divided by the quantum yield of MR121 labeled GS peptide without quencher. All samples show low dynamic quenching. Comparison of the two distinct measures of QYst show equal values.[BBP+11]

QYss are always measured in comparison to free dye samples by cuvette measurements. For comparison the same cuvette and the same spectrometer settings were used to record fluorescence spectra. QYss (eq. (71)) of free dye MR121, MR121-$(GS)_8W$, and MR121-$(SGalG)_8W$ are shown in tab. 1. All quantum yields are normalized by the respective measured quantum yield of singly labeled GS_5K. The labeling process itself often induces fluorescence enhancement, as it does in this case. The QYss values of $(GS)_8W$ and $(SGalG)_8W$ are lower compared to free dye by a factor of two, while the QYss of $(GS)_8W$ is significantly lower than the QYss of $(SGalG)_8W$. Therefore the glycosylated peptide is altogether brighter than the non-glycosylated.

The comparison of QYss to QYdyn yields no difference between those values for MR121. MR121-$(GS)_8W$ and MR121-$(SGalG)_8W$ are both stronger quenched due to static quenching than dynamic quenching. These oligopeptides differ in QYst and QYdyn. While QYst of MR121-$(SGalG)_8W$ is lower than the QYst value of MR121-$(GS)_8W$, QYdyn is higher for MR121-$(SGalG)_8W$ compared to MR121-$(GS)_8W$. This is a hint for less contacts of quencher and dye of MR121-$(SGalG)_8W$. The QYst reflects either dye quencher interactions or changes in conformational dynamics.

FCS measurements can reveal more detailed insights into dynamic and static interactions in comparison to the ensemble spectrometer results. For GS polypeptides it was shown [28, 76] that peptides with a chain length of more than 10 AAs can be estimated as Gaussian chains (compare sec. 2.6.1). It was concluded that contact kinetics measured via PET-FCS are diffusion controlled. To test the behaviour of glycosylated peptides, measurements of non- and glycosylated peptides with FCS were performed.

The diffusional behaviour of glycosylated peptides was determined as described in sec. 3.2 using eq. (74). Correlation curves of MR121-$(GS)_8W$ and a singly labeled GS-peptide control sample are shown in fig. 26 measured in Phosphate Buffered Saline (PBS) at 293 K. The diffusion time τ_D is given by the correlation time, where the correlation G drops to the half of the amplitude that gives the inverse mean particle number.

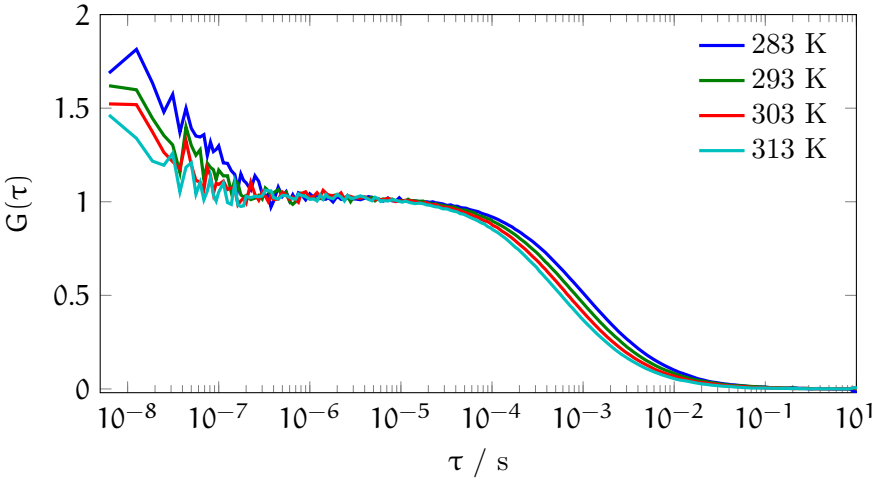

Figure 29: FCS data of MR121-$(SGalG)_8W$ measured at temperatures of 283 K, 293 K, 303 K, and 313 K. The curves are plotted after normalization to the same particle number and computational elimination of triplet effects.[BBP+11]

Measurements at 293 K with 200 µW laser intensity, where the excitation profile of FCS is approximately Gaussian shaped[1], yield significantly different diffusion constants of $D_{MR121-(GS)_8W} = (262 \pm 8)\ \frac{\mu m^2}{s}$ for MR121-$(GS)_8W$ and $D_{MR121-(SGalG)_8W} = (221 \pm 8)\ \frac{\mu m^2}{s}$ for MR121-$(SGalG)_8W$. Due to the Stokes-Einstein equation eq. (21) this is a hint for an expanded conformation of the glycosylated sample compared to the non-glycosylated.

Correlation curves of MR121-$(GS)_8W$ show exponential decays in the range of milli- to nanoseconds (fig. 26 and fig. 29). As explained before, conformation dynamics are represented by nanosecond decays for GS-peptides. Correlation curves taken at 1 mW laser power were fitted via eq. (60) and yield K and τ_K. The static quantum yields QYst of the peptides that fluoresce in the detection volume[2] eq. (65) are equal to the quantum yields measured in ensemble experiments (compare tab. 1). This indicates that the loss of brightness is due to the quenching interactions measured with FCS and other interactions can be neglected.

Changes of solvent environment reveal the underlying processes for contact formation of oligopeptide ends. These measurements can be biased if the reporter system severely changes the energy landscape of contact formation. These changes are negligible in this chapter. Therefore I go ahead with temperature and viscosity dependent measurements.

In fig. 30 viscosity corrected temperature dependence of diffusion constants of glycosylated and non-glycosylated samples are shown. A linear fit of the data gives a gradient of $m_{glyco} = 4.9 \cdot 10^{-16}\,\frac{N}{m^2} \pm 2\%$

1 This is not perfectly right.[SBND13] But in the accuracy needed here the approximation is fine. Compare also sec. 4

2 This is emphasized due to the results of sec. 6

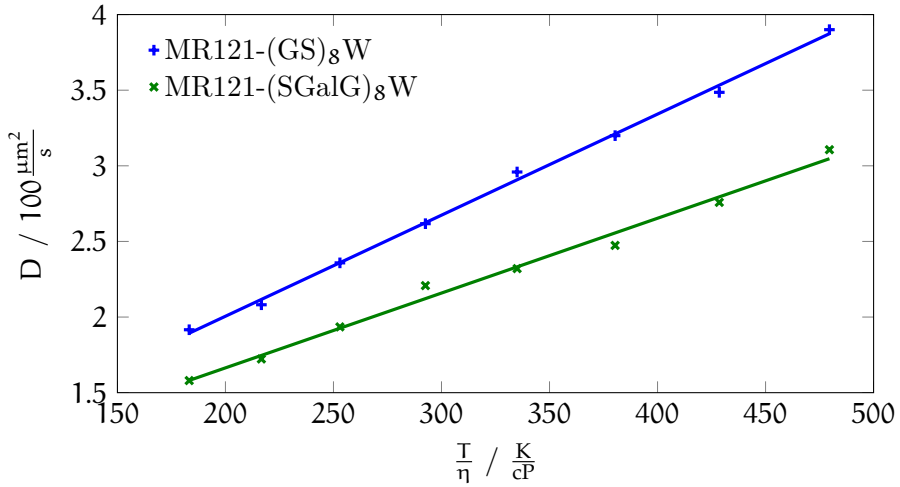

Figure 30: Temperature dependent diffusion constants D of MR121-(SGalG)$_8$W (x) and MR121-(GS)$_8$W (+).[BBP+11] Linear fits indicate Stokes-Einstein eq. (21) behaviour of D. The fits reveal a slope of $6.7 \cdot 10^{-16} \frac{Kg}{K \cdot s}$ ($4.9 \cdot 10^{-16} \frac{Kg}{K \cdot s}$) and y-intercept of 67 $\frac{\mu m^2}{s}$ (67 $\frac{\mu m^2}{s}$) for MR121-(GS)$_8$W (MR121-(SGalG)$_8$W).

($m_{non-glyco} = 6.7 \cdot 10^{-16} \frac{N}{m^2} \pm 2\%$) for the glycosylated (non-glycosylated) peptides indicating diffusion following the Stokes-Einstein equation eq. (21). Evaluation yields hydrodynamic radii of $R_{non-glyco}$ =(1.10 ± 0.02) nm for the non-glycosylated and R_{glyco} = (1.40 ± 0.03) nm for the glycosylated polypeptide with a ratio of $\frac{R_{non-glyco}}{R_{glyco}} = 0.74 \pm 0.03$. Because of this we suggest that glycosylated peptides have a significant larger conformation and diffuse slower in phosphate buffer than the non glycosylated.

The amplitudes K and relaxation times τ_K on the nanosecond timescale are assumed to be described by a two state process (compare sec. 2.6.4). They give (eq. (64)), opening k_o and closing k_c rates of the peptides. The contact (opening) rates of MR121-(GS)$_8$W are $k_c^{non-glyco} = (2.3 \pm 0.2) \cdot 10^7 s^{-1}$ ($k_o^{non-glyco} = (2.3 \pm 0.2) \cdot 10^7 s^{-1}$) compared to $k_c^{glyco} = (0.8 \pm 0.1) \cdot 10^6 s^{-1}$ ($k_o^{glyco} = (1.2 s^{-1} \pm 0.1) \cdot 10^7 s^{-1}$) for MR121-(SGalG)$_8$W. The contact rates slow down fourfold during glycosylation of GS-peptides. Opening rates behave in a similar way, but the rates decrease by a factor of two.

To study enthalpic contributions of the differences in folding dynamics regarding eq. (70), temperature dependent FCS data was also analyzed. In fig. 31 opening and closing rates of glycosylated and non-glycosylated peptides are shown. To compare results with published data[76] rates of non-glycosylated peptides were measured parallel to glycosylated sample. These results are shown in fig. 31. With increasing temperature all rates increase. According to eq. (70) the natural logarithm of the rates are plotted in fig. 31 versus the inverse temperature. Linear fits were made to extract activation enthalpies. The slope

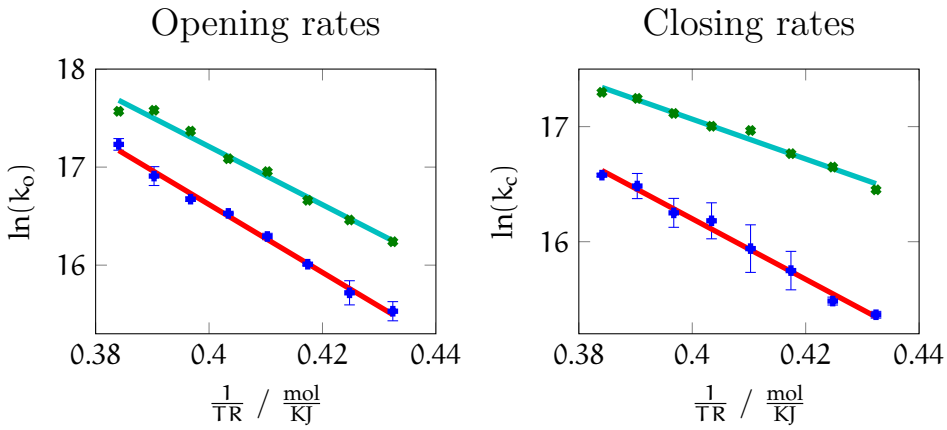

Figure 31: Logarithmic plot of opening (left) and closing (right) rates of glycosylated (blue) and non-glycosylated (green) GS-peptides. Linear fits to these datasets yield slopes of -34.6 kJ/mol, -35.8 kJ/mol for opening rates and -27.5 kJ/mol, -17.3 kJ/mol for closing rates of glycosylated, non-glycosylated peptides, respectively. Measurement errors are extracted from two distinct measurements. [BBP+11]

Sample	r_0^{PBS}	θ^{PBS} / ns	r_0^{GdCl}	θ^{GdCl} / ns
$(SGalG)_8W$	0.25 ± 0.01	0.61 ± 0.03	0.22 ± 0.01	1.33± 0.05
$(GS)_8W$	0.25 ± 0.01	0.35 ± 0.02	0.21 ± 0.01	0.92± 0.04

Table 2: Results of anisotropy decay fits. Fundamental anisotropy r_0 and anisotropy decay time θ are given for glycosylated MR121-$(SGalG)_8W$ and non-glycosylated MR121-$(GS)_8W$ samples in PBS and GdCl solvent, respectively.

of the data yields activation enthalpy for opening and closing rates that consist of enthalpy contributions by solvent solute interactions, interactions of Trp/MR121, and by intrachain interactions. Enthalpy barriers for opening of the polypeptide are for both samples significantly higher than the enthalpy barrier of the phosphate buffer solvent of $H^*_{aq} \approx 17 \frac{kJ}{mol}$. The closing enthalpy energy barriers for the glycosylated sample is also with $27 \frac{kJ}{mol}$ about 1.7 times higher than H^*_{aq}, whereas the non-glycosylated sample has in accordance to Neuweiler et al. [76] $H^*_{non-glyco} \approx H^*_{aq}$. There are several possible reasons for this enthalpy change.

To deduce possible interaction between dye and sugar residues slowing down conformational changes, time dependent anisotropy measurements were done. Therefore micromolar solutions of MR121-$(GS)_8W$, MR121-$(SGalG)_8W$, and MR121 were measured in PBS and 7.7 M GdCl at (294 ± 1) K. The fundamental anisotropy $r_0 = r(t = 0)$ and the steady state anisotropy θ (s. sec. 2.1.2.2) of the oligopeptides are listed in tab. 2. The IRF and sample measurements were taken in GdCl and PBS using excitation at 637 nm with 20 MHz pulse repetition rate yielding a 50 ns time windows for fluorescence decay. The measure-

Sample	τ^{PBS} / ns	τ^{GdCl} / ns
MR121	1.85 ± 0.01	2.33 ± 0.01
MR121-$(GS)_8W$	1.77 ± 0.01	2.35 ± 0.03
MR121-$(SGalG)_8W$	2.38 ± 0.01	2.38 ± 0.01

Table 3: Fluorescent lifetimes τ of MR121, non-, and glycosylated peptides measured in magic angle conditions at room temperature.

ments in magic angle conditions in PBS and GdCl gave fluorescence lifetimes shown in tab. 3. The measurements in PBS reflect the changes in QYdyn already shown in tab. 1. In GdCl all fluorescence lifetimes increase with unchanged order compared to PBS. For anisotropy measurements lifetimes were fitted biexponentially with one rotational time using eq. (73). Data of MR121-$(GS)_8W$ are mean values of MR121-$(GS)_7W$ and MR121-$(GS)_9W$. Measurement uncertainties given in tab. 2 are due to fit uncertainties when varying initial values of fits and are due to averaging of MR121-$(GS)_7W$ and MR121-$(GS)_9W$ data.

Comparison of results for both samples shows no difference in the fundamental anisotropy for each solvent. Factors of anisotropy decays of glycosylated/non-glycosylated samples are 1.7 ± 0.2 in PBS and 1.44 ± 0.14 in GdCl. So the glycosylated sample has in both solvents an about 1.5fold higher anisotropy.

Assuming no interactions between dye and sugar residues, viscosity related studies were made to differentiate viscosity related mechanisms like internal and solution based slow down contact formation by glycosylation. As solvent, mixtures of water/sucrose with w/v ratios between 0% and 50% were used. As mentioned in sec. 4, in high sucrose concentration two fast correlation decays had to be used for fitting. The new fast decay is due to polarization anisotropy.

Focusing on the kinetic part of the FCS curves in sucrose, the viscosity dependence of glycosylated peptides for 293 K and 313 K is plotted in fig. 32 (left) up to 10 cP viscosity. Like in Neuweiler et al. [76] for non-glycosylated GS peptides already shown, the closing rates show here a linear relationship. Linear fits in this range indicate because of linear behaviour and zero intercepts diffusion limited contact rates. Variation of the fit limits yields fit uncertainties for y-intercepts of about 5×10^{-8} s. So the values for y-intercepts of $\tau_{c,o}^{293K} = k_{c,o}^{293K\,-1} = -3.6 \cdot 10^{-8}$s ($\tau_{c,o}^{313K} = -3.7 \cdot 10^{-8}$s) for the closing times and $\tau_{o,o}^{293K} = k_{o,o}^{293K\,-1} = 2.3 \cdot 10^{-8}$s ($\tau_{o,o}^{313K} = 0.8 \cdot 10^{-8}$s) for the opening times show that the accuracy of this series of measurements the y-intercept is zero. Therefore the linear behaviour shows hints for diffusion limited behaviour.

In addition to the results by Neuweiler et al. [76] we see not only a linear behaviour of the glycosylated polypeptide. In the range of 0 cP to 5 cP the inverse rates show linear behaviour, but the higher the

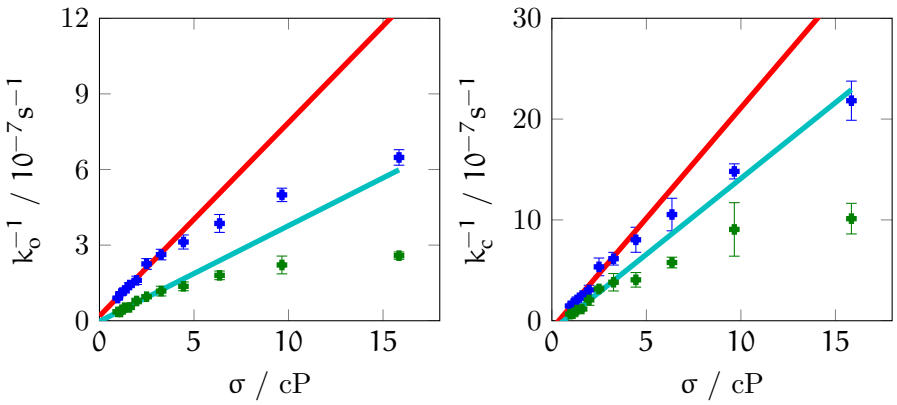

Figure 32: Dependence of inverse opening (left) and closing (right) rates of glycosylated GS-peptides at 293 K (blue) and 313 K (green) on solvent viscosity. Viscosity was controlled by changing sucrose concentration in the solvent.[BBP+11]

viscosity enhancement by more sucrose concentration is, the less linear behaviour is seen by us. We have recently investigated this and saw that this behaviour is related to the molecular reporter system.[SBND13]

5.2 DISCUSSION

Glycosylated GS-peptides can be compared to previously characterized GS-peptides[14, 61, 74, 76], They also show end-to-end conformational dynamics on the 10 ns-timescale. The organic fluorophore MR121 and the amino-acid Trp show PET induced quenching interactions[110]. The quenching process is contact induced quenching by complex formation of MR121 and Trp. The nature of the quenching interaction is the same for glycosylated and non-glycosylated dyes. Therefore the change of the energy landscape governing the relaxation time of end-to-end contact formation is negligible.

Like in Doose et al. [28, 29] the following conclusions on the energy surface of the end-to-end contact formation of the glycosylated polypeptide itself can be made[14, 76].

Fast correlation decays which are not due to polarization or triplet effects are well described as a single exponential decay. Zhu et al. [125] found no significant heterogeneity of quenching of ATTO655, a dye similar to MR121, by Trp. They state that angle dependencies of contact formation of ATTO655 and Trp are negligible for quenching interaction. This backs Doose et al. [28], who states that quenching occurs contact induced at subnanometer distance being applicable to study conformational dynamics of polypeptides. However, it is still possible to have a combination of different conformational changes happening on the same time scale that cannot be differentiated by fitting procedures.[48] Our data shows clearly, that end-to-end contacts are in our precision a

two state process. And because MR121 attached to a GS-polypeptide without Trp is not quenched, only interactions between MR121 and Trp are responsible for this quenching.

The opening rates k_o as determined for the various peptides are for MR121/Trp always larger than closing-rates k_c. When determining the equilibrium constant $K_{eq} = 61 M^{-1}$, Doose et al. [28] had to use in their study a model that considered not only differentiation between static and dynamic quenching. They also needed a term to compensate for a quenching sphere of action[64]. This means that in a range of distances up to 1.9 nm quencher and dye are interacting. This is a process that influences especially $k_o = \frac{1}{\tau_o}$ giving the mean time that complexes exist plus the mean time the fluorophore needs to diffuse out of the sphere of action. In sec. 6 we will see, that a change of end-to-end contact reporter system from MR121/Trp to MR121/MR121 can be, regarding rates, foremost seen in k_o. These interpretations are supported by Arrhenius analysis of non-glycosylated GS-samples having a activation enthalpy of $\Delta H^*_{o,(GS)8W} = 35.8 \frac{kJ}{mol}$. This energy barrier is significantly higher than the characteristic energy of viscid forces in water[6, 76]. Therefore the value for glycosylated GS-peptides of $\Delta H^*_{o,(SGalG)8W} = 34.6 \frac{kJ}{mol}$ can also only report on interactions between dye and Trp, that show similar values.

The closing rates k_c measured with the MR121/Trp reporter system are however diffusion limited with a small change of the energy landscape[28, 76] of the free oligopeptide. This is again shown by $\Delta H^*_{c,(GS)8W} = 17.3 \frac{kJ}{mol}$ being the value of the energy barrier for end-to-end contact formation of Gaussian chains in water. Glycosylated samples show a different behaviour with higher activation enthalpies for contact formation of $\Delta H^*_{c,(SGalG)8W} = 27.5 \frac{kJ}{mol}$. The Arrhenius behaviour of eq. (70) yields $\Delta k_c \propto \exp(-\frac{\Delta H^* \cdot N_A}{k_B T})$. The change in activation enthalpy would induce a 30fold decrease of k_c from non- to glycosylated probe. Comparing the measured values of k_c directly, here the measured difference in contact rates of non- and glycosylated samples at 293 K in aqueous solution is only fourfold. Following eq. (70), k_c is a product of a temperature dependent exponential part with the activation enthalpy in its exponent, a temperature independent part dependent on entropy effects, and a factor being inversely proportional to viscosity.

Interactions between dye and sugar residues are negligible in this case, because a comparison of anisotropy decays of glycosylated and non-glycosylated probes in PBS and phosphate buffer with high denaturing salt concentrations shows no significant difference in fundamental anisotropy of non- and glycosylated sample.[49] Therefore dyes linked to glycosylated GS-peptides are rotating as free as dyes linked to non-glycosylated GS-peptides of this study.

Viscosity dependent measurements indicate that attractive intramolecular interactions between glycans are not the reason for slow down of

peptide dynamics. Than interactions of these peptide compartements with solvent sugar residues and water molecules would be expected. But we do not see a viscosity dependent offset in our measurements up to 5 cP viscosity that is an indicator for internal friction.[50] For higher viscosities that we produced by high sucrose concentrations a deviation towards a linear behaviour of contact rates versus viscosity was observed. To elucidate the reasons therefore work is in progress. On the one hand we have a look on the fitting procedure of our FCS data.[SBND13] We see that for complicated correlation data with additional decays due to polarization other algorithms like fingerprint[77] reveal better estimates for relaxations times τ_D.[SBND13] However, at the moment this technique is not able to reveal opening k_o and closing rates k_c. Studies of the ability of several non-glycosylated proteins in the presence of high concentrations of saccharide such as glycerol, glucose, galactose , α,α-trehalose[23], and sucrose have shown that these glycans stabilize folded proteins.[102] Even if we have chosen sucrose as co-solute, because of its low chemical reactivity, there might be other interactions that cannot be described only by enhanced or decreased viscosity. Therefore, referring to the data in low concentrated sucrose, interactions between glycans and peptide backbone or steric effects are left as possible reasons for for the slow down of the peptide dynamics for the glycine-serine oligopeptides by glycosylation.

It is well known that chain thickness imposes stringent restrictions on conformational space[2]. Banavar et al. [12] invented a description of biomolecules, where three protein units in a row as a larger compartment with defined radius. In this model they varied the thickness of N-unit chains and also varied the interacting number of different constituents of the chain. They got directly secondary structures of proteins as favorable structures, showing that thickness of amino-acid chains can explain steric repulsion. In this model attached glycans thicken GS-peptides. The temperature dependent change of end-to-end contact rates of glycosylated peptides indicating a much higher difference that we see by direct comparison of contact rates can be explained by this fact. The glycans give steric constraints limiting the space the backbone of the GS-peptide has for changing its structure. However, this may have a slowing down or speeding up contribution to peptide dynamics.

Activation enthalpy of glycosylated peptides are increased compared to non-glycosylated samples, because additional motion of glycans about their linker to the peptide backbone is possible. We interpret the ratio of hydrodynamic radii of glycosylated and non-glycosylated GS-peptides of 0.74 at 293 K with the conclusions drawn by Szabo-Szabo-Schulten theory (s. sec. 2.6.1): A Gaussian chain with excluded volume by its constituents has a rate constant that is proportional to $R_h^{1/3}$. Here we expect therefore for glycosylation of the GS-peptide a slow down of rate constants only by a factor of 2.5. The direct compari-

son of rate constants of FCS data fits at 293 K gives a fourfold decrease of rate constants. Therefore there has to be some compensation of the enthalpic barrier of the contact formation of the GS oligopeptides.

The analysis of serine-glycine glycopeptides in comparison to non-glycosylated serine-glycine and glycine-serine peptides shows enthalpic and entropic contributions of glycosylation. This study was compared to proteins on two easy model systems giving new experimental results in detail to elucidate the general question, how glycosylation changes the energy landscape of proteins for the glycosylation of serine-glycine peptides at every serine residue.

6

PEPTIDE DYNAMICS MONITORED BY DIMERIZATION

In this chapter dimerization of the oxazine dye MR121 is used to characterize end-to-end dynamics of GS-oligopeptides. In the chapter sec. 5 we have seen, that PET is an interaction that can be used to monitor conformational dynamics of non- and glycosylated GS-oligopeptides. Generally, reporter systems for determination of end-to-end contact kinetics of biomolecules must be tailored to the molecule of interest. MR121 and Trp are an excellent reporter system for reporting end-to-end contacts of GS polypeptides with 2 to 15 GS-building blocks.[76]

The relaxation time τ_K for end-to-end contact kinetics of $(GS)_5W$ are in the range of 10 ns. This range is well separated from triplet and anti-bunching times of MR121 in PBS. So extraction of FCS intramolecular kinetic data becomes possible.[SBND13]

The correlation function eq. (60) gives reliable results of end-to-end kinetics if the ratio K of the time a particle is in a fluorescent state to the time it is non-fluorescent, is high enough, so that the exponential describing kinetics is distinguishable from statistical noise of the measured correlation function. For MR121-$(GS)_5W$ this is the case (compare sec. 5). The accuracy of fitting parameters for long polypeptide chains are relatively low, because amplitudes of the exponential decay on the correlation curve decrease. Similarly, in high denaturant solutions amplitudes of FCS measurements also decrease, too. Therefore there might be other reporter systems having properties fitting better in these circumstances to measure end-to-end contact formation.

MR121 is known to form non-fluorescing dimer complexes upon contact.[68] It is shown in this chapter, that MR121 dimerization can be used for end-to-end contact measurements in denaturant conditions. In PBS the dimerization of MR121 at the ends of $(GS)_5K$ is so strong that in 1 ms only 10 % of the sample fluoresces. This may have applications in super-resolution imaging.

6.1 RESULTS

Singly labeled GS-peptides ($(GS)_5$K-MR121; D = MR121 here) and doubly (MR121-$(GS)_5$K-MR121) labeled GS-peptides are purified as described in sec. 3.3. $(GS)_5$K-MR121 is used as control sample with non-quenched fluorescence emission.

Comparing QYss of the probes in tab. 4 to QYss of the free dye MR121 shows enhanced fluorescence of $(GS)_5$K-MR121, whereas MR121-$(GS)_5$K-MR121 is strongly quenched. MR121-$(GS)_5$K-MR121

Sample	QY_{ss}	D	B	$\frac{N}{c}$	$\frac{\tau}{\tau_0}$
	%	$10^{-6}\frac{cm^2}{s}$	kHz		%
MR121	90 ± 10	4.3 ± 0.1	11 ± 1	11.0 ± 0.2	96 ± 1
$D(GS)_5K$	100	2.8 ± 0.2	12 ± 1	11.0 ± 0.8	100 ± 1
$(GS)_5KD$	100	2.8 ± 0.3	11 ± 1	12.2 ± 0.4	100 ± 1
$D(GS)_5KD$	3 ± 2	3.1 ± 0.4	5 ± 1	3.2 ± 0.2	96 ± 1

Table 4: Steady-state quantum yield QY_{ss} relatively to the value for singly labeled peptides, diffusion constant D, brightness per molecule B, particle number N normalized to the sample concentration c, fraction of optical densities at 608 nm and at 660 nm, fluorescence lifetime τ of MR121, with MR121 singly-labeled $(GS)_5K$-oligopeptides, and doubly-labeled $(GS)_5K$-oligopeptides MR121-$(GS)_5K$-MR121. All measurements were performed at 293 K in PBS buffer. Lifetime measurements were done in 7.7 M GdCl.[BLSD11] MR121-$(GS)_5K$-MR121 is strongly quenched due to static quenching.

has only 3 % fluorescence compared to $(GS)_5K$-MR121. Dynamic quantum yields QYdyn of tab. 4 in 7.7 M GdCl have maximal differences of 4 % between MR121, $(GS)_5K$-MR121 and MR121-$(GS)_5K$-MR121. Although measured in different solvents, a comparison of peptides using PET in tab. 1 of sec. 5 the dynamic quenching rates are similar.

MR121-$(GS)_7W$ in GdCl has QYdyn $= \frac{\tau}{\tau_0}$ of 98%. TCSPC measurements of MR121-$(GS)_5K$-MR121 in PBS show the same fluorescence lifetimes as $(GS)_5K$-MR121. This is accompanied by an increase of the amount of time to get accurate photon statistics for TCSPC measurements of MR121-$(GS)_5K$-MR121. Because of this, the concentration of MR121-$(GS)_5K$-MR121 in PBS was increased to 10 μM to shorten measurement time. While a 1 μM $(GS)_5K$-MR121 sample lasts 30 s for 4000 counts of the maximum of its TCSPC histogram, the measurement of the more concentrated MR121-$(GS)_5K$-MR121-solution lasts two days. Higher concentrations are not used due to concentration dependent aberrations. However, the dimer reporter system is slightly more quenched dynamically than the PET reporter system.

Looking at the absorption and fluorescence spectra of $(GS)_5K$-MR121 and MR121-$(GS)_5K$-MR121 in PBS at 293 K underlines changes in QYss. As shown in fig. 33, the spectrum of the $(GS)_5K$-MR121 sample is in the range between 230 nm to 900 nm comparable to the MR121 absorption spectrum. The comparison of their spectral shapes in fig. 33 (left) exhibits that the maximum absorption of MR121-$(GS)_5K$-MR121 is shifted hypsochromically to $(GS)_5K$-MR121. The fraction $\frac{OD_{660}}{OD_{608}} = 0.47 \pm 0.08$ of MR121-$(GS)_5K$-MR121 is 5fold smaller than its equivalent for $(GS)_5K$-MR121 (2.3 ± 0.1) and free dye (2.5 ± 0.4). In the range of 250 nm and 470 nm all spectra are equal. So the static quenching is accompanied by the strong spectral change of MR121-$(GS)_5K$-MR121 absorption.

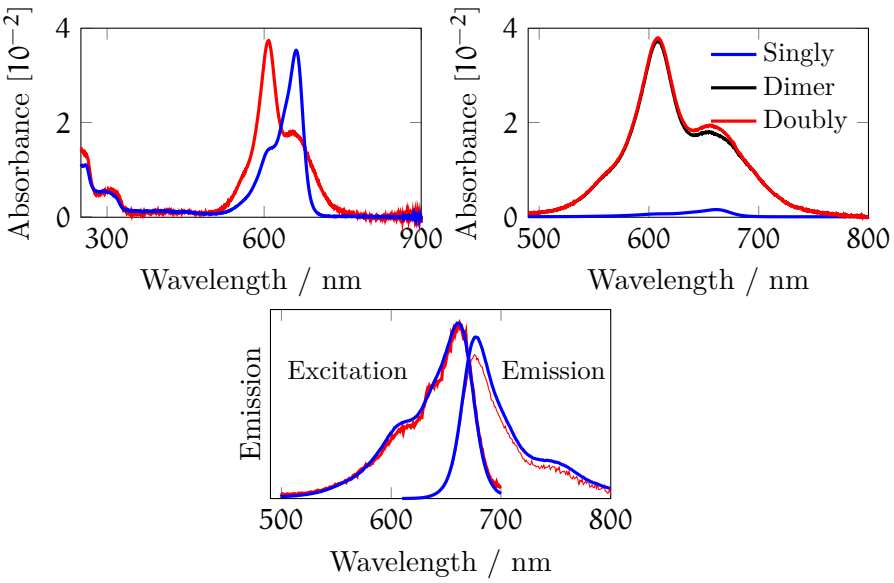

Figure 33: Absorption, emission, and excitation spectra for MR121-labeled peptides. Left: Absorption spectra of MR121-$(GS)_5$K-MR121 (red) and $(GS)_5$K-MR121 (blue) samples. MR121-$(GS)_5$K-MR121 distinguishes from $(GS)_5$K-MR121 a peak at (608 ± 1) nm with a shoulder peak at (655 ± 1) nm. Right: Absorption spectra for the pure MR121-dimer. The spectrum is calculated by subtraction of a normalized $(GS)_5$K-MR121 (blue)absorption spectrum from the MR121-$(GS)_5$K-MR121 (red)absorption spectrum. The normalization of the $(GS)_5$K-MR121 spectrum is done by multiplication of a factor that is the fluorescence emission ratio between $(GS)_5$K-MR121 and MR121-$(GS)_5$K-MR121. Below: Excitation (emission at 730 nm) and emission spectra (excitation at 600 nm) of $(GS)_5$K-MR121 and MR121-$(GS)_5$K-MR121. The data for MR121-$(GS)_5$K (not shown) equal those for $(GS)_5$K-MR121. The emission data curves are normalized to the area under the $(GS)_5$K-MR121 (blue)excitation spectrum.[BLSD11]

Excitation and emission spectra of $(GS)_5$K-MR121 and MR121-$(GS)_5$K-MR121 have the same wavelength dependence. In fig. 33 (B), emission spectra of $(GS)_5$K-MR121 and MR121-$(GS)_5$K-MR121 are normalized by their maximal emission ($I^{max}_{(GS)_5K-MR121}$, $I^{max}_{MR121-(GS)_5K-MR121}$) using the ratio f as defined in eq. (75). The spectral shape of all curves in fig. 33 is the same as the corresponding spectrum of the free dye MR121. Now the fluorescence emission ratio f is used to calculate the part of the the MR121-$(GS)_5$K-MR121 absorption spectrum that does not fluoresce. Therefore the fluorescent $A_{fluor.}$ part of the absorption spectrum is calculated via eq. (76) assuming that fluorescence is due to dye species having the properties of $(GS)_5$K-MR121. So the absorption of $(GS)_5$K-MR121 $A_{(GS)_5K-MR121}$ is responsible for fluorescence. Subtracting $A_{fluor.}$ from the absorption spectrum of MR121-$(GS)_5$K-MR121 $A(\lambda)_{MR121-(GS)_5K-MR121}$ gives the absorption spectrum of non-fluorescing species $A(\lambda)_{dimer}$ that has a 6 % smaller 660 nm shoulder peak.

$$f = \frac{I^{max}_{(GS)_5K-MR121}}{I^{max}_{MR121-(GS)_5K-MR121}} \tag{75}$$

$$A_{fluor.} = \frac{A_{(GS)_5K-MR121}}{f} \tag{76}$$

Because absorption spectra of MR121-$(GS)_5$K-MR121 in PBS are hypsochromically shifted compared to $(GS)_5$K-MR121 and because MR121-$(GS)_5$K-MR121 is strongly quenched, the quenching is surely due to H-dimerization of MR121. The form of excitation and emission spectra suggest that the 3 % fluorescence still existing are due to non interacting dyes. Therefore the calculated spectrum of non-fluorescing species $A(\lambda)_{dimer}$ is assumed to be a pure dimer spectrum. In the following, this assumption is tested.

To get an accurate estimate for the dimerization constant of MR121 according to Würthner et al. [120] absorption and ensemble fluorescence experiments of free dye in aqueous solution were measured. MR121-NHS dyes were dissolved in phosphate buffer at pH 7.7 and after incubation of one day purified by extracting the peak of abreacted MR121. The dried sample was dissolved at different concentrations in PBS in cuvettes with path lengths ranging from 0.1 mm to 1 cm. Similar to $(GS)_5$K-MR121 and MR121-$(GS)_5$K-MR121 absorption, in the range between 230 nm and 470 nm no changes of the spectral shape of MR121 absorption are visible. A shoulder next to the maximal peak is visible at (660 ± 2) nm. Normalizing all spectra to the absorption value at 280 nm, which is depending only at the concentration, this shoulder evolves to a second peak. The peak at 660 nm decreases relatively to this shoulder. Fig. 34 shows two isosbestic points at $\omega_{iso1} = (608 \pm 1)$ nm and $\omega_{iso2} = (680 \pm 1)$ nm. In the range of 1 µM to 100 µM excitation spectra do not change. Because of the inner filter effects of high

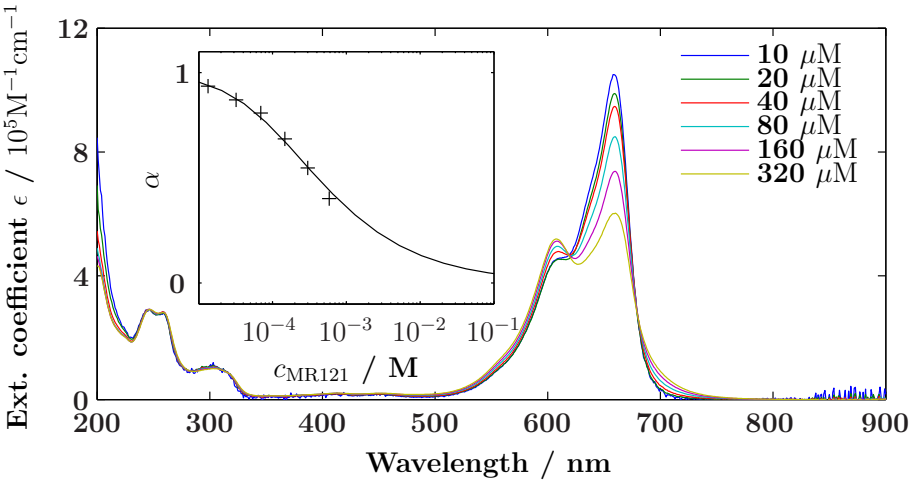

Figure 34: Absorption spectra of MR121 normalized to fluorophore concentration. Data curves yield two isosbestic points at 618 and 680 nm. Spectral shape of absorption is equal in the 230 nm to 470 nm range. Inset: molar monomer fractions a are calculated by fitting a linear superposition of pure MR121-monomer and -dimer spectra to the measured absorption spectra. Data are fitted by a sigmoidal curve with a reflection point at (2600 ± 240) M^{-1}.[BLSD11]

concentrated samples, excitation measurements of high concentrated dye solutions are distorted. Because of this all solutions have two interconverting species - a fluorescing and a non-fluorescent one. The non-fluorescent one consists of dimerized fluorophores.

This two state system consists of interconverting monomeric and dimeric dye species with concentrations c_M and c_D. An equilibrium binding constant K_{eq} is given in thermodynamic equilibrium by eq. (77). Here α and c_0 are the monomeric fraction and the total concentration of fluorophores in the solution, respectively. Because dimers consist of two dyes the dimer concentration is given by $c_D = (1-\alpha)\frac{c_0}{2}$.[116, 120] Thus the binding constant follows eq. (77)

$$K_{eq} = \frac{c_D}{c_M^2} = \frac{1-\alpha}{2\alpha^2 c_0}. \tag{77}$$

$$A_{misc}(\lambda) = \alpha \cdot A_{mono}(\lambda) + d \cdot A_{dimer}(\lambda) \tag{78}$$

Spectra having concentrations under 1 µM do not change anymore when further diluted. Therefore we assume that they are pure monomer spectra. The pure monomer $A_{mono}(\lambda)$ and pure dimer spectra $A_{dimer}(\lambda)$ can be fitted to every absorption spectrum by eq. (78). Data measured with sample concentrations between 10 µM and 400 µM in fig. 34 yield α for every concentration. Via eq. (77) K_{eq} is then calculated to be $K_{eq} = (2600 \pm 240) M^{-1}$ at 293 K (s. inset of fig. 34).

To get the extinction coefficient of MR121-dimers in aqueous solution at 293 K the absorption spectra $A(\lambda)_{(GS)_5K-MR121}$ and $A(\lambda)_{MR121-(GS)_5K-MR121}$ are normalized by their absorption. This

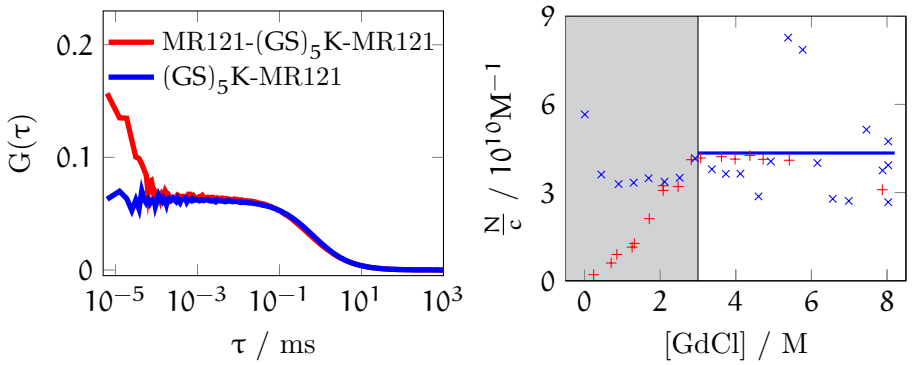

Figure 35: Left: FCS curves of $(GS)_5$K-MR121 (blue) in PBS and MR121-$(GS)_5$K-MR121 (red) in PBS + 0.24 M GdCl at 293 K. Right[BLSD11]: Number of fluorescent molecules N diffusing through the focal FCS volume, relative to the concentration c. The values are extracted from MR121-$(GS)_5$K-MR121 (+) and $(GS)_5$K-MR121 (+) FCS curves as a function of GdmCl concentration.

factor is chosen, so that the absorption between 270 nm and 470 nm are equal in the normalized spectra. In a second step, both spectra are multiplied by the same factor, so that the spectrum of $(GS)_5$K-MR121 has a maximum value of $1.05 \cdot 10^5 M^{-1}cm^{-1}$. This is the extinction coefficient of MR121.[68] It gives a maximum extinction coefficient of a dimer of $\epsilon^{max}_{dimer} = (140000 \pm 14000)M^{-1}cm^{-1}$ for the dimer. This value is splitted to $\epsilon^{p.d.max}_{dimer} = (70000 \pm 7000)M^{-1}cm^{-1}$ for the maximum extinction coefficient of a single dye molecule of the dimer.

So the interactions occurring between similar dyes are due to self-quenching. What is the outcome this may have for single molecule experiments? Therefore we tested the reporter system for end-to-end contact rate measurements. We measured $(GS)_5$K-MR121 and MR121-$(GS)_5$K-MR121 samples in nanomolar concentrations using confocal FCS in aqueous solutions. Fig. 35 exemplifies curves of $(GS)_5$K-MR121 in PBS and MR121-$(GS)_5$K-MR121 in solution consisting of PBS with 0.24 M GdHCl. The shapes of both curves are comparable to the ones described in sec. 4. There the FCS curves of $(GS)_5$K-MR121 and MR121-$(SGalG)_9$W are compared in fig. 26.

So like in sec. 5 for peptides with Trp/MR121, the 10 ns decay is identified as exponential reporting on end-to-end contact. For data fitting a 2D Gaussian model is used. Data of MR121-$(GS)_5$K-MR121 followed eq. (59). At higher laser intensities and at high denaturant concentration in the solution a small additional exponential part arises in all FCS-curves in the range of 1 µs. Because of this eq. (60) is used for data analysis. The exponential is power dependent and that occurs in the typical time range for triplet states (1 µs - 100 µs)[30]. Therefore we consider it as triplet blinking.

In FCS measurements the mean focal particle number N is used to establish constant measurement conditions with N between 5 and 20. To accomplish this in PBS solvent with MR121-$(GS)_5$K-MR121, concentrations of MR121-$(GS)_5$K-MR121 are of over an order of magnitude higher than for the corresponding peptide with a PET reporter system. This effect might be due to species that do not fluoresce while diffusing through the focal volume. To test if it is due to dimerization of the fluorophores attached to the oligopeptides, we tested if N increases by addition of the denaturant GdCl to the solution.

In a PBS solution with 0.24 M GdCl about 10 particles are fluorescing while diffusing through the focal volume of the FCS-setup. In 4 M GdCl, concentration of the solute MR121-$(GS)_5$K-MR121 has to be 10fold lower to still measure with the same particle number in the focal volume. In the latter solution, the mean concentration normalized particle number of $(GS)_5$K-MR121 is $N_{(GS)_5K-MR121} = (3.5 \pm 0.9) \cdot 10^{10} M^{-1}$, while it is for MR121-$(GS)_5$K-MR121 $N_{MR121-(GS)_5K-MR121} = (4.0 \pm 0.4) \cdot 10^{10} M^{-1}$. The concentration dependent results of GdCl-concentration normalized particle numbers are shown in fig. 35. The FCS measurements of MR121-$(GS)_5$K-MR121 and $(GS)_5$K-MR121 only give the same results in denaturant solvent concentrations of over 3 M, while for low denaturant concentration there are less particles fluorescent while diffusing through the detection volume.

We calculate the equilibrium constant using the differences of N in PBS. Approximating the equilibrium constant K_{eq} via eq. (77) with $\alpha = 0.1$ and the concentration of two molecules tethered in a volume of $2.1 \cdot 10^{-24}$ l, the equilibrium constant for dimerization is $K_{eq}^{M} R121 - (GS)_5K - MR121 \approx 1800 M^{-1}$. Regarding the two different types of determination this value is near to the equilibrium constant estimated with free dyes MR121. We will use this kind of estimating the equilibrium constant K_{eq} for dimerization later in sec. 7.

While on average only 10 % of MR121-$(GS)_5$K-MR121 fluoresce in PBS, the relaxation amplitude K (s. fig. 36) reports on average 50 % fluorescing molecules of MR121-$(GS)_5$K-MR121 sample in PBS. This is a hint for a heterogeneous distribution of fluorescing molecules blinking with relaxation times of 20 ns. Now a further examination on the outcome of the dimerization on kinetic parameters estimated via fitting the FCS data of MR121-$(GS)_5$K-MR121 follows.

We used an Arrhenius analysis for determining enthalpic influences of dimerization of the reporter system. At 3 M GdCl all MR121-$(GS)_5$K-MR121 molecules are fluorescent. In this concentration range we did temperature dependent measurements. According to Möglich et al. [73], rates of GS-polypeptides are dependent on solvent viscosity η by $k_c \propto \eta^{-0.94}$. Therefore we corrected closing rates k_c and opening rates k_o by η of the GdCl solution. Therefore an empirical equation of Perl et al. [80] was used to determine η.

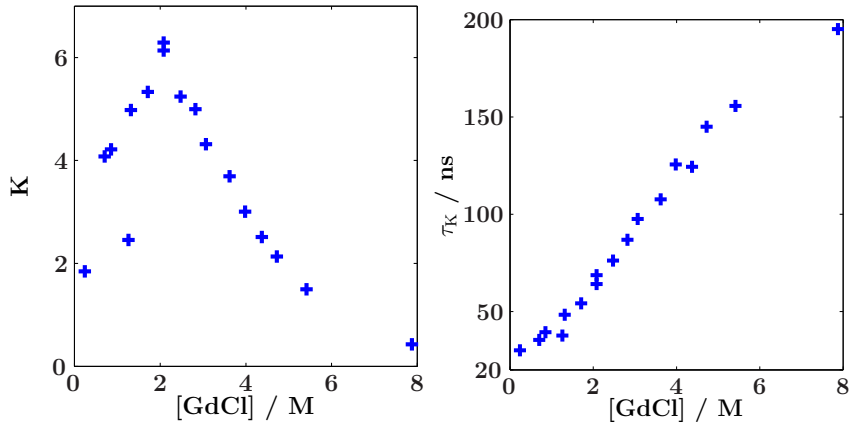

Figure 36: Relaxation amplitudes K and relaxation times τ_K GdCl are shown solvent concentration dependent. τ_K is linear dependent on [GdCl], K has a maximum at 3 M [GdCl]. If all molecules are at least several times fluorescing in the focal volume, K is a measure for the fraction of non-fluorescing to fluorescing molecules. The fraction $\frac{N_{doubly}}{N_{singly}}$ differs to K in the range from 0 to 3 M GdCl. Therefore there is a subset of molecules that does not fluoresce in the focal detection volume.

$$\begin{aligned}\eta =&\{a + b\exp(c[GdCl])\}\\ &+\{d + e\exp(f[GdCl])\}\\ &\cdot\exp[(-g + h[GdCl] + j\cdot 10^{-8}[GdCl]^2)(T - 273.15)]\end{aligned} \tag{79}$$

with a = 0.178, b = 0.1225, c = 0.2028, d = 1.4376, e = 0.01674, f = 0.5802, g = 0.0331, h = 0.0004424 and j = 2.272. The viscosities of GdCl were calculated ranging from 1.228 mPa at 293 K for 3.11 M GdCl to 0.639 mPa at 333 K for 3.11 M GdCl. Viscosity-corrected (fig. 37) measurements show an Arrhenius like (eq. (69)) temperature dependence of contact rates. A linear fit to the semilogarithmic plotted data has a slope of $(-1640 \pm 500)\cdot 10^3$ K, yielding an activation enthalpy barrier of (14 ± 4)kJ mol^{-1} for the peptide conformation. Without viscosity correction the barrier is (27 ± 6)kJ mol^{-1}. This is the conformational intramolecular enthalpy barrier plus solvent enthalpy barrier for end-to-end contact formation. This gives us informations about the energy landscape of contact formation, but we still have to test, if the contact kinetics we measure give the right closing rates k_c.

In fig. 38 the viscosity corrected k_c and k_o of MR121-$(GS)_5$K-MR121 and MR121-$(GS)_5$W are shown dependent on GdCl-concentration. The behaviour of k_c and k_o differs in general. k_c of both samples decreases with increasing [GdCl]. The k_c-values of MR121-$(GS)_5$K-MR121 are smaller than the ones of MR121-$(GS)_5$W by 60 % while showing the same qualitative [GdCl] dependent behaviour. k_o of MR121-$(GS)_5$W increases with increasing [GdCl]. This is different for MR121-$(GS)_5$K-MR121: Its k_o decrease by increase of [GdCl] until 3 M [GdCl]. At

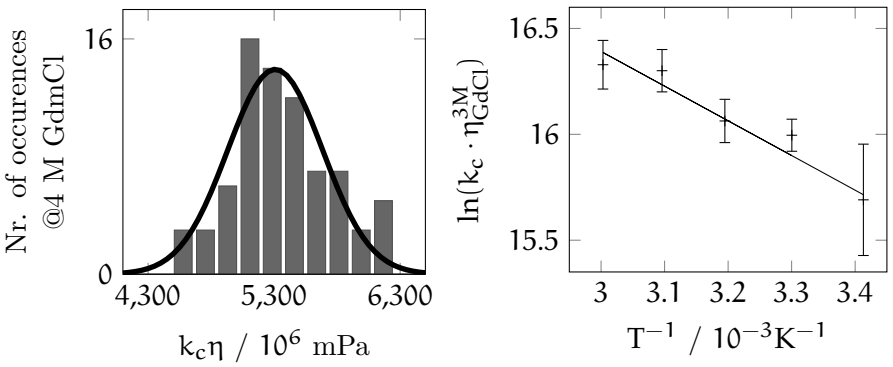

Figure 37: Contact rates. Left: Histogram of viscosity corrected contact rates of MR121-$(GS)_5$K-MR121. 76 viscosity corrected k_c values are distributed into bins that have a width of 0.18×10^6 mPa. A Gaussian fit to this distribution gives a mean value of $\mu = 5.3 \times 10^6$ mPa having a standard deviation of $\sigma = 0.4 \times 10^6$ mPa. Right: Arrhenius analysis of MR121-$(GS)_5$K-MR121. Viscosity corrected closing rates k_c of MR121-$(GS)_5$K-MR121 in 3 M GdCl solution. Data are fitted by a linear regression yielding a slope of $(-1640 \pm 500) \cdot 10^3$ K and a y-intercept of 21 ± 1. Error bars represent standard deviation of three measurements.

about 3 M [GdCl] the k_o values have a local minimum and increase for increasing [GdCl] for concentrations over 3 M. In the range from 3 M [GdCl] to 8 M [GdCl] k_o of both samples differ for every datapoint for by about an order of magnitude. The minimum of the opening rates of MR121-$(GS)_5$K-MR121 coincides with the beginning of the plateau of its particle number in fig. 35.

Furthermore statistical fluctuations of the rates of both samples show a different behaviour: Opening and Closing rates of MR121-$(GS)_5$K-MR121 are fluctuating less in high GdCl solvent concentrations compared to rates of MR121-$(GS)_5$W. Particle number and triplet effect corrected FCS curves, exemplified in fig. 39, have in the 10 - 400 ns range exponential decays with end-to-end contact kinetics. The MR121-$(GS)_5$W samples produce FCS curves with kinetic exponential functions with a small amplitude. If the GdCl concentration is increased, this exponential decreases. While it is still possible to fit these curves, this is accompanied with greater uncertainties for fit parameters K and τ_K. The standard deviation of closing rates of MR121-$(GS)_5$W is about 20 % for k_c in 4 M GdCl solution at 293 K. For MR121-$(GS)_5$K-MR121 samples it is only 8 %. So the statistical noise of the fitting procedure itself decreases.

6.2 DISCUSSION

Kinetics of GS peptides can be measured using MR121 dimerization as reporter for end-to-end contacts in denaturing solvent. Dimerization of

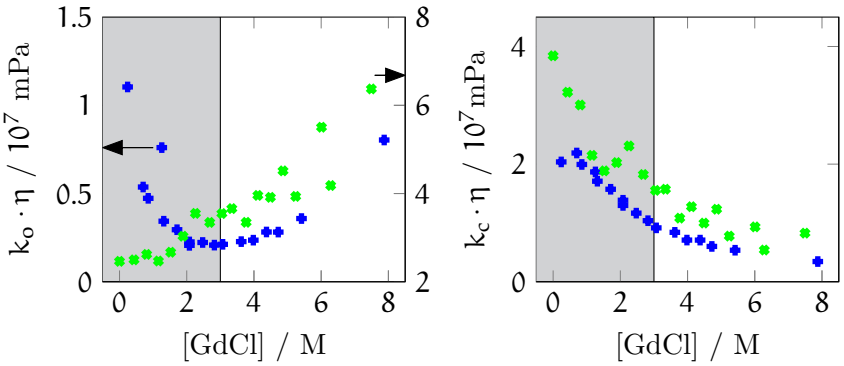

Figure 38: Closing rate k_c (left plot) and opening rates k_o (right plot) of MR121-$(GS)_5$K-MR121 (+) and MR121-(GS)5-W (x), multiplied by the viscosity η, are shown as a function of GdCl concentration.[BLSD11] The closing rates decrease with increasing GdCl-concentration. The values for k_c of MR121-$(GS)_5$K-MR121 are 60 % smaller. Opening rates increase on increasing GdCl-concentration for MR121-$(GS)_5$-W. The k_o for MR121-$(GS)_5$K-MR121 decrease with increasing GdCl-concentration, have a minimum at about 3 M [GdCl] and increase afterwards.

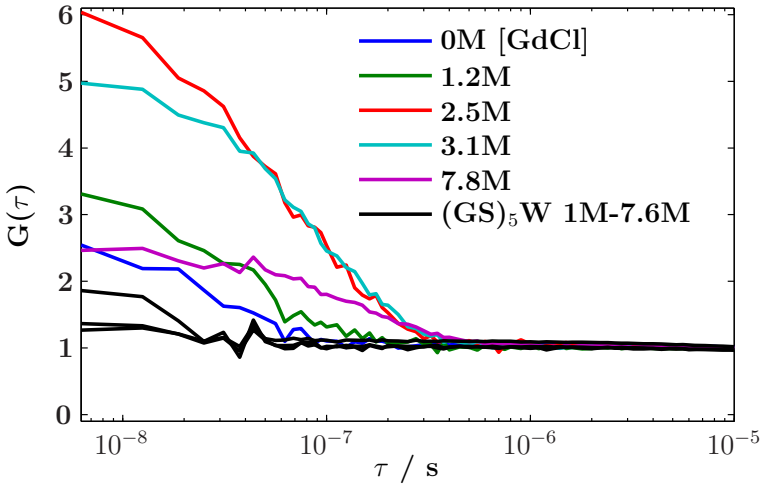

Figure 39: FCS data for MR121-labeled peptides. Coloured curves show FCS data for MR121-$(GS)_5$K-MR121 in 0-7.8 M GdCl solutions, normalized by molecule number N and corrected for triplet effects. For comparison of the fast kinetics part, FCS data of MR121-(GS)5W in aqueous solutions with different GdCl concentrations are shown in black.[BLSD11]

the oxazine MR121 was characterized. More than 90 % of all MR121-$(GS)_5$K-MR121 are quenched with an off-time longer than 1 ms.

Excitation, emission and absorption spectra in GdCl-rich solutions show minor differences between MR121 and $(GS)_5$K-MR121. In PBS the absorption spectrum of MR121-$(GS)_5$K-MR121 has a maximum at 618 nm with a shoulder at 660 nm. In contrast to this, $(GS)_5$K-MR121, has a peak at 660 nm with a shoulder at 618 nm. Excitation and emission spectra of $(GS)_5$K-MR121 and MR121-$(GS)_5$K-MR121 have the same shape. To find out, whether the change in absorption is due to dye-dye or dye-peptide interaction, we made absorption measurements of concentrated dyes in solution.

Steady-state ensemble experiments with free MR121 dyes show in the range of 500 nm to 850 nm concentration dependent changes in absorption spectra. Such absorption spectra have two isosbestic points at 618 nm and 680 nm. At high MR121 concentrations a new peak arises at 608 nm. The peak position is at the same position as the highest peak of the MR121-$(GS)_5$K-MR121 absorption spectrum. Spectra with different MR121 concentrations can be fitted by a linear combination of the absorption spectrum of $(GS)_5$K-MR121 and an absorption spectrum of pure non-fluorescent probe $A(\lambda)_{dimer}$. The emission spectra of all MR121 samples with different dye concentrations exhibit the same shape of emission and excitation spectra. In an investigation on aggregation properties of MR121[68], it was argued with exciton theory that here equal excited-state energy levels of two monomer dyes split into two different levels upon dimerization. One energy level has a higher energy than the one of the monomer and is characteristic for H-type dimers. Additionally, in exciton theory the blue shifted absorption band of a H-dimer[34] is broad compared to thin spectral shapes of J-dimers. The absorption spectrum of MR121-$(GS)_5$K-MR121 shows a peak which is as broad as the $(GS)_5$K-MR121-peak.

All these results underline the strong dimerization of MR121 in the spectrum of MR121-$(GS)_5$K-MR121. The new absorption peak is blue shifted to the $(GS)_5$K-MR121 absorption maximum, and the steady-state quantum yield of MR121-$(GS)_5$K-MR121 is (3 ± 2) %. Also, the emission spectrum of MR121-$(GS)_5$K-MR121 is similar to the one of MR121. Therefore it is very likely, that quenching is due to self-dimerization of MR121. Then every MR121 dye pair that is dimerized is fully quenched and has an extinction coefficient of $\epsilon = 140000 \pm 14000$.

The shapes of MR121 absorption spectra below 470 nm do not change with dye concentration. One gets clearly visible isosbestic points by normalization to such wavelengths. These isosbestic points are also visible when normalizing the curves by dilution factors. Therefore maxima at wavelengths in the range of 250 nm to 470 nm can be used for concentration normalization.

The non-fluorescent MR121 dimers give in fluorescence lifetime measurements of MR121-$(GS)_5$K-MR121 no contributions. The contributions to TCSPC histograms of MR121-$(GS)_5$K-MR121 are

- opened MR121-$(GS)_5$K-MR121 peptides,
- peptides with one destroyed dye.

A QYdyn of $\frac{\tau}{\tau_0} = 96\%$ MR121-$(GS)_5$K-MR121 in 7.7 M GdCl indicates, that in GdCl the quenching of MR121 here is due to diffusional limited quenching. The fact that MR121-$(GS)_7$W has a QYdyn of $\frac{\tau}{\tau_0} = 98\%$ reflects the length difference to MR121-$(GS)_5$K-MR121.

The equilibrium constant K_{eq} in eq. (77) reports of the strength of dimerization. Here we show a new estimation for K_{eq} of dimerization of organic dyes, called dimerization estimation by oligopeptides only Dimerization Estimation by oligopeptides Only (DEO), using ensemble spectroscopy and FCS. The QYss in PBS (293 K) of MR121-$(GS)_5$K-MR121 is 3%, so the fraction of dimerized dyes of MR121-$(GS)_5$K-MR121 is 97 %. At 293 K the viscosity of water is 1 mPas. With the diffusion constant of MR121-$(GS)_5$K-MR121 tab. 4, the hydrodynamic radius $R_h = 0.77$ nm of MR121-$(GS)_5$K-MR121 is calculated, using the Stokes-Einstein equation eq. (21). We define a model in which R_h is the mean radius of a sphere that one dye diffuses freely around the other dye. In this model the effective concentration of the two dyes in MR121-$(GS)_5$K-MR121 is $c_{eff} = 1.8$. With these values the equilibrium constant is $K_{eq} = 300\ M^{-1}$. Upper and lower bounds are $K_{eq_l} = 100\ M^{-1}$ and $K_{eq_u} = 2800\ M^{-1}$ that follow from the uncertainties of QYss (compare tab. 4). Compared to the dimerization constant $K_{eq} = (2600 \pm 240) M^{-1}$ that we obtain *via* MR121 concentration dependent absorption measurements the DEO determination of K_{eq} has advantages and disadvantages: Advantages are the small amounts of dyes to get estimates of K_{eq} if standard spectrometers are used. For concentration dependent dimerization measurements for MR121 concentrations over $320\mu M$ are necessary. Dyes having lower dimerization constants need more sample concentration to get better statistics to examine the dimerization itself. In sec. 7 we can use the estimation of K_{eq} by DEO to obtain differences in K_{eq} also for dimerization of different dyes. This is possible notwithstanding that the uncertainty in determination of K_{eq} is high. The latter is a disadvantage of this kind of determination.

Even if the peptide is considered as a Gaussian chain, there will be still interactions between solvent and peptide pulling dimerized dyes apart. This is the reason, why K_{eq} measured by diffusion of bound dyes is estimated too low. As a second cause the hydrodynamic radius is for non-spherical particles smaller than the rotational radius of a molecule, because the hydrodynamic radius also reflects hydration interactions between molecule and solvent. Considering this effect, c_{eff} is estimated too high and therefore the estimation of K_{eq} is too low

using the effective volume method. The calculation of the length of a stretched peptide yields ≈ 5 nm using carbon-carbon link lengths of 120 pm. The measured mean hydrodynamic radius is small compared to the 5 nm of a stretched peptide. Therefore the peptide is most of the time in a compact form. Spherical particles are compact so this might be a small effect.

The determination of K_{eq} of MR121 was already examined by Marmé et al. [68]. Their K_{eq} of $(3300 \pm 300)\ M^{-1}$ is in the 2σ interval of $K_{eq} = 2600 \pm 240$ we determined with the technique similar to theirs. A weighted mean of the results of both working groups gives a $K_{eq} = (2900 \pm 200)\ M^{-1}$.

So, the determination of K_{eq} via hydrodynamic radii gives a good estimation of dimerization strength. After the characterization of dimerization, now we focus on determination of biomolecular dynamics. Dimerization of MR121 was used to extract end-to-end dynamics information of GS oligopeptides.

In aqueous solution contact rates are hardly applicable due to strong dimerization. Having at least 3 M GdCl denaturant in the solvent, all MR121-$(GS)_5$K-MR121 are fluorescent while diffusing through the focal volume of our FCS-setup. We suggest using MR121-$(GS)_5$K-MR121 peptides with MR121 in high denaturant solution for monitoring conformational dynamics of long GS peptides. Nevertheless, contact dynamics of MR121-$(GS)_5$K-MR121 samples are also in aqueous solution comparable to dynamics of MR121-$(GS)_5$W chain dynamics.

Temperature dependent measurements of MR121-$(GS)_5$K-MR121 in 3 M GdCl show activation enthalpy barriers of 14 $\frac{KJ}{mol}$ additional to solvent interactions. In the Kramers-rate model (eq. (70)), this additional enthalpy barrier induces a 26fold contact rate decrease. The direct comparison of closing rates of MR121-$(GS)_5$K-MR121 and MR121-$(GS)_5$W shows only a 0.6fold decrease of contact rates. Therefore there must be entropic compensation to the activation energy for end-to-end contacts.

There will always be influences of reporter systems on kinetic measurements of biomolecules. The question is, how strong they are to estimate possible implications for the experiment. The MR121 dimer reporter system shows lower fitting uncertainties than the MR121/Trp reporter system in high denaturant solvents. The longer GS-peptides are, the smaller kinetic amplitudes in FCS curves of end-to-end contacts are. In measurements of biomolecular systems, where the kinetic amplitudes get low, reporter systems with higher association constants can lower uncertainties to compare biomolecular kinetics.

FCS measurements at 293 K in phosphate buffer are hardly applicable, because only 10 % of MR121-$(GS)_5$K-MR121 are luminescent. The fluorescent part of MR121-$(GS)_5$K-MR121 is furthermore only fluorescent for a time much shorter than the diffusion time through the focal volume of our experiment of 0.6 miliseconds. This is an interesting result for applications in super-resolution microscopy, where long

lasting dark states of fluorophores are needed to record single molecules with some kHz frame rates. There were several mechanisms reported to achieve good blinking ratios of dyes to record dense structures from buffer conditions to enhance dye blinking to molecular switches.

7

HOW FUNCTION OF HETERODIMERS INFLUENCES FLUORESCENCE

Besides contact induced quenching mechanisms, FRET has become a routine tool in biochemical studies on structural and dynamic properties of biomolecules. While the contact induced quenching mechanisms - used and discussed in sec. 6 and sec. 5 - give reliable results on intra- and intermolecular contact, FRET efficiencies E of energy transfer between donor (D) and acceptor (A) molecules are a measure of A-to-D distances. A and D being the same (homo-FRET) or different molecules (hetero-FRET). Non-randomized orientation of D and A, molecular linkers between biomolecules and D/A, dye blinking, and photodestruction distort precise distance dependent FRET measurements.

Nowadays the use of FRET to study dynamic biomolecules increases. In particular questions regarding unfolded or denatured protein states have gained much interest to understand the process of protein folding or to characterize intrinsically disordered proteins.[93] As it was seen in sec. 6, dimerization by overlap of molecular orbitals of fluorophores influences the energy landscape for the conformations of flexible unstructured polypeptides.

We tested a selection of D/A pairs that are popular in single-molecule FRET studies for contact-induced fluorescence quenching interactions. Quenching processes are identified, and quantitative estimates for contact-induced interactions in homogeneous and heterogeneous fluorophore pairs are given. This will help to identify and quantify contact-induced quenching effects in FRET studies with highly dynamic biomolecules.

Hydrophobicity and charges are responsible for different dimerization behaviour of dyes,[44, 85, 96] although there is at least one publication that states hydrophobicity is not important for dimerization[79]. We tested dyes used for distance-dependence FRET measurements and quantify their dimerization constants. FCS measurements showed that there are obvious differences between opening and closing rates of contact rate measurements using H-dimerization of MR121 as contact reporter.[BLSD11] Knowing the behaviour of single dyes in solution, we investigate their properties regarding quenching effects comparing doubly labeled unstructured glycine-serine peptides, with Fl_1 and Fl_2 denoting different fluorophores at N-terminus and lysine side chain $\mathsf{Fl}_1{-}(\mathsf{GS})_5\mathsf{K}{-}\mathsf{Fl}_2$ or Fl denoting same fluorophores at both peptide ends $\mathsf{Fl}{-}(\mathsf{GS})_5\mathsf{K}{-}\mathsf{Fl}$.

Results are compared to singly labeled peptides $(GS)_5K{-}Fl_1$ and $(GS)_5K{-}Fl_2$, because labeling influences the quantum yields and lifetimes of dyes.

In the next sections we show that cyanine dyes show negligible self-dimerization if measured in aqueous solution in sub-millimolar concentrations. Oxazine and rhodamine dyes used here show H-dimerization with self-quenching in even lower concentration ranges. We quantify the dimerization strength of $Fl{-}(GS)_5K{-}Fl$-constructs by calculating equilibrium constants of dimerization K_D. Then we investigated $Fl_1{-}(GS)_5K{-}Fl_2$ constructs to estimate dimerization strengths of different dyes held at about 1 nm distance. One would expect that the same classes of dyes show similar behaviour concerning dimerization. However, hetero-labeled probes with only cyanine or only rhodamine dyes show H-dimerization with self-quenching. Mixtures of sorts of dyes seem to inhibit H-dimerization effects, but still quenching occurs. We estimate dimerization constants and quantify brightness of dimerized samples in phosphate buffer and denaturant solution. At the end we suggest Cy3/Cy5 as the best dye pair of this study as reporter dyes in FRET measurements, because of its brightness in dimer and denatured state.

7.1 HOMODIMERIZATION

In sec. 6 we have seen, that constraining MR121 via unstructured oligopeptides into a volume of the order of 10^{-25}l can give estimates of self-dimerization constants. The technique used in sec. 6 is on the one hand tested here for other organic dyes and will help on the other hand to interpret heterodimer data.

7.1.1 *Measurements and results*

To understand dimerization of dyes themselves we measured highly concentrated solutions (2 mM - 25 µM) and solutions containing low dye concentrations $< 1\mu M$ (s. fig. 42).

Retention times of different probes in RP-HPLC using gradients of polar and non-polar solvents like water and ACN can give hints to hydrophobicity of the probed samples. ATTO488 is an anionic and the most hydrophilic of the dyes used in this study. Cy5 (manuf. info), Cy3/Cy3B[22] are moderately hydrophobic dyes and Cy3 and Cy5 are anionic. Chromatography using reverse phase HPLC on the pentafluorophenyl (PFP)-column show that more hydrophobic solvent elutes Cy5 from the PFP phase than the other cyanine dyes. ATTO532 is eluted by a slightly more non-polar solvent than the Cy-dyes. ATTO647N and ATTO565 are eluted by the most non-polar environment of this study, whereas ATTO520 is eluted in 56 % ACN.

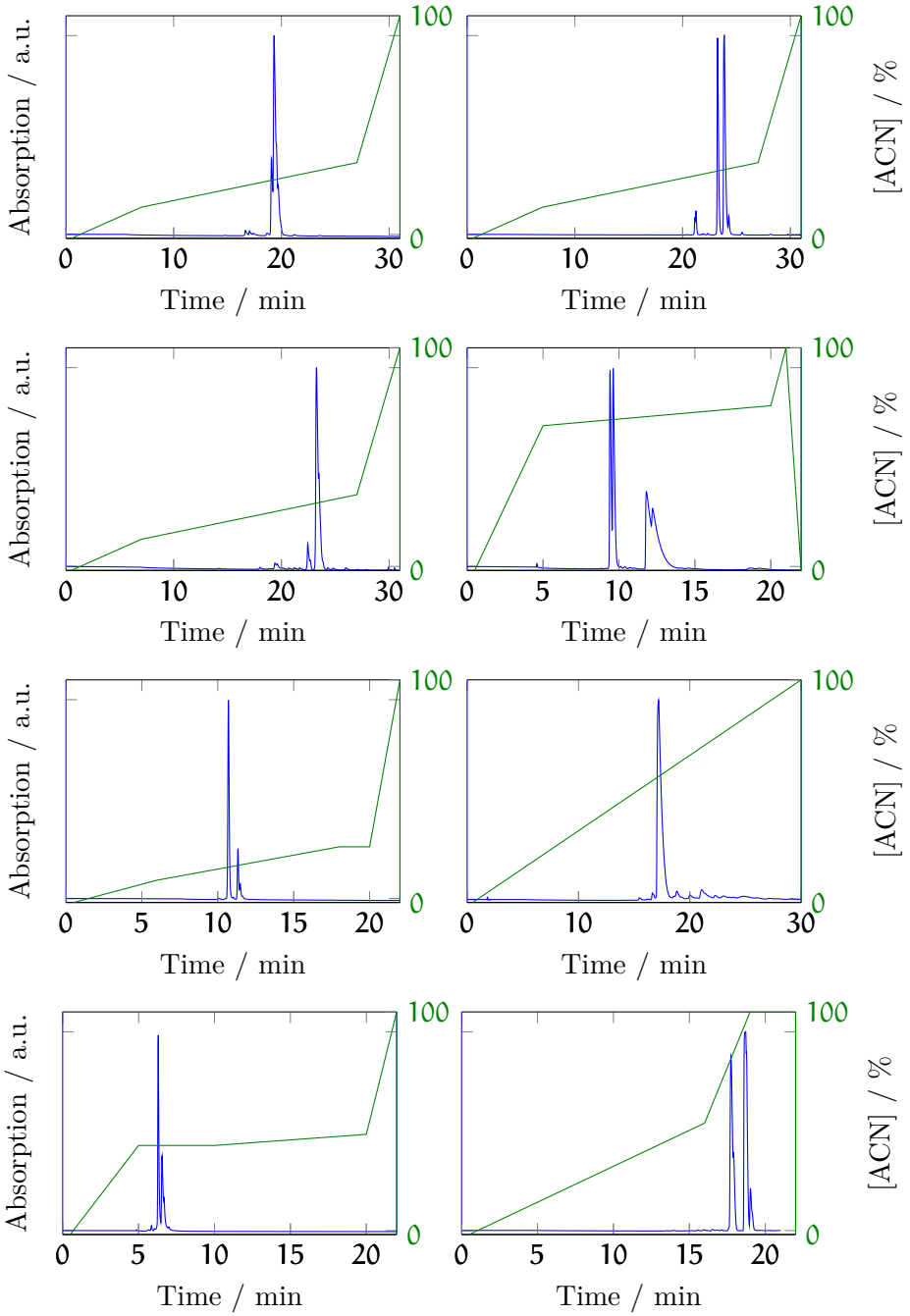

Figure 40: Gradients (-) from H_2O to ACN and chromatograms (-) of (from top left to bottom right) Cy3, Cy5, Cy3B, ATTO647N, ATTO488, ATTO520, ATTO532, and ATTO565. The gradients shown are the ones we used for separating labeled and unlabeled GS peptides.

For measuring highly concentrated samples in ensemble experiments we used cuvettes with pathlengts of 0.1 mm or 0.2 mm that are taken from a NanoPhotometer (Implen; Munich, Germany). The measurements were made using absorption and fluorescence spectrometer as described in sec. 3.1. For all samples used in this study the shapes of absorption spectra between 250 nm and 400 nm are identical for different sample concentrations and are proportional to dye concentrations. We estimated the concentration of highly concentrated samples by normalization to the dye specific absorption maximum in this range considering different cuvette path-lengths for low and high concentration measurements. All highly diluted dyes, which structures are shown in fig. 41 show expected absorption maxima and spectral shapes in comparison to manufacturer informations (s. fig. 42). Besides their characteristic absorption maximum all dyes show blue shifted shoulders originating from other vibrational absorption bands[34].

In measurements up to optical densities at maximum of 2.5 in a 0.1 mm path-length cuvette Cy3B (Cy3) shows at 550 μM (900 μM) a slightly enhanced increase of the shoulder peak at 510 nm (514 nm). Cy5, ATTO532 and ATTO488 show no change compared to highly diluted samples (s. fig. 42). In measurements where Cy5 is so concentrated that absorption between 620 and 670 is too high to give reliable results about the spectrum in that range, a new peak at 602 nm ± 2 nm is observed (data not shown). ATTO647N, and ATTO565 have new peaks at 603 nm and 531 nm respectively, while ATTO520 has a new shoulder at 490 nm.

For a quantitative description on self-dimerization association constants were derived.[BLSD11][68] Absorption and excitation spectra of $(GS)_5K{-}Fl$ and $Fl{-}(GS)_5K{-}Fl$ samples were taken. The shape of excitation spectra of $(GS)_5K{-}Fl$ and $Fl{-}(GS)_5K{-}Fl$ are identical for all dyes except Cy3 and Cy3B. These dyes show 10% enhanced excitation at $511\text{nm} \pm 1$ nm and $515\text{nm} \pm 1$ nm. All absorption spectra have hypsochromic shifted peaks arising at 509 nm (Cy3), 604 nm (ATTO647N), 531 nm (ATTO565) and 603 nm (Cy5).

We conclude that absorption spectra changes are due to H-dimerization. In the case of Cy3/3B this might not be the only case and the observed changes of excitation spectra give 10% uncertainty for the following evaluation of dimerization constants.

Absorption spectra of $(GS)_5K{-}Fl$ are normalized by excitation spectra of $(GS)_5K{-}Fl$ and $Fl{-}(GS)_5K{-}Fl$ for a specific dye D, to get the fraction of not dimerized dye species of $Fl{-}(GS)_5K{-}Fl$. All $Fl{-}(GS)_5K{-}Fl$ samples are strongly quenched compared to $(GS)_5K{-}Fl$.

Subtraction of normalized $(GS)_5K{-}Fl$ from $Fl{-}(GS)_5K{-}Fl$ absorption spectra yield homodimer spectra (fig. 44). Assuming that the extinction coefficient of dyes does not change upon labeling, absorption spectra of $(GS)_5K{-}Fl$ are normalized to known extinction coefficients of the free dye (s. tab. 5) at the absorption maximum. Then

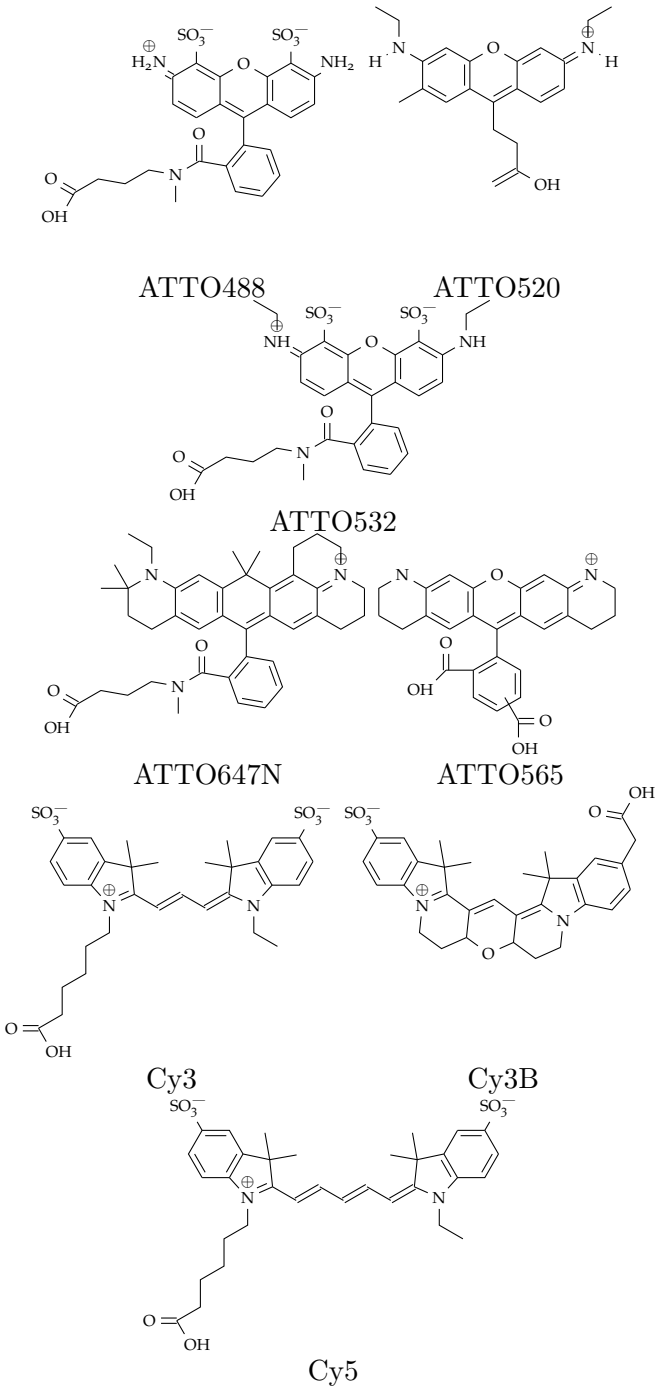

Figure 41: Molecular structures of ATTO488, ATTO520, ATTO532[32], ATTO 565, ATTO647N[32], Cy3B[22], Cy3[22] and Cy5[109]

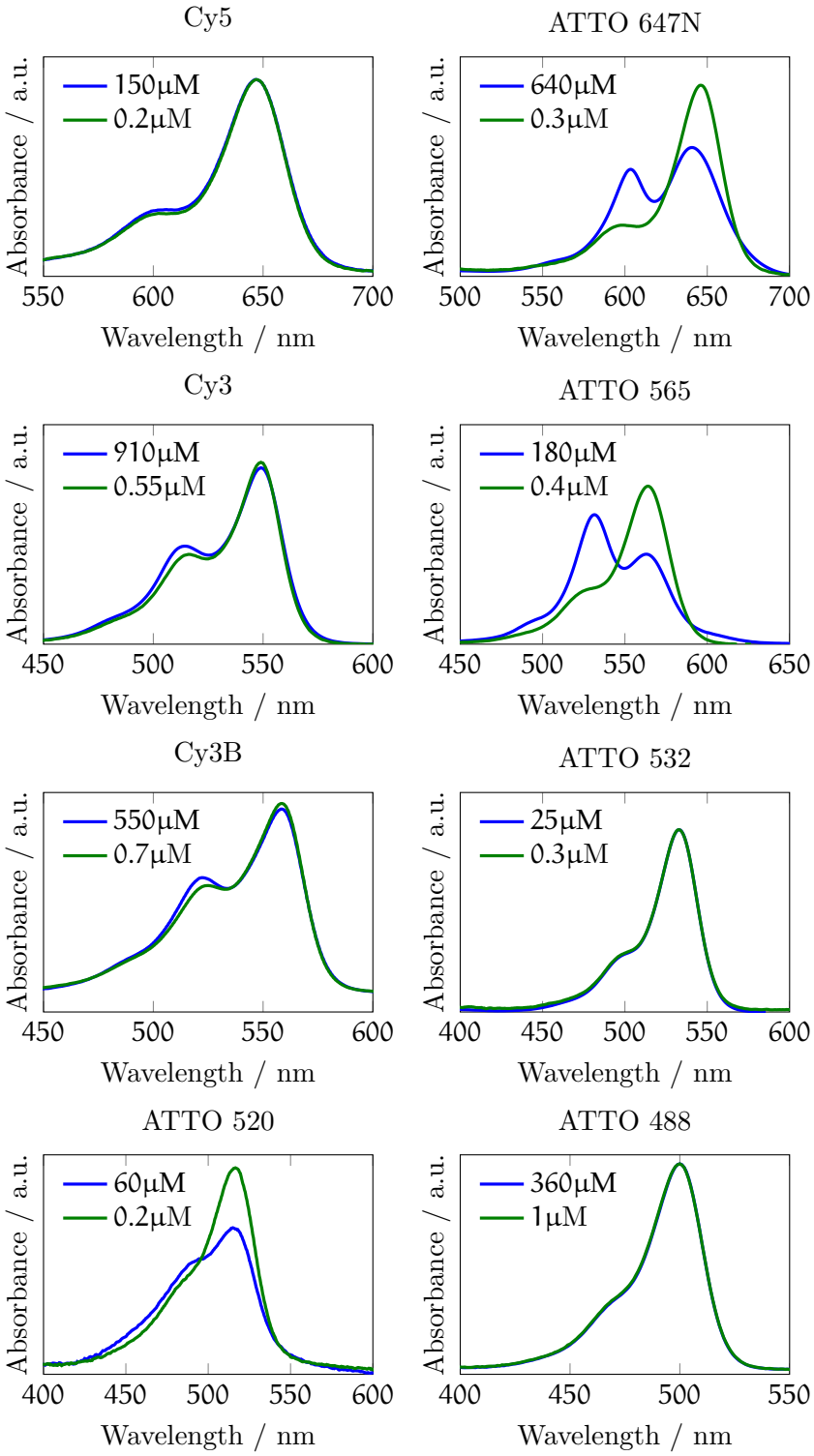

Figure 42: Absorption spectra of free dyes from upper left to bottom right: Cy5, ATTO647N, Cy3, ATTO565, Cy3B, ATTO532, ATTO520, ATTO488 - highly diluted (green) and concentrated (blue) in 20°C H_2O.

Fl−$(GS)_5$K−Fl and homodimer samples are normalized by the value of the maximum at 250 to 400 nm to the maximum of the $(GS)_5$K−Fl spectrum. The extracted homodimer extinction spectra of Cy5 and ATTO565 have a main peak at 603 nm and 531 nm with a shoulder at wavelengths where the spectrum of $(GS)_5$K−Fl shows maximal extinction (s. tab. 5). Extracted Cy3 and ATTO647N extinction spectra show also an hypsochromic peak, but they still have a peak, where peaks of monomeric species are.

Extracted H-Dimer spectra of organic dyes shoulders shoulders[BLSD11][56]. The H-dimer spectrum of rhodamine dyes shows not only a shoulder at wavelengths where the corresponding monomers have their maximum, there are also peaks in the H-dimer spectrum. This was also seen by Fujii et al. [43].

Notwithstanding the low tendency to form dimers in solution of most dyes in solution (compare fig. 42), evaluation of low concentrated dyes in solution $OD < 0.1$, yield spectra of doubly labeled peptides showing blue shifted enhanced absorption, and calculated pure dimer spectra in fig. 44 show isosbestic points and no enhanced absorption to higher wavelengths. Therefore it can be stated, that these changes in spectra are due to a reaction of two species - dimers and monomers.

For comparison we extracted then dimerization constants K_D using two methods shown in tab. 5: We used the high and low (HL) concentration spectra of fig. 42 for the determination of the equilibrium constant K_D^{HL} and the $(GS)_5$K−Fl and Fl−$(GS)_5$K−Fl spectra (Pept.) for the determination of the equilibrium constant K_D^{Pept}. First monomer, dimer and mixed spectra were normalized to fit in the UV wavelength range. Then a linear combination of normalized monomer $Abs_{mono}(\lambda)$ spectrum - low concentration or $(GS)_5$K−Fl- and dimer $Abs_{dimer}(\lambda)$ spectrum was fitted to the spectrum of the mixed species $Abs_{mixed}(\lambda)$ - high concentration and Fl−$(GS)_5$K−Fl spectrum.

$$Abs_{mixed}(\lambda) = \alpha \cdot Abs_{mono}(\lambda) + \beta \cdot Abs_{dimer}(\lambda). \tag{80}$$

With monomeric fraction α and total concentration c_T we calculated dimerization constants K_D using

$$K_D = \frac{1-\alpha}{2\alpha^2 c_T}. \tag{81}$$

One gets total concentrations c_T of $Abs_{mixed}(\lambda)$ of highly concentrated samples directly by the normalization factor of low and high concentrated spectra in the UV-range and the concentration of the low concentrated sample. The last mentioned is determined using literature extinction coefficients (s. tab. 5). For Fl−$(GS)_5$K−Fl an effective concentration c_T of dyes held together in an effective volume is calculated using hydrodynamic radii R_h of 0.84 nm measured by FCS for samples containing Cy5 as acceptor dye and 0.82 nm for samples with

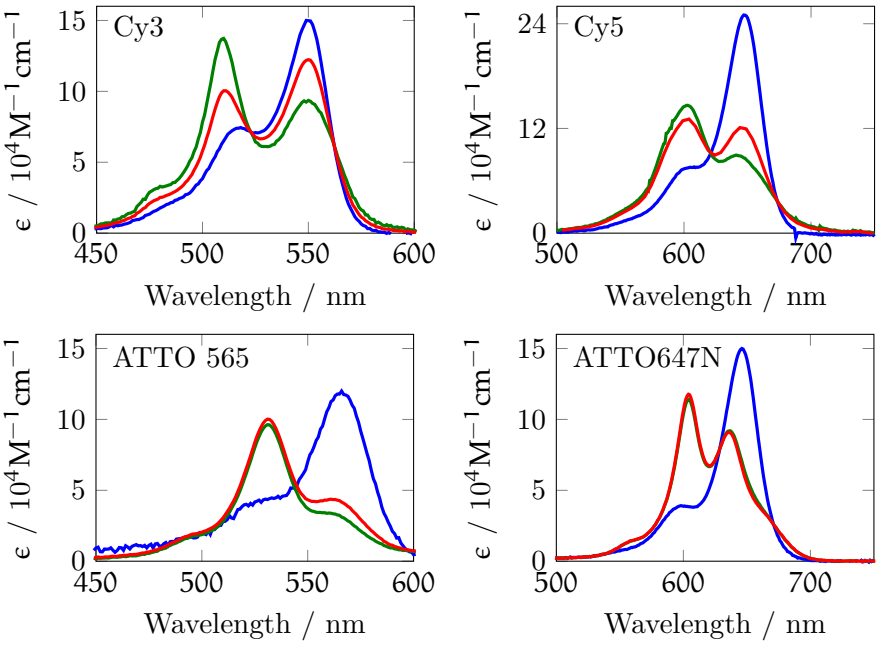

Figure 43: Normalized absorption spectra of doubly, singly labeled peptides and calculated dimer spectrum.

ATTO647N as acceptor dye. The effective volume $V_{eff} = \frac{4}{3}\pi R_h$ is a sphere in which one dye can diffuse around the other one[BLSD11]. With these values the effective concentration is for Cy5 sample 1.35 M and for ATTO647N 1.46 M.

Measurement uncertainties arise mainly from noise in the UV-range of the raw data ($\approx 10\%$). Hence, dimer extinction spectra are not exact and we estimate from the fits an uncertainty for α of 35 %. If one uses this measurement uncertainty, the dimerization constants of the concentrated samples of Cy3, Cy5 and also ATTO565 and ATTO647N are not distinguishable. Assuming for Cy-dyes a 50 % uncertainty, the dimerization constants are still significantly lower. An analogue argumentation for the Fl−$(GS)_5$K−Fl dimerization constants leads to the same result.

Comparing K_D^{HL} and K_D^{Pept} dye by dye we see strong differences. K_D^{Pept} is consequently by one or two magnitudes smaller than K_D^{HL}. Still both experiments give the same dependencies and therefore they are systematic. Keeping this in mind, K_D^{Pept} of Fl_1−$(GS)_5$K−Fl_2 samples are determined for heterogeneous dye pairs.

7.1.2 *Discussion*

Intermolecular free dye self-dimerzation and intramolecular self-dimerization of closely bound organic fluorophores ATTO488, Cy3, Cy3B, Cy5, ATTO520, ATTO532, ATTO565, and ATTO647N were tested. It was possible to compare spectra of free diffusing concentrated solutions

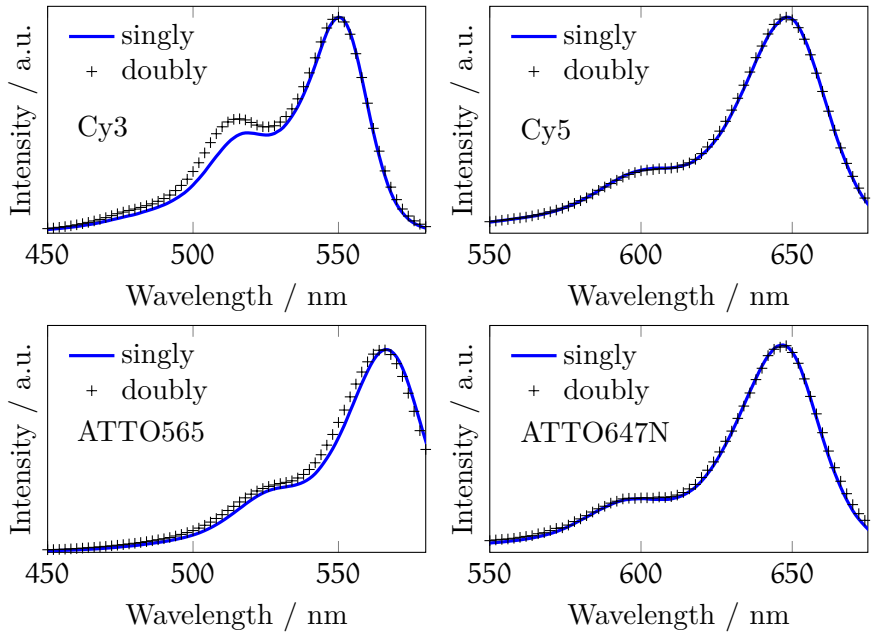

Figure 44: Excitation spectra of $(GS)_5K$–Fl and Fl–$(GS)_5K$–Fl in PBS. The fluorophores Fl are Cy5, ATTO647N, Cy3, and ATTO565. Cy5 and ATTO647 show no differences in their spectral characteristics. ATTO565-$(GS)_5$K-ATTO565 has a slight bathochromic shift to $(GS)_5$K-ATTO565 and Cy3 shows a 10% higher excitation at its shoulder at 511 nm. The excitation of Cy5 and ATTO647N was recorded at an emission wavelength of 680 nm, while Cy3 and ATTO565 excitation was recorded at 580 nm emission.

Sample	λ_M^{max}	λ_D^{max}	ϵ_M^{max}	ϵ_D^{max}
	nm	nm	$M^{-1}cm^{-1}$	$M^{-1}cm^{-1}$
ATTO647N	646	604	150000	79000
ATTO565	566	531	120000	150000
Cy3	549	510	150000	125000
Cy5	647	603	250000	130000

Table 5: Wavelength of absorption maxima of monomeric λ_M^{max} dye species, dimeric λ_D^{max} dye species, maximal extinction coefficient of monomeric ϵ_M^{max} and dimerized ϵ_D^{max} dyes.

Sample	$K_{ass}^{pept}{}^{+\Delta_+}_{-\Delta_-}$ / M^{-1}	$K_{ass}^{HL}{}^{+\Delta_+}_{-\Delta_-}$ / M^{-1}
ATTO647N	170^{692}_{73}	7200^{8000}_{3900}
ATTO565	$40\ ^{167}_{17}$	11000^{16000}_{5000}
Cy3	$0.7\ ^{4.1}_{0.1}$	230^{500}_{170}
Cy5	$7\ ^{30}_{2.6}$	190^{570}_{185}

Table 6: Association constants K_{ass} of ATTO647N, ATTO565, Cy3, and Cy5 determined by measurements of high and low concentrated dye solutions K_{ass}^{HL} and by comparison of $(GS)_5$K–Fl and Fl–$(GS)_5$K–Fl absorption spectra K_{ass}^{pept}. Δ_+ and Δ_- are upper and lower confidence intervals.

of all dyes. For Cy3, Cy5, ATTO565, and ATTO647N we determined dimerization constants of dyes freely diffusing in solution. Pure dimer spectra are encountered and extinction coefficients for the homodimer species were determined.

The organic dyes ATTO647N and ATTO565 are eluded from the HPLC column when the used gradient uses much non-polar solvent. They are showing strong dimerization effects in absorption spectra. The most hydrophilic dye of this study - ATTO488 - has no tendency to form molecular dimers in solution in the concentration range in which we can measure its absorption. The cyanine dyes show low dimerization behaviour in solution. ATTO647N and ATTO565 have only one positive charge that is delocalized over the chromophoric part of the molecule. Therefore we have here a mixture of interaction effects. Polar groups at these dyes provide hydrophilicity. Electrostatic interaction of the charges at the polar groups is also possible and has a repulsive effect. This might explain, why labeling of ATTO488, ATTO532, and Cy3B to $(GS)_5K$ peptides is difficult. This was also seen by other workgroups, who established labeling chemistry with NHS esters or maleimid coupling.[81] Therefore ATTO647N and ATTO565 show the strongest dimerization of this study.

The changes in absorption spectra in fig. 44 that are seen for ATTO647N, ATTO565, ATTO520, and also slightly for Cy3 and Cy3B are all bathochromical shifts of over 40 nm. These bathochromic shifts are characteristic for H-dimerization of organic molecules. Attached to Fl−$(GS)_5$K−Fl ATTO647N and ATTO565 show dimerization with the same shift of absorption bands but the bathochromic shift is larger. Here also Cy5 and Cy3 show dimerization with maxima which are shifted bathochromic. The fact, that the fraction of fluorescing species are for Cy5 and Cy3 Fl−$(GS)_5$K−Fl samples higher than for ATTO647N and ATTO565 reflects the known behaviour of free dye sample. The hypothesis of H-dimerization of the dyes is also supported by excitation spectra of Fl−$(GS)_5$K−Fl samples showing only fluorescence excitation of monomeric species of Fl−$(GS)_5$K−Fl sample, because H-dimers do not fluoresce. Cy3 deviates with an increased fluorescence for the excitation at the bathochromic shifted dimer peak. This deviation is rather small compared to the elevated absorption at this wavelength and can be taken into account in simulations for further analysis of the characteristics of the Cy3 dimerization itself.

Compared to Cy3 and Cy5 the dimerization constant of ATTO565 and ATTO 647N is at least an order of magnitude higher. This is shown for free dyes in high concentrated solution and also by measuring the dimerization constant for the dyes with the method using Fl−$(GS)_5$K−Fl constructs to limit the effective volume the dyes can move.

The dimerization constant determined by different dye concentrations is always higher than the one determined for Fl−$(GS)_5$K−Fl sam-

ples. This might be due to enthalpic contributions of the GS peptide. This is an effect we have already seen in sec. 6.

Extinction coefficients of pure dimers of Cy3, Cy5, ATTO647N, and ATTO565 were determined and show values similar to monomeric dyes. The molecular extinction coefficients range from 79000 $M^{-1}cm^{-1}$ for ATTO647N to 150000 $M^{-1}cm^{-1}$ for ATTO565. This might be interesting for switchable absorbers where chemical structures change their structure light induced[95] or by electric pulses.

7.2 INTRAMOLECULAR DIMERIZATION BETWEEN DIFFERENT DYES

self-dimerization of molecules and especially of fluorophores is not only of academic interest. It is used as reporter for contact formation[44, 123] or can give unwanted effects in FRET-experiments. In single-molecule FRET experiments of very flexible biomolecules dye pairs may introduce artifacts because of unwanted dye flickering arising from dimer quenching, that may come from overlapping of molecular orbitals. This quenching can lower acceptor intensities and shift distance distributions to higher values. Quantification of such effects and its relation to interaction strength of dye dimers in solution is usually not examined.

Here we present a technique that helps to compare dimerization constants of different heterogeneous and homogeneous dye pairs. Therefore we use the technique established calculating K_D^{Pept} in sec. 6. An effective concentration of two bound dyes at oligopeptides together with the fraction of monomeric species given by absorption measurements of this sample yields K_D^{Pept}.

7.2.1 *Measurements and results*

Five $Fl_1-(GS)_5K-Fl_2$ samples with Fl_1/Fl_2 pairs (A) Cy3B/Cy5, (B) Cy3/Cy5, (C) ATTO532/ATTO647N, (D) ATTO565/ATTO532 and (E) ATTO488/Cy5 were purified using HPLC as described in sec. 3.3 as well as $(GS)_5K-Fl_1$ and $(GS)_5K-Fl_2$. Steady-state ensemble absorption spectra, fluorescence spectra, TCSPC and FCS measurements of a purified sample were recorded. $Fl_1-(GS)_5K-Fl_2$ samples showed significant alterations after two to three weeks. Experiments were made by diluting concentrated stocks in PBS and GdCl solution by three orders of magnitude.

Excitation spectra in fig. 46 at acceptor emission of $Fl_1-(GS)_5K-Fl_2$ are superpositions of donor and acceptor only excitation spectra. Exceptions are $Fl_1-(GS)_5K-Fl_2$ samples with Cy3 and Cy3b as Fl_1 showing slightly increased excitation at $511\ nm \pm 1$ nm and $515\ nm \pm 1$ nm.

Absorption spectra of samples, dissolved in PBS and GdCl containing under 1 µM sample concentrations, are shown in fig. 48. For compari-

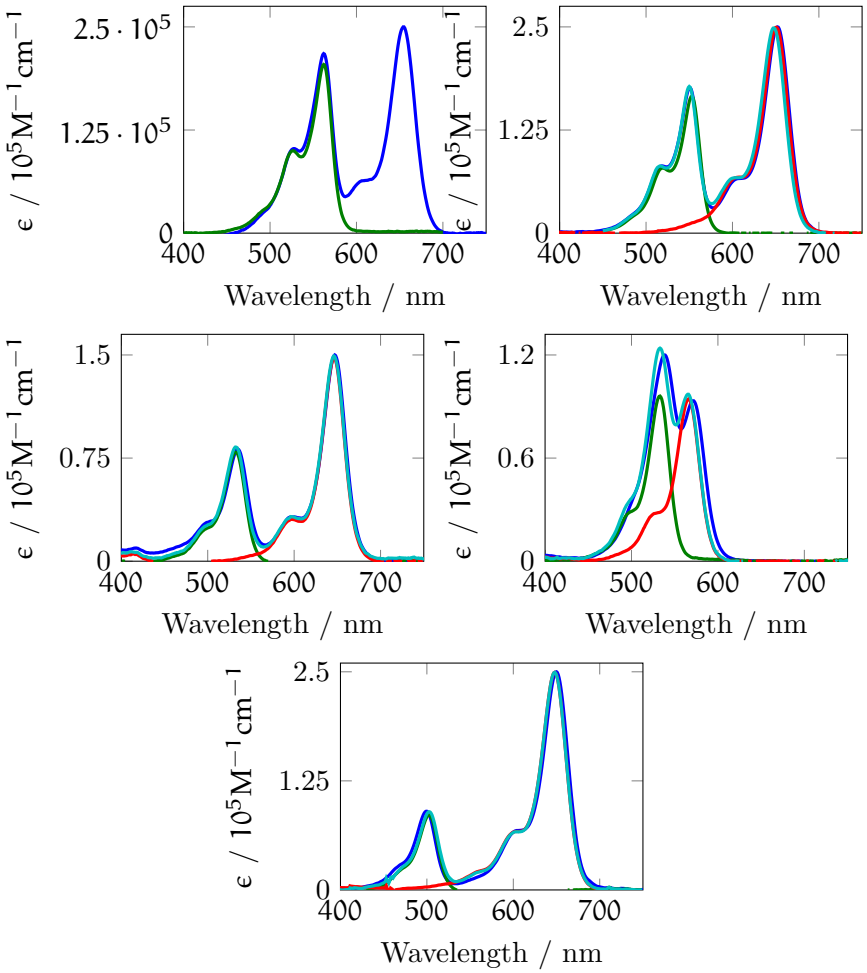

Figure 45: Fl_1−$(GS)_5$K−Fl_2-spectra in 7 M GdCl of Cy5/Cy3B, Cy5/Cy3, ATTO647N/ATTO532, ATTO565/ATTO532, and Cy5/ATTO488 (top left - bottom). The Fl_1−$(GS)_5$K−Fl_2-spectra are linear combinations of Donor-$(GS)_5$K and Acceptor-$(GS)_5$K-spectra, which were shifted up to 3 nm for fitting. The fit is in good accordance to the raw data.

son $(GS)_5$K−Fl_1 and $(GS)_5$K−Fl_2 samples shown in fig. 47. All singly labeled samples have bathochromic shifts between 4 nm (ATTO647N) and 8 nm (Cy5) in GdCl solvent compared to PBS. All GdCl absorption spectra of Fl_1−$(GS)_5$K−Fl_2 are superpositions of Fl_1 and Fl_2 GdCl absorption spectra (see fig. 45). We assume therefore, that acceptor peaks are in GdCl not influenced by dye interactions. Absorption spectra of Cy5-$(GS)_5$K-Cy3B (A), Cy5-$(GS)_5$K-Cy3 (B) and Cy5-$(GS)_5$K-ATTO488 (E) have new peaks arising blue shifted to the donor only absorption maximum. For (A), (B) and (C) and (E) shapes of the acceptor part of Fl_1−$(GS)_5$K−Fl_2 are identical [(C) has a slight shift at the ATTO647N shoulder].

We conclude, that new absorption bands only occur near the donor maximum. Therefore PBS and GdCl absorption spectra of all absorption spectra are shifted analogue to $(GS)_5$K−Fl acceptor spectra

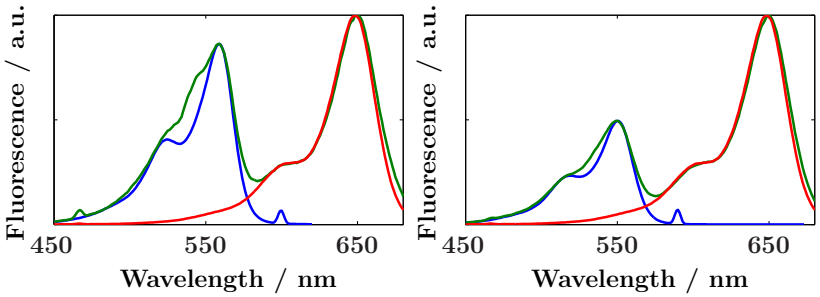

Figure 46: Excitation spectra of $(GS)_5K{-}Fl_1$, $(GS)_5K{-}Fl_2$, and $Fl_1{-}(GS)_5K{-}Fl_2$ samples of Fl_1/Fl_2 Cy3B/Cy5 (left) and Cy3/Cy5 (right) in PBS. Besides Cy3 and Cy3B all $Fl_1{-}(GS)_5K{-}Fl_2$-spectra are a linear combination of $(GS)_5K{-}Fl_1$ and $(GS)_5K{-}Fl_2$.

and are normalized to the acceptor maximum. Assuming that extinction coefficients of free acceptors are also valid for labeled peptides in PBS and GdCl for $(GS)_5K{-}Fl_2$ and $Fl_1{-}(GS)_5K{-}Fl_2$, difference spectra can be calculated to get the spectra of the dimer species of the $Fl_1{-}(GS)_5K{-}Fl_2$ samples itself.

To calculate difference spectra, GdCl spectra of $Fl_1{-}(GS)_5K{-}Fl_2$ are shifted to overlap with their PBS absorption spectrum in the acceptor absorption wavelength range. The subtraction of normalized GdCl from normalized PBS spectra yield difference spectra that are interpreted as heterodimer spectra (s. fig. 48). In these difference spectra oscillations occur at acceptor wavelength range. The difference spectrum of Cy5-$(GS)_5$K-Cy3B shown in fig. 48 (A) has a peak blue shifted to the Cy3B absorption in GdCl and to the donor only spectrum of both solvents. It looks like a usual dye spectrum with a shoulder blue shifted to its maximum at 542 nm. The difference spectrum of Cy5-$(GS)_5$K-Cy3 in fig. 48 (B) has a new blue shifted peak at 535 nm, whereas fig. 48 (C) shows only oscillations at donor wavelength like those at acceptor wavelength. Fig. 48 (D) shows a new peak blue shifted to the ATTO532 peak at 516 nm and in fig. 48 (E) a peak at the maximal absorption wavelength ATTO488 shows slightly larger absorption than the acceptor wavelength oscillations.

Normalization of $Fl_1{-}(GS)_5K{-}Fl_2$ spectra in the UV-range to GdCl spectra gives spectra depicting same fluorophore concentrations. Difference spectra show only small oscillations for Cy5-$(GS)_5$K-Cy3 and Cy5-$(GS)_5$K-Cy3B. Therefore we can deduce from changes of acceptor absorption from GdCl to PBS solution dimerization constants $K_D^{Cy5-(GS)_5K-Cy3}$ and $K_D^{Cy5-(GS)_5K-Cy3B}$ by taking the difference of UV-range normalized acceptor absorption maxima. This is not possible for ATTO565-$(GS)_5$K-ATTO532 and Cy5-$(GS)_5$K-ATTO488. Either donor absorption overlaps with acceptor absorption or no new dimer peak is distinguishable in our studies (s. fig. 48). Nevertheless, we get for the monomeric fraction α of Cy3/Cy5 $\alpha = 58.4\%$ and for Cy3B/Cy5 an $\alpha = 50.7\%$. With hydrodynamic radii of 1.41 nm one

gets dimerization constants of $K_D^{Cy5-(GS)_5K-Cy3} = 0.07^{0.2}_{0.007} M^{-1}$ and $K_D^{Cy5-(GS)_5K-Cy3B} = 0.7^{1.1}_{0.43} M^{-1}$ respectively.

Normalization by comparing excitation spectra like it was done for $Fl-(GS)_5K-Fl$ samples in sec. 6, where we were inspired by Marmé et al. [68], is not possible here. We must take the FRET efficiency E_{FRET} as an unknown parameter, even if the peptides are constructed in a way, that the efficiency is up to 1. With other quenching effects real FRET can still be below 1 and even if we use freshly purified samples there is an uncertainty about how many dyes are still intact. But by analysis of FRET values, we get from the data, we get insight into quenching strength by electronic transfer and dimerization effects.

Usually FRET efficiencies are measured by intensities I or fluorescence lifetimes τ[64]

$$E_{FRET} = 1 - \frac{I_{DA}}{I_D} \tag{82}$$

$$= 1 - \frac{\tau_{DA}}{\tau_D} \tag{83}$$

$$= \left(1 + \frac{r^6}{R_0^6}\right). \tag{84}$$

DA denoting samples having donor and acceptor and D means only donor species. The distance dependency of E_{FRET} depends on Förster radius $R_0^6 = \frac{9000(\ln 10)\kappa^2 Q_D}{128\pi^5 n^4} \int_0^\infty F_D(\lambda)\epsilon_A(\lambda)\lambda^4 d\lambda$. $Fl_1-(GS)_5K-Fl_2$ samples with Cy5 and ATTO647N as acceptors have hydrodynamic radii of about 0.837 nm to 0.816 nm measured by FCS. Assuming κ^2 of 2/3, using quantum yield data given in tab. 8 we get förster radii between 5.3 nm and 7 nm tab. 9 for all samples. Therefore E_{FRET} should deviate at maximum by 0.2% from 1 for all $Fl_1-(GS)_5K-Fl_2$ samples.

In tab. 7 experimental values for E_{FRET} in PBS and GdCl are given. In all cases FRET efficiencies do not vary between solvents. On the other hand we know, remembering the aforementioned results, that dimerization with acceptor and donor quenching happens in $Fl_1-(GS)_5K-Fl_2$ constructs in PBS. Therefore molecular brightness quality factors are established in eq. (85).

$$P = \frac{\frac{I^D_{DA}}{\phi_D} + \frac{I^D_{AD}}{\phi_A}}{\frac{I^D_D}{\phi_D}} \tag{85}$$

$$P_{acc} = \frac{I^A_{AD}}{I^A_A} \tag{86}$$

$$\phi_{D/A} = \frac{\hat{I}^{D/A}_{D/A}}{OD_{D/A}} \tag{87}$$

$$I^x_y = \frac{\hat{I}^x_y}{OD_x} \tag{88}$$

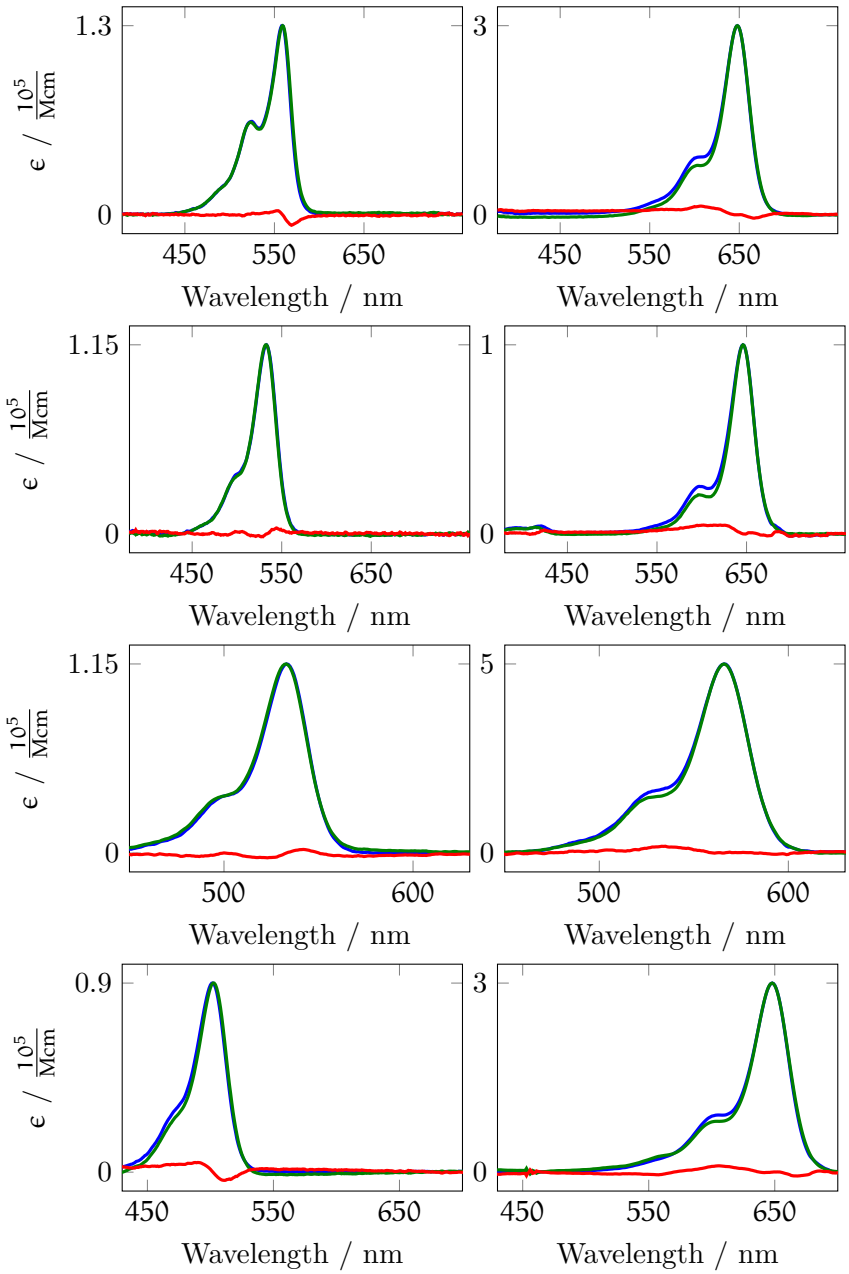

Figure 47: Extinction spectra of $(GS)_5K$—Fl samples of (A) Cy3B and Cy5, (B) Cy3 and Cy5, (C) ATTO532 and ATTO647N, (D) ATTO532 and ATTO565, (E) ATTO488 and Cy5. All items are $(GS)_5K$—Fl-spectra acceptor (left) and donor (right) extinction in pbs (blue), gdcl (green) and a difference spectrum of both (red). $(GS)_5K$—Fl-spectra are normalized to the maximal extinction coefficient of free fluorophore.

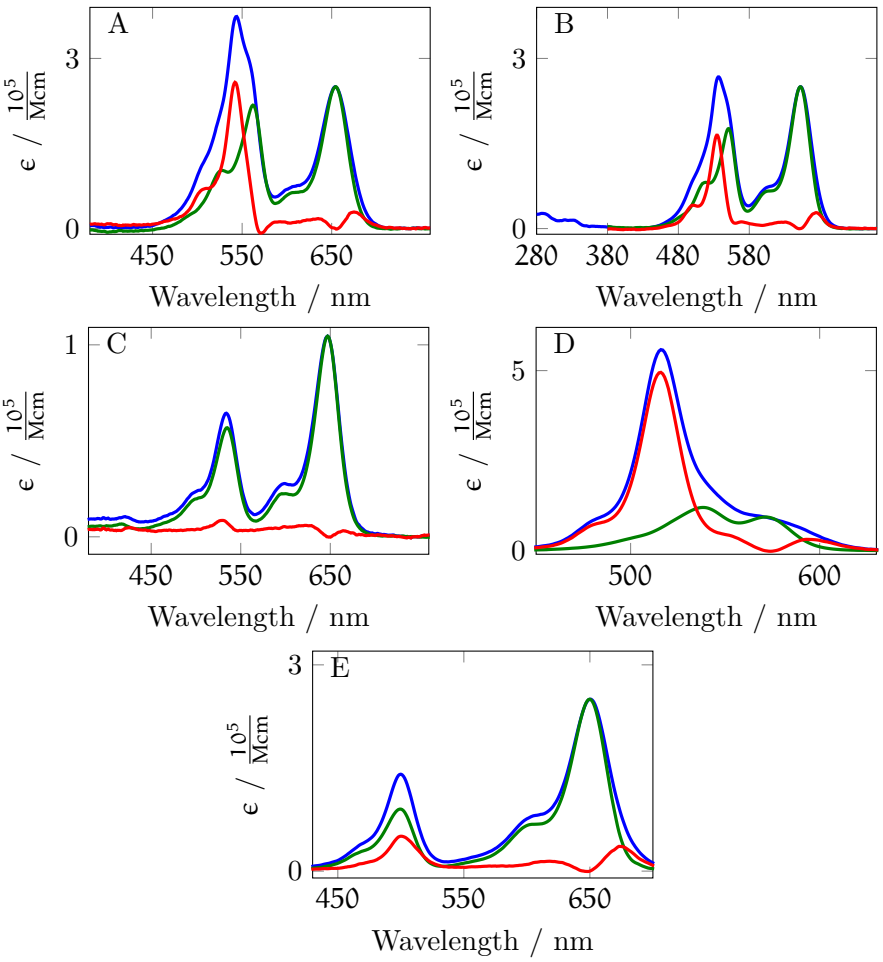

Figure 48: Extinction spectra of $Fl_1-(GS)_5K-Fl_2$ samples of (A) Cy5/Cy3B, (B) Cy5/Cy3, (C) ATTO647N/ATTO532, (D) ATTO565/ATTO532 and (E) Cy5/ATTO488. Shown are absorption spectra of $Fl_1-(GS)_5K-Fl_2$ in PBS (blue), GdCl (green) and a difference spectrum of both (red) are plotted. All spectra were corrected for spectral shifts. GdCl absorption spectra are always bathochromic shifted to PBS absorption spectra: Cy3 and Cy3B are 7 nm, ATTO 532 is 5 nm, ATTO647N is 4 nm, ATTO565 and ATTO488 are 6 nm shifted. The spectra are normalized at acceptor maximum to literature values of the free acceptor fluorophore.

P quantifies how many photons, which are available for donor emission or via FRET for acceptor emission upon donor excitation, are emitted by $Fl_1-(GS)_5K-Fl_2$. To accomplish this, raw intensities $\hat{I}$, that is the maximum of the intensity spectrum, are corrected by the optical density at the excitation wavelength to yield intensities I (eq. (88)). If a dye is excited and the dyes are only coupled by FRET interactions, the emission of each dye is weighted by its quantum yield ϕ. Therefore intensities of donor or acceptor at $Fl_1-(GS)_5K-Fl_2$ sample $I^D_{DA/AD}$ excited at donor wavelength are furthermore normalized by quantum yields of donor ϕ_D (eq. (87)). The intensities of $(GS)_5K-Fl$ labeled with donor excited at donor wavelength are normalized in the same way by quantum yields of donor/acceptor $\phi_{D/A}$. P is then the comparison of donor only labeled and $Fl_1-(GS)_5K-Fl_2$ species intensity. If P is 100%, a $Fl_1-(GS)_5K-Fl_2$ construct is as bright as its donor. A lower P indicates fluorescence quenching of the whole $Fl_1-(GS)_5K-Fl_2$ molecule. P_{acc} defined in eq. (86) shows in contrast, how strong the quenching of non dimerized acceptors is. Comparison of both values gives hints to the interactions of the quenching processes.

The measurements were always made with the same spectrometer settings. Only excitation wavelengths of donor and acceptor species were varied according to different optical properties of the dyes. All fluorescence spectra were in this study corrected for wavelength dependent emission and detection efficiencies of the fluorometer.

Cy3/Cy5 (Cy3B/Cy5) has in PBS P = 35% (40%) and in GdCl solvent 97% (100%). Therefore the excitation energy available by the donor is, besides usual quenching processes of the dyes themselves, fully converted to fluorescence by both dyes in high denaturant. In PBS about 2.5 times less photons are emitted by both constructs. Results for P_{acc} are similar. P_{acc} amounts to 43% (30%) for Cy3/Cy5 (Cy3B/Cy5) in PBS and 93% (95%) in GdCl. Cy5 of Cy3-$(GS)_5$K-Cy5 and Cy3B-$(GS)_5$K-Cy5 is in GdCl as bright as acceptor only species in GdCl, but is strongly quenched in PBS. For Cy3/Cy5 it is clear, that the FRET-efficiency in GdCl shows the real FRET of the construct, because whether Cy3 nor Cy5 are quenched and the FRET value in GdCl is 90 %. The difference to 100% FRET efficiency may be due to heterogeinity in the sample with donor only species resulting from acceptor bleaching. For Cy3B/Cy5 we get FRET-efficiencies of 74 and 72 % in PBS and GdCl, while Cy3B nor Cy5 are quenched in GdCl. Besides, $P > P_{acc}$ in PBS shows more luminescence of Cy5 at the construct when excited at 630 nm than luminescence of Cy5-only species when excited at 630 nm. Because E_{FRET} is significantly lower than 100%, while P_{acc}, P are 100 % in GdCl indicating that the construct is as bright as donor species itself and no quenching of the dyes occurs, we conclude, that the constructs show a significant amount of donor only species.

$Fl_1-(GS)_5K-Fl_2$	E_{FRET} / %		P / %		P_{acc} / %	
Fl_1/Fl_2	PBS	GdCl	PBS	GdCl	PBS	GdCl
Cy3/Cy5	93 ± 3	90 ± 2	35 ± 3	97 ± 15	43 ± 1	93 ± 4
Cy3B/Cy5	74 ± 2	72 ± 2	40 ± 4	100 ± 10	30 ± 2	95 ± 7
ATTO532/ATTO647N	98 ± 1	95 ± 1	30 ± 1	73 ± 3	85 ± 24	103 ± 2
ATTO488/Cy5	96± 1	90 ± 1	22 ± 1	70 ± 1	52 ± 1	97 ± 1

Table 7: FRET efficiency E_{FRET} vs. molecular brightness quality factors P of the whole $Fl_1-(GS)_5K-Fl_2$-constructs and P_{acc} of the acceptor in $Fl_1-(GS)_5K-Fl_2$. FRET efficiencies are nearly 100 % for all samples, while P is in PBS significantly lower by factor 2-3. In GdCl P values show, that acceptors are not quenched, while for ATTO532-$(GS)_5$K-ATTO647N and Cy5-$(GS)_5$K-ATTO488 even in GdCl quenching of the whole construct occurs. Therefore donors are quenched in these constructs.

E_{FRET} of ATTO532/ATTO647N and ATTO488/Cy5 in PBS and GdCl indicates high FRET with values near 100 %, but both have P values of 70 % in GdCl. In PBS these are 2.5 to 3 times lower. This indicates that the constructs show strong quenching in PBS and are still quenched in GdCl solvents. High P_{acc} of 103% and 97 % in GdCl suggest that in both samples quenching is mainly due to quenched donors.

7.2.2 *Discussion*

In this section we have determined dimerization behaviour of heterodimers analogue to sec. 7.1, where it was done for homodimerization. We are able to determine pure heterodimer spectra and heterodimer extinction coefficients of Cy5-$(GS)_5$K-Cy3B, Cy5-$(GS)_5$K-Cy3, and ATTO565-$(GS)_5$K-ATTO532. The brightness of a heterodimer is characterized indicating other quenching processes than H-dimerization for ATTO488-$(GS)_5$K-Cy5 and ATTO532-$(GS)_5$K-ATTO647N.

Absorption and excitation spectra of $Fl_1-(GS)_5K-Fl_2$ are a linear combination of corresponding $(GS)_5K-Fl_2$ and $(GS)_5K-Fl_1$ spectra. We found a small solvent chromophore bathochromic shift of ≈ 6 nm of $(GS)_5K-Fl_2$ and $(GS)_5K-Fl_1$. Otherwise, there is no change or maximal 10% change in spectral shape between PBS and GdCl solvent for monomeric dyes. Spectra of ATTO488-$(GS)_5$K-Cy5 and ATTO532-$(GS)_5$K-ATTO647N are a linear combination of monomeric spectra in PBS. Cy5-$(GS)_5$K-Cy3, Cy5-$(GS)_5$K-Cy3B, and ATTO647N-$(GS)_5$K-ATTO532 however change their absorption spectrum due to H-dimerization. H-dimerization manifests itself by new bathochromically shifted absorption bands that are not fluorescent.

All $Fl_1-(GS)_5K-Fl_2$ samples however are quenched to an overall brightness of 20 % - 40% in PBS. This is the fraction of the overall num-

ber of photons that are expected to be emitted, when considering quantum yields of the dyes themselves. For Cy3-$(GS)_5$K-Cy5 and Cy3B-$(GS)_5$K-Cy5 in GdCl the overall fluorescence is as high as expected for the two dyes whether FRET occurs or not, whereas ATTO532-$(GS)_5$K-ATTO647N and ATTO488-$(GS)_5$K-Cy5 still show 70 % quenching in GdCl. Therefore there are other mechanisms responsible for quenching than H-dimerization. This may be pure electronic transfer mechanisms. Cy3-$(GS)_5$K-Cy5 is the brightest sample in our analysis and Cy3B-$(GS)_5$K-Cy5 is slightly more quenched.

As far as we know, there exist only few spectroscopic datasets in the literature analyzing dimerization in detail.[46, 78, 79] Here we have exactly two dyes at one peptide and see therefore interactions of only these two dyes. Because of clear chromatograms from RP-HPLC we have a sample purity of over 99%. Comparison of spectra of free and singly-labeled dyes show negligible changes in spectral properties of the dyes by the labeling procedure itself. Therefore the shape of pure dimer spectra that we present here are precise up to 10 %, due to uncertainties in normalization of noisy data in the UV-wavelength range.

This enables us to determine dimerization constants of $K_D^{Cy5-(GS)_5K-Cy3} = 0.07^{0.2}_{0.007}M^{-1}$ and $K_D^{Cy5-(GS)_5K-Cy3B} = 0.7^{1.1}_{0.43}M^{-1}$ for Cy3-$(GS)_5$K-Cy5 and Cy3B-$(GS)_5$K-Cy5. Dimerization constants of these constructs are biased by influences of the oligopeptides. Therefore these values might be higher for dyes that are constrained to stay in a 10^{-24}l volume without any other influences besides stacking of the dye molecules. Groups have measured spectra containing heterodimers.[46, 78, 79, 88, 122] We now present here the first experimentally determined pure heterodimer spectra of organic dyes in solution.

An interesting property of Cy3 and Cy3B complexes with Cy5 is, that these molecular complexes show absorption changes that we attribute to H-dimerization, but also show fluorescence emission of its dimerized species. This might be due to coupling of locally separated bands that yield fluorescence emission. An analogous effect was also seen for homodimers of Cy3 and Cy3B, but not for Cy5. Therefore we account this effect to be a specific property of Cy3 and Cy3B.

Regarding analysis of molecular brightness of the hetero-labeled samples, one has to bear in mind, that due to deterioration of dyes, especially acceptor dyes are sensitive to photodestruction[90] and it is known that ozone destroys cyanine dyes even without irradiation.[38] Therefore the analysis of the data is prone to errors by deterioration, if no single-molecule studies are made, where signals of single molecules can be sorted into signals originating from FRET-samples and donor/acceptor only species.[5] Nevertheless, hetero labeled samples checked against changes in fluorescence properties right after labeling and it was determined that the Fl–$(GS)_5$K–Fl constructs are

stable for up to a week. Measurements were taken three workdays in a row and it was no trend seen in spectroscopic data.

Because Cy3-$(GS)_5$K-Cy5 has the highest molecular brightness quality factor and the lower dimerization constant in PBS compared to Cy3B-$(GS)_5$K-Cy5 we suggest to use the Cy3/Cy5 pair as FRET pair in ensemble and single-molecule studies of very flexible structures. The data will be the least influenced by complexation due to H-dimerization and they will yield the highest photon statistics.

8

CONCLUSION AND OUTLOOK

This work elucidates changes in end-to-end contact dynamics of unstructured glycine-serine oligopeptides by glycosylation and attachement of organic fluorophores at peptide ends. We studied the effects of glycosylation and denaturing conditions on peptide dynamics. The strong interactions of organic fluorophores in aqueous solution as cause for fluorescence quenching were then further examined with regard to the nature of these interactions. We identified different fluorescence quenching interactions and quantified their contribution for all investigated fluorophore combinations.

Changes in the energy landscape from non- to glycosylated unstructured glycine-serine oligopeptides were found using PET quenching of MR121 and Trp to estimate end-to-end contact rates via FCS. We found that β-galactose attached to serine residues via O-glycosylation increases the hydrodynamic radius of the used glycine-serine peptides. Rate constants at different temperatures are viscosity-controlled. No internal friction was detected, but the temperature dependence of end-to-end contact rates shows increased activation enthalpies for glycosylated peptides that are partially compensated by entropy effects.[BBP$^+$11]

In the literature there is no consistent picture about the question how glycans influence the biophysical properties of glycoproteins. For N-glycosylated proteins removal of glycans from folded proteins has not shown any effect on their activity, but their stability and folding kinetics were altered.[97]. It was recently shown for glycosylated dihydrofolate reductase, that glycosylation of the protein increased the stability of the protein against thermal denaturation.[102] In a study, where O-glycosylation of a Gc-MAF-analogue was analyzed, a loss of about 1 kcal/mol per glycosylation event in the folded– unfolded transition was observed.[100]

We have examined a small oligopeptide glycosylated at every repeating unit. Other reports show, that specific glycosylation can strongly alter the kinetic behaviour in a way that for now is unpredictable. A systematic exploration of the GS oligopeptides, where selected serine units are specifically glycosylated could help with a better understanding of this question.

Concluding, PET combined with FCS and TCSPC reveals biophysical properties of oligopeptides especially on conformational dynamics. The results affirm qualitatively previously formulated assumptions regarding changes in end-to-end contacts. Enthalpic contributions to protein folding were quantified. Predictions of dynamic behaviour of biomolecules entirely based on their structure are nevertheless still not possible.

Another interesting question is if there are other reporter systems that can report on end-to-end contact for use in FCS. We have changed the reporter system from PET quenching reporters to reporters quenching via dimerization. Therefore Trp was exchanged at the carboxylic end of glycine-serine oligopeptides by Lys-MR121. This slightly alters the energy landscape of the whole oligopeptide. For measurements in high denaturant solution, end-to-end contact formation rates of the glycine-serine oligopeptides could be determined within a factor of 1.7 compared to PET-quenching experiments.

Besides, in solutions containing less than 3 M denaturant [GdCl] the observed fluorescence signal in a confocal FCS measurement rapidly decreases. This is because of the strong dimerization constant of MR121. Over 90 % of MR121-$(GS)_5$K-MR121 do not fluoresce for more than a few milliseconds and thus while diffusing through the focal volume. The less GdCl from 3 M GdCl is in the solution, the less accurate are the determined contact rates.

On the one hand, the PET reporter system of MR121 and Trp is a good choice to measure end-to-end contact kinetics in aqueous solution. On the other hand, in denaturant solution the MR121 dimerization based reporter system has advantages regarding accuracy of fits to the correlation curves. A smaller complex stability of quencher and fluorescent molecule in unstructured proteins result also in a decreased amplitude of the correlation curve decay. Therefore a reporter system with a higher binding constant can be advantageous to Trp/MR121.

The strong dimerization process of some organic fluorophores that translates into fluorescence on-off blinking might further be applied in modern super-resolution microscopy. Fluorophores that are non-fluorescent over sufficiently long time can enhance resolution of wide-field microscopy setups when single-molecule localization and successive image reconstruction is used. In this approach most fluorescent reporters are turned in an off-state while the few remaining single-molecule signals are imaged with high precision. There are two possibilities, where the long lasting non-fluorescing states of homodimers might be used:

- Having the right salt and buffer conditions, fluctuations of opening and closing dimer-peptide probes specifically attached at binding sites of interest on macromolecules in buffer or cells could be used for further resolution enhancement.

- It might also be possible to attach these probes at specific binding sites, tune conditions such that all fluorophores are dimerized, and then irradiate them. As soon as single fluorophores within a dimer complex get photobleached, the other fluorophore can switch on and fluoresce until it is also photobleached.

The reconstruction methods give resolution enhancements by determination of the center of point spread functions of single emitters that

are spatially isolated such, that the distance between two emitters is greater than the size of the point spread function as determined by diffraction. Thus spatial resolution is enhanced by stretching spatial informations in time. This needs emitters that do not fluoresce for a long time compared to the time they are in a fluorescent state. The ratio between non-fluorescent time and fluorescent time r and localization uncertainties of single emitters σ_{se} are values limiting resolution of super-resolution techniques.[119]

$$r = \frac{k_c}{k_o} = K \tag{89}$$

$$\sigma_{se} = \frac{\sigma}{\sqrt{N}} \tag{90}$$

For the stochastic optical reconstruction method, $r = 100$ is desirable with fluorescent times of the emitters of at least 1 ms.[112] The whole MR121-$(GS)_5$-MR121 construct has $r = K \approx 10$ in PBS. Getting fast cameras in the future with high frame rates up to 10 kHz, it might be possible to use it as such an emitter. One could integrate a reactive amino acid into into the middle of the oligopeptide to bind it specifically to an antibody. If this antibody binds specifically at structures of a cell, then the fluctuations that both fluorophores produce can be used as an emitter reporting the position of this specific structural element of the cell. Then the blinking rate is only dependent on the used biomolecule holding the two fluorophores together.

At last we examined the interactions of different organic fluorophores that are typically used in single-molecule FRET measurements to examine distance distributions in biomolecules. These fluorophores were Cy5, ATTO647N, Cy3, Cy3B, ATTO488, ATTO565, ATTO520, and ATTO532. For very flexible structures that exist e.g. in intrinsically disordered proteins, distance dependent FRET measurements can be distorted by fluorescence quenching of the acceptor fluorophore due to dimerization or other contact induced quenching.

Consequently, we looked at the dimerization interactions analogue to the MR121 investigation by coupling of two fluorophores of the same kind at the amino end of the $(GS)_5K$ oligopeptide and the amino side chain of the attached lysine. We tested a new method that only uses absorption spectra of singly and doubly labeled peptides to get pure dimer spectra of homo-dimers and equilibrium constants of dimerization. Comparison of dimerization constants shows that ATTO565 and ATTO647N have stronger homodimerization interactions than Cy5 and Cy3. Both techniques showed the same order of magnitude for dimerization constants for the freely dissolved fluorophores, contrasting the significantly lower values for fluorophores that are attached to the oligopeptide. This might be due to influences from the unstructured oligopeptide statistically pulling at the dimerized fluorophores.

Hypsochromic shifts give evidence for H-dimerization. The strong dimerization of ATTO647N, ATTO565 (s. fig. 42) and MR121 (s. sec. 6) fit into suggestions made by other groups. [19, 69] It is still an open question if larger chromophoric systems in fluorophores favor so called pi-pi interactions.[69] We are not able to answer this, there might be a tendency of enhanced aggregation of fluorophores with larger chromophoric system.

It was reported that steric effects of bulky substituents may drastically decrease or prevent the aggregation of molecules.[19] Our data reveal these steric effects. Dimerization properties of ATTO565 are similar to properties found for MR121.[BLSD11][68] ATTO520 and ATTO647N show also high selfdimerization. Although Cy5 is also a hydrophobic fluorophore, its equilibrium constant for selfdimerization is low. Cy3, ATTO488, ATTO532, and Cy3B also show a low tendency for selfdimerization and together with Cy5, all of them have at least one SO_3^- group hindering aggregation.

Extinction coefficients of several H-dimers of organic fluorophores were measured and reported in this work. The maximal extinction coefficients of H-dimers of ATTO565 and Cy3 are roughly the maximal extinction coefficients of their monomeric fluorophore species. Extinction coefficients of Cy5 and ATTO647N are much smaller for their H-dimers than for their monomeric species.

H-dimers are non-fluorescent. If one attaches fluorophores at specific binding sites in conditions such that the fluorophores are dimerized, the maximal absorption is hypsochromically shifted to the monomeric flourophore species. Using these dimers as FRET acceptors, they can be used as dark quencher molecules in future applications.

Heterodimerization was tested intramolecular. From all tested fluorophore pairs Cy5-$(GS)_5$K-Cy3, Cy5-$(GS)_5$K-Cy3B, and ATTO565-$(GS)_5$K-ATTO532 show significant H-dimerization. Absorption does not change for $(GS)_5K{-}Fl_2$ and $(GS)_5K{-}Fl_1$, while new peaks arise bathochromically shifted to $(GS)_5K{-}Fl_2$ and $(GS)_5K{-}Fl_1$ in PBS for $Fl_1{-}(GS)_5K{-}Fl_2$. In GdCl the spectral changes are not seen for any sample. The spectral changes are not due to fluorophore solvent interactions, because $(GS)_5$K-MR121 spectra do not change at these wavelengths upon solvent change. There are small bathochromic shifts of the spectral fractions of $Fl_1{-}(GS)_5K{-}Fl_2$ in GdCl that is attributed to the spectra of non interacting fluorophores.

In excitation spectra of Cy3-$(GS)_5$K-Cy3 and Cy3B-$(GS)_5$K-Cy3B small contributions of fluorescence excitation bathochromically shifted to $(GS)_5$K-MR121 were seen. It is known that even if H-dimers are most often entirely non-fluorescing complexes, in some cases this assumption does not hold. For instance, it was reported for merocyanine fluorophores that dimerized states do fluoresce.[89] We do not know, if it is the same effect here for Cy3 and Cy3B dimers. Since the dimerized fluorescing species described here and in[89] are cyanine dimers,

the underlying interactions might be very similar. Because we calculate in this work brightness quality factors using maxima of fluorescing species, this small amount of fluorescence from apparently dimerized species contributes to a systematic uncertainty in estimation of brightness quality for Cy3/Cy3B constructs. We are, nevertheless, able to compare the brightness quality and dimerization constants.

In contrast to the high extend of H-dimers in the spectra of $Fl_1-(GS)_5K-Fl_2$, J-dimerization was not indicated at all. It seems to be a general property of the organic fluorophores in solution constrained by flexible structures into a volume with nanometer radius, that they aggregate in stacked geometries with properties resembling pure H-dimers.

The dimerization constant of intramolecular dimerization of Cy3-$(GS)_5$K-Cy5 were estimated as 0.07 M^{-1} being one order of magnitude smaller than the dimerization constant of Cy3B-$(GS)_5$K-Cy5. Dimerization constants of heterodimers for both constructs Cy3B-$(GS)_5$K-Cy5 and Cy3-$(GS)_5$K-Cy5 were smaller than the homodimerization constants we derived for any other fluorophore. Cy3-$(GS)_5$K-Cy5 turns out to be the brightest construct of organic FRET fluorophore pairs in this study, followed by Cy3B-$(GS)_5$K-Cy5 with slightly stronger quenching interactions. Both fluorophore pairs are therefore useful FRET labels whenever contact between the two fluorophores cannot be entirely excluded.

Even if the method for determination of dimer spectra presented in[68] corrects the raw ensemble spectra for fractions of the sample that are singly labeled, we can present here pure dimer spectra of heterodimers. It was found for ATTO488-$(GS)_5$K-Cy5 that its quenching is not exclusively due to H-dimerization. Also the acceptor molecule ATTO647N of the ATTO532-$(GS)_5$K-ATTO647N construct is not quenched in GdCl, but the whole ATTO532-$(GS)_5$K-ATTO647N molecule is. Thus it is likely, that a mixture of quenching interactions including e.g. photoinduced electron transfer quenching only the donor molecule ATTO532 is involved.

The heterodimerization studies done in this work have led to quantification of homodimer and heterodimer association constants. Dimer absorption and fluorescence spectra of commercially available fluorophores were reported, most of them the first time, and we estimated their extinction coefficients. We found out, that H-dimerization is a defining feature of fluorophore interactions for fluorophores held at a distance of 1 nm. We saw that there are differences for these processes. Based on the overall molecular brightness of very small and flexible FRET pairs at glycine-serine oligopeptides we encourage to use a reporter system consisting of a Cy5/Cy3 pair.

To conclude, continuing on investigations on unstructured glycine-serine peptides we have shown that O-glycosylation slows down structural dynamics of glycine-serine peptides. It is difficult to apply the

used PET reporter system to measure contact rates for structural dynamics in high denaturant solutions. A reporter system that uses dimerization of the organic fluorophore MR121 overcomes this drawback in high denaturant solvents. The fact that in aqueous solutions most of the MR121 glycine-serine oligopeptides used are in a dimerized state, that they do not fluoresce in confocal FCS measurements, raises the issue if two different fluorophores used as reporters for FRET measurements are reliable. Therefore, interactions of different commercially available fluorophores at small distances were attached at the very flexible glycine-serine oligopeptides so that they were nearly free diffusing. We quantified the first time how much fluorophores are quenched. For all fluorophore combinations the fluorescence is quenched at molecular contact, either due to photoinduced electron transfer process or the more common H-dimerization process. We got dimer spectra that can be further analyzed e.g. with algorithms using Coherent Excitation Approximation. The given association constants will help to estimate if the fluophores are applicable for FRET measurements in unstructured peptides and proteins.

9 APPENDIX

9.1 MULTIPOLE EXPANSION

For distances $|\vec{r}|$ far away from a charge density $\rho(\vec{r}')$ the electric potential of ρ in eq. (91) can be expressed in a power series of $\vec{r}$ in eq. (92). Neglecting terms decreasing stronger than $\vec{r}^{-2}$, $\phi(\vec{r})$ depends can be splitted into two parts. The one summand in eq. (93) depends on the net charge of ρ decreases with $|\vec{r}|^{-1}$ and the dipole moment $\vec{p}$ with $|\vec{r}|^{-2}$.

$$\phi(\vec{r}) = \int d^3\vec{r}' \frac{\rho(\vec{r}')}{|\vec{r}-\vec{r}'|} \tag{91}$$

$$\begin{aligned}
\frac{1}{|\vec{r}-\vec{r}'|} &= \frac{1}{\sqrt{\sum_{i=1}^{3} (x_i - x'_i)^2}} \\
&= \frac{1}{|\vec{r}|} + \vec{r}' \left(\vec{\nabla}' \frac{1}{|\vec{r}-\vec{r}'|}\bigg|_{\vec{r}'=0} \right) + \mathcal{O}(|\vec{r}-\vec{r}'|^2) \qquad (92) \\
&\approx \frac{1}{|\vec{r}|} + \vec{r}' \frac{\vec{r}}{|\vec{r}|^3} \\
\Rightarrow \phi(\vec{r}) &\approx \frac{1}{r} \int d^3\vec{r}' \rho(\vec{r}') + \frac{\vec{r}}{|\vec{r}|^3} \int d\vec{r}' \vec{r}' \rho(\vec{r}') \\
&= \frac{q}{r} + \frac{\vec{p}\vec{r}}{|\vec{r}|^3} \qquad (93)
\end{aligned}$$

9.2 POLARIZABILITY OF SINGLY DIPOLES

For an ideal dipole ($\rho(\vec{r}) = q(\delta(\vec{r} + \frac{d}{2}\vec{e}_x) - \delta(\vec{r} - \frac{d}{2}\vec{e}_x))$) the dipole moment $\vec{p}$ is then, because of vanishing overall charge

$$\vec{p} = q \cdot \vec{d}. \tag{94}$$

In a lorentzian model every charge is driven by the force $\vec{F} = q\vec{E}$ in an electric field $\vec{E}$. Let this field consist of planar electromagnetic waves like in a low monocromatic laser field $\vec{E}(t) = \vec{E}_0 \exp(-i\omega t)$. This field induces oscillations of charge pairs in the molecule. Let b be a friction matrix that models dissipative forces in the molecule, which has a mass m. For a special coordinate system, where b has diagonal form, an equation of motion gives the differential equation in z-direction

$$\frac{\partial^2}{\partial t^2} d_z(t) + b \frac{\partial}{\partial t} d_z(t) + \omega_0 d_z(t) = \vec{E}_0 \exp(-i\omega t). \tag{95}$$

A general solution is

$$d_z(t) = \frac{q\vec{E}_0}{m} \frac{\exp(-i\omega t)}{\omega_0^2 - \omega^2 - i\omega b} \tag{96}$$

$$\Rightarrow \vec{p} = q \cdot d_z(t) \tag{97}$$

$$= q d_z \exp(-i\omega t) \tag{98}$$

For the other axes one gets similar results by substituting d_z by d_x, d_y. If one identifies the time independent part here as the polarizability $\tilde{\alpha}$, one gets for singly dipoles with $\tilde{\alpha}(\omega) = \frac{q^2}{m(\omega_0^2 - \omega^2 - i\omega b)}$

$$\vec{p} = \tilde{\alpha} \cdot \vec{E}(t) \tag{99}$$

9.3 POLARIZATION OF AN ENSEMBLE OF FREE DIPOLES

The polarization of an ensemble of ideal N dipole molecules is the sum over all existing dipole moments. In the calculations one has to take a basis of a coordinate system not varying between molecules. Therefore $\tilde{\alpha}$ is again a 3×3 matrix that can be diagonalized for each molecule and then calculation of sec. 9.2 hold.

$$\vec{p} = \sum_{m=1}^{3} \sum_{i=1}^{3} \tilde{\alpha}_{im} E_i \vec{e}_m \tag{100}$$

$$\Rightarrow \vec{P} = \sum_{k=1}^{N} \sum_{m=1}^{3} \sum_{i=1}^{3} \tilde{\alpha}_{imk} E_i \vec{e}_m \tag{101}$$

$$= \sum_{m=1}^{3} \sum_{i=1}^{3} E_i \vec{e}_m \sum_{k=1}^{N} \tilde{\alpha}_{imk} \tag{102}$$

$$= \sum_{m=1}^{3} \sum_{i=1}^{3} \alpha_{im} E_i \vec{e}_m \tag{103}$$

$$= \alpha \cdot \vec{E} \tag{104}$$

Here, $\tilde{\alpha}_{imk}$ is introduces as polarizability matrix of molecule k. Finally, the polarizability matrix $\alpha = \sum_{k=1}^{N} \tilde{\alpha}$ describes the polarizability of the whole ensemble of molecular dipoles. Again, one can find a coordinate system, where α is diagonal. Therefore one may describe an ensemble like a single dipole, but with its own frequency ω_0 and dissipation constant b.

9.4 CORRELATION FUNCTION FOR TWO-DIMENSIONAL DIFFUSION WITH ISOMERIZATION

This is the calculation of the correlation function $G(\tau)$ by [60] for two dimensional diffusion with conformational changes between a floures-cent state (quantum yield of species A QY) and a non-fluorescent one

($QY_B = 0$). It is presented here to give a coherent overview of the assumptions made in the calculations of the correlation function that is fitted to the data of the FCS experiments in this work.

It is assumed that the diffusion constant D of both isomers is the same. Also excitation and emission volume V are the same. The absorbed and emitted intensity is proportional to the intensity profile that is gaussian $I(\vec{r}) = I_0 \exp -\frac{2(x^2+y^2)}{\omega_{xy}^2}$. In many FCS applications oil lenses are used while the particles of interest are in aqueous solution. The beam profile stretches then and therefore a two dimensional approximation is sufficient. The number of collected photons at the detector is then given by eq. (105) and fluctuations of the photon count from the mean $\tilde{n}$ follow in eq. (106).

$$n(t) = \Delta t \int d^2\vec{r} I(\vec{r}) Q C(\vec{r}, t) \tag{105}$$

$$\delta n(t) = n(t) - \tilde{n} = \Delta t \int d^2\vec{r} I(\vec{r}) Q \delta C(\vec{r}, t) \tag{106}$$

The correlation $G(t)$ is in experiments determined by the time average of products of intensity fluctuations normalized to the average intensity eq. (107). Due to ergodicity $t = 0$ is chosen in .

$$G(t) = \frac{1}{\tilde{n}^2 T} \sum_{i=0}^{T-1} \delta n(t') \delta n(t'+t) \tag{107}$$

$$= \frac{1}{\tilde{n}^2} \langle \delta n(0) \delta n(t) \rangle \tag{108}$$

$T\Delta t$ is the total measurement time of the experiment. t corresponds to delay channel m with $m = \frac{t}{\Delta t}$ and $\delta n(t') = n_i - \tilde{n}, \delta n(t'+t) = n_{i+m} - \tilde{n}$. n_i are the numbers of photon counts at times $t' = i\Delta t$.[60] Using eq. (105) and eq. (108), the correlation function is

$$G(t) = \frac{(\Delta t)^2}{\tilde{n}^2} \int d^2r \int d^2r' I(r) I(r') Q^2 \left\langle \delta C(\vec{r}, 0) \delta C(\vec{r}', t) \right\rangle \tag{109}$$

$$\begin{aligned} &A \underset{k_{BA}}{\overset{k_{AB}}{\rightleftharpoons}} B \\ &\frac{\partial \delta C_A(\vec{r}, t)}{\partial t} = D\nabla^2 \delta C_A(\vec{r}, t) - k_{AB} \delta C_A + k_{BA} \delta C_B(\vec{r}, t) \\ &\frac{\partial \delta C_B(\vec{r}, t)}{\partial t} = D\nabla^2 \delta C_B(\vec{r}, t) + k_{AB} \delta C_A - k_{BA} \delta C_B(\vec{r}, t) \end{aligned} \tag{110}$$

After a Fourier-transform ($\tilde{C}(\vec{q},t) = (2\pi)^{-2}\int d\vec{r}\exp i\vec{q}\vec{r}C(\vec{r},t)$) of the system of equations in eq. (110) the matrix M is given by eq. (113). It has eigenvalues and eigenvectors $\lambda_{1,2}, \vec{x}_{1,2}$.

$$\frac{\partial}{\partial t}\begin{pmatrix}\delta C_A\\ \delta C_B\end{pmatrix} = M\cdot\begin{pmatrix}\delta C_A\\ \delta C_B\end{pmatrix} \tag{111}$$

$$M = \begin{pmatrix}-Dq^2 - k_{AB} & k_{BA}\\ k_{AB} & -Dq^2 - k_{BA}\end{pmatrix}. \tag{112}$$

$$\begin{aligned}\lambda_1 &= -Dq^2 \qquad \vec{x}_1 = \begin{pmatrix}1\\ \frac{k_{AB}}{k_{BA}}\end{pmatrix}\\ \lambda_2 &= -Dq^2 - k_{BA} - k_{AB} \qquad \vec{x}_2 = \begin{pmatrix}1\\ -1\end{pmatrix}\end{aligned} \tag{113}$$

Using the starting conditions $\delta C_A(\vec{q},0) = \delta C_A(\vec{q},t=0)$ and $\delta C_B(\vec{q},0) = \delta C_B(\vec{q},t=0)$, the solution for the fluorescing species can be calculated in eq. (114). In the following derivation of the correlation $\langle\delta C(\vec{r},0)\delta C(\vec{r}',t)\rangle$ it is assumed that positions of different species are decorrelated (in eq. (115) and eq. (116)) and that molecules of the same species at different locations are locally decorrelated (in eq. (117)).

$$\begin{aligned}\delta C_A(\vec{q},t) = \frac{1}{1+K}\cdot[&\exp(\lambda_1 t)\,(\delta C_A(\vec{q},0) + \delta C_B(\vec{q},0)) +\\ &\exp(\lambda_2 t)\,(K\delta C_A(\vec{q},0) - \delta C_B(\vec{q},0))]\end{aligned} \tag{114}$$

$$\Rightarrow \left\langle\delta C(\vec{r},0)\delta C(\vec{r}',t)\right\rangle =$$

$$(2\pi)^{-1}\int_{-\infty}^{\infty} d^2\vec{q}\exp\left(-i\vec{q}\vec{r}'\right)\langle\delta C(\vec{r},0)\delta C(\vec{q},t)\rangle \tag{115}$$

$$\begin{aligned}&= (2\pi)^{-2}\int_{-\infty}^{\infty} d^2\vec{q}\exp(-iq\vec{r}')\int_{-\infty}^{\infty} x''\exp(iqr'')\cdot\ldots\\ &\quad\frac{1}{1+K}\left\langle\exp(\lambda_1 t)\delta C_A(\vec{r},0)\left(\delta C_A(\vec{r}'') + \delta C_B(\vec{r}'',0)\right) + \ldots\right.\\ &\quad\left.\delta C_A(\vec{r},0)\left(K\delta C_A(\vec{r}'',0) - \delta C_B(\vec{r}'',0)\right)\right\rangle\\ &= (2\pi)^{-2}\int_{-\infty}^{\infty} d^2\vec{q}\exp(-iq\vec{r}')\int_{-\infty}^{\infty} x''\exp(iqr'')\cdot\ldots\\ &\quad\frac{1}{1+K}\left\langle\delta C_A(\vec{r},0)\delta C_A(\vec{r}'',0)\right\rangle(\exp(\lambda_1 t) + K\exp(\lambda_2 t))\end{aligned} \tag{116}$$

$$\begin{aligned}&= \frac{\tilde{C}_A}{(1+K)(2\pi)^2}\cdot\ldots\\ &\quad\int_{-\infty}^{\infty} d^2\vec{q}\exp(-iq\vec{r}')\,(\exp(\lambda_1 t) + K\exp(\lambda_2 t))\end{aligned} \tag{117}$$

In eq. (107) one can use, that $I(\vec{r}) = I(-\vec{r})$ to introduce its Fourier transform of $\tilde{I}(\vec{q}) = (2\pi)^{-1} \int_{-\infty}^{\infty} d^2\vec{r} I(\vec{r}) exp(-i\vec{q}\vec{r})$. The average number of collected photons is $\bar{n} = \Delta t \int_{-\infty}^{\infty} d^2\vec{r}\ I(\vec{r}) Q C_A = 2\pi \tilde{I}(0) Q C_A$

$$G(t) = \frac{(\Delta t)^2}{(\bar{n})^2} \int_{-\infty}^{\infty} d^2\vec{q}\ \tilde{I}(\vec{q})^2 Q^2 \left\langle \delta C(\vec{r},0)\delta C(\vec{r}',t)\right\rangle \tag{118}$$

$$= \frac{1}{(2\pi)^2(1+K)\tilde{C}_A} \int_{-\infty}^{\infty} d^2\vec{q}\ \frac{\tilde{I}(\vec{q})^2}{\tilde{I}(0)^2} \left(\exp(\lambda_1 t) + K\exp(\lambda_2 t)\right) \tag{119}$$

$$\frac{\tilde{I}(\vec{q})}{\tilde{I}(0)} = (2\pi I(0))^{-1} \int_{-\infty}^{\infty} dx \exp(-iq_x x) exp(-\frac{2x^2}{\omega_{xy}^2}) \cdot \ldots$$

$$\int_{-\infty}^{\infty} dy \exp(-iq_y y) exp(-\frac{2y^2}{\omega_{xy}^2}) \tag{120}$$

$$= \frac{1}{\tilde{I}(0)} \frac{\omega_{xy}^2}{4} \exp\left(-\frac{\vec{q}^2\omega_{xy}^2}{8}\right) \tag{121}$$

$$= \exp\left(-\frac{\vec{q}^2\omega_{xy}^2}{8}\right) \tag{122}$$

Here the relaxation time $\tau_K = (k_{AB} + k_{BA})^{-1}$ was introduced. The equilibrium constant is given by $K = \frac{k_{AB}}{k_{BA}} = \frac{\bar{N}_B}{\bar{N}_A}$ and in the two dimensional excitation/emission volume, particle number N_A of the fluorescing species is connected with its concentration via $\bar{N}_A = \tilde{C}_A \omega_{xy}^2 \pi$

$$G(t) = \frac{1}{(2\pi)^2(1+K)\tilde{C}_A} \int_{-\infty}^{\infty} d^2\vec{q}\ \exp\left(-\frac{\vec{q}^2\omega_{xy}^2}{4} - Dtq^2\right)\left(1 + K\exp(-\frac{t}{\tau_K})\right)$$

$$= \frac{\left(1 + K\exp(-\frac{t}{\tau_K})\right)}{4\pi(1+K)\tilde{C}_A} \frac{1}{\frac{\omega_{xy}^2}{4} + Dt}$$

$$= \frac{\left(1 + K\exp(-\frac{t}{\tau_K})\right)}{\tilde{\pi}\omega_{xy}^2 C_A(1+K)} \frac{1}{1 + \frac{t}{\tau_D}}$$

$$= \frac{1}{1 + \frac{t}{\tau_D}} \frac{2\bar{N}_A\left(1 + K\exp(-\frac{t}{\tau_K})\right)}{\bar{N}_A + \bar{N}_B}$$

$$= \frac{1}{N\left(1 + \frac{t}{\tau_D}\right)} \left(1 + K\exp(-\frac{t}{\tau_K})\right)$$

This is the two dimensional correlation function for unimolecular isomerization reactions with one fluorescing species.

D_1/D_2	R_{FRET} / nm
Cy5/Cy3	5.3
Cy5/Cy3B	6.9
ATTO647N/ATTO532	6.5
ATTO532/ATTO565	7.1
Cy5/ATTO488	6.3

Table 9: FRET radii calculated with ensemble data, $\kappa^2 = \frac{2}{3}$, and QYss from tab. 8

9.5 QUANTUM YIELDS OF ORGANIC DYES

Dye	QYss / %
Cy3	20[27, 99]
Cy3B	28[22]
ATTO488	74[20]
ATTO532	90[99]

Table 8: Quantum yields of organic dyes in aqueous solution.

BIBLIOGRAPHY

[1] URL http://www.ebi.ac.uk/uniprot/TrEMBLstats/.

[2] *Protein folding handbook*. Wiley-VCH, Weinheim, 2005. ISBN 978-3-527-30784-5, 3-527-30784-2.

[3] *New Oxford American Dictionary*. Oxford University Press Inc., 2nd edition, 2005.

[4] The initial step of dna hairpin folding: a kinetic analysis using fluorescence correlation spectroscopy. *Nucleic Acids Res*, 34(9):2516–2527, 2006. ISSN 1362-4962 (Electronic). doi: 10.1093/nar/gkl221.

[5] Periodic acceptor excitation spectroscopy of single molecules. *Eur Biophys J*, 36(6):669–674, Jul 2007. ISSN 0175-7571 (Print). doi: 10.1007/s00249-007-0133-7.

[6] *CRC handbook of chemistry and physics*. 2009. ISBN 978-1-4200-9084-0.

[7] Photoinduced formation of reversible dye radicals and their impact on super-resolution imaging. *Photochem. Photobiol. Sci.*, 10:499–506, 2011. doi: 10.1039/C0PP00317D. URL http://dx.doi.org/10.1039/C0PP00317D.

[8] Jan 2013. URL http://en.wikipedia.org/wiki/N-glycosylation.

[9] Ernst Abbe. Beiträge zur theorie des mikroskops und der mikroskopischen wahrnehmung. *Archiv für Mikroskopische Anatomie*, 1873.

[10] David L. Andrews. A unified theory of radiative and radiationless molecular energy transfer. *Chemical Physics*, 135 (2):195 – 201, 1989. ISSN 0301-0104. doi: 10.1016/0301-0104(89)87019-3. URL http://www.sciencedirect.com/science/article/pii/0301010489870193.

[11] David L. Andrews and David S. Bradshaw. Virtual photons, dipole fields and energy transfer: a quantum electrodynamical approach. *European Journal of Physics*, 25(6):845, 2004. URL http://stacks.iop.org/0143-0807/25/i=6/a=017.

[12] Jayanth R. Banavar, Amos Maritan, Cristian Micheletti, and Antonio Trovato. Geometry and physics of proteins. *Proteins: Structure, Function, and Bioinformatics*, 47(3):315–322, 2002. ISSN 1097-0134. doi: 10.1002/prot.10091. URL http://dx.doi.org/10.1002/prot.10091.

[13] Valerie Belle, Sabrina Rouger, Stephanie Costanzo, Elodie Liquiere, Janez Strancar, Bruno Guigliarelli, Andre Fournel, and Sonia Longhi. Mapping alpha-helical induced folding within the intrinsically disordered c-terminal domain of the measles virus nucleoprotein by site-directed spin-labeling epr spectroscopy. *Proteins*, 73(4):973–988, Dec 2008. ISSN 1097-0134 (Electronic); 0887-3585 (Linking). doi: 10.1002/prot.22125.

[14] Oliver Bieri, Jakob Wirz, Bruno Hellrung, Mike Schutkowski, Mario Drewello, and Thomas Kiefhaber. The speed limit for protein folding measured by triplet-triplet energy transfer. *Proceedings of the National Academy of Sciences USA*, 96(17):9597–9601, 1999. URL `http://www.pnas.org/content/96/17/9597.abstract`.

[15] Noël Boens, Wenwu Qin, Nikola Basarić, Johan Hofkens, Marcel Ameloot, Jacques Pouget, Jean-Pierre Lefèvre, Bernard Valeur, Enrico Gratton, Martin vandeVen, Norberto D. Silva, Yves Engelborghs, Katrien Willaert, Alain Sillen, Garry Rumbles, David Phillips, Antonie J. W. G. Visser, Arie van Hoek, Joseph R. Lakowicz, Henryk Malak, Ignacy Gryczynski, Arthur G. Szabo, Don T. Krajcarski, Naoto Tamai, and Atsushi Miura. Fluorescence lifetime standards for time and frequency domain fluorescence spectroscopy. *Analytical Chemistry*, 79(5):2137–2149, 2007. doi: 10.1021/ac062160k. URL `http://pubs.acs.org/doi/abs/10.1021/ac062160k`.

[16] Carsten Budke. *Hemmung der Eisrekristallisation in wässrigen Lösungen durch Antigefrierglykopeptide*. 2010. URL `http://pub.uni-bielefeld.de/publication/2302646`.

[17] Paola Ceroni and Vincenzo Balzani. Photoinduced energy and electron transfer processes. In Paola Ceroni, editor, *The Exploration of Supramolecular Systems and Nanostructures by Photochemical Techniques*, volume 78 of *Lecture Notes in Chemistry*, pages 21–38. Springer Netherlands, 2012. ISBN 978-94-007-2041-1. doi: 10.1007/978-94-007-2042-8_2. URL `http://dx.doi.org/10.1007/978-94-007-2042-8_2`.

[18] Krishnananda Chattopadhyay, Elliot L. Elson, and Carl Frieden. The kinetics of conformational fluctuations in an unfolded protein measured by fluorescence methods. *Proceedings of the National Academy of Sciences USA*, 102(7):2385–2389, 2005. doi: 10.1073/pnas.0500127102. URL `http://www.pnas.org/content/102/7/2385.abstract`.

[19] Zhijian Chen, Andreas Lohr, Chantu R. Saha-Möller, and Frank Würthner. Self-assembled [small pi]-stacks of functional dyes in solution: structural and thermodynamic features. *Chem. Soc. Rev.*,

38:564–584, 2009. doi: 10.1039/B809359H. URL http://dx.doi.org/10.1039/B809359H.

[20] Alexey I. Chizhik, Ingo Gregor, Benedikt Ernst, and Jörg Enderlein. Nanocavity-based determination of absolute values of photoluminescence quantum yields. *ChemPhysChem*, 14(3):505–513, 2013. ISSN 1439-7641. doi: 10.1002/cphc.201200931. URL http://dx.doi.org/10.1002/cphc.201200931.

[21] Claude Cohen-Tannoudji. *Quantenmechanik/1*. 2007. ISBN 978-3-11-019324-4.

[22] M. Cooper. Cy3b: Improving the performance of cyanine dyes. *Journal of Fluorescence*, 14(2):145–150, 2004.

[23] John H. Crowe, Lois M. Crowe, and Dennis Chapman. Preservation of membranes in anhydrobiotic organisms: The role of trehalose. *Science*, 223(4637):701–703, 1984. doi: 10.1126/science.223.4637.701. URL http://www.sciencemag.org/content/223/4637/701.abstract.

[24] Thomas Dertinger, Victor Pacheco, Iris von der Hocht, Rudolf Hartmann, Ingo Gregor, and Jörg Enderlein. Two-focus fluorescence correlation spectroscopy: A new tool for accurate and absolute diffusion measurements. *ChemPhysChem*, 8(3):433–443, 2007. URL http://dx.doi.org/10.1002/cphc.200600638.

[25] D. L. Dexter. A theory of sensitized luminescence in solids. *The Journal of Chemical Physics*, 21(5):836–850, 1953. doi: 10.1063/1.1699044. URL http://link.aip.org/link/?JCP/21/836/1.

[26] Nicolas Di Fiori and Amit Meller. The effect of dye-dye interactions on the spatial resolution of single-molecule fret measurements in nucleic acids. *Biophysical Journal*, (98):2265–2272, 2010.

[27] Anja Dietrich, Volker Buschmann, Christian Müller, and Markus Sauer. Fluorescence resonance energy transfer fret and competing processes in donor and acceptor substituted dna strands: a comparative study of ensemble and single-molecule data. *Reviews in Molecular Biotechnology*, (82):211–231, 2002.

[28] Sören Doose, Hannes Neuweiler, and Markus Sauer. A close look at fluorescence quenching of organic dyes by tryptophan. *ChemPhysChem*, 6:2277–2285, 2005.

[29] Sören Doose, Hannes Neuweiler, and Markus Sauer. Fluorescence quenching by photoinduced electron transfer: A reporter for conformational dynamics of macromolecules. *ChemPhysChem*, 10 (9-10):1389–1398, 2009. URL http://dx.doi.org/10.1002/cphc.200900238.

[30] K. H. Drexhage. *Dye Lasers*, chapter 4. Springer, 1973.

[31] H. J. Dyson and P. E. Wright. Intrinsically unstructured proteins and their functions. *Molecular Cell Biology*, 6:197–208, March 2005.

[32] Christian Eggeling, Christian Ringemann, Rebecca Medda, Gunter Schwarzmann, Konrad Sandhoff, Svetlana Polyakova, Vladimir N. Belov, Birka Hein, Claas von Middendorff, Andreas Schonle, and Stefan W. Hell. Direct observation of the nanoscale dynamics of membrane lipids in a living cell. *Nature*, 457(7233):1159–1162, 02 2009. URL `http://dx.doi.org/10.1038/nature07596`.

[33] A. Einstein. Über die von der molekularkinetischen theorie der wärme geforderte bewegung von in ruhenden flüssigkeiten suspendierten teilchen. *Annalen der Physik*, 322(8):549–560, 1905. ISSN 1521-3889. doi: 10.1002/andp.19053220806. URL `http://dx.doi.org/10.1002/andp.19053220806`.

[34] A. Eisfeld and J.S. Briggs. The j- and h-bands of organic dye aggregates. *Chemical Physics*, 324(2-3):376 – 384, May 2006. ISSN 0301-0104. doi: 10.1016/j.chemphys.2005.11.015. URL `http://www.sciencedirect.com/science/article/pii/S030101040500563X`.

[35] A. Eisfeld, L. Braun, W. T. Strunz, and J. S. Briggs. Vibronic energies and spectra of molecular dimers. *The Journal of Chemical Physics*, 122, 2005.

[36] David Eliezer. Biophysical characterization of intrinsically disordered proteins. *Curr Opin Struct Biol*, 19(1):23–30, Feb 2009. ISSN 1879-033X (Electronic); 0959-440X (Linking). doi: 10.1016/j.sbi.2008.12.004.

[37] Jörg Enderlein and Ingo Gregor. Using fluorescence lifetime for discriminating detector afterpulsing in fluorescence-correlation spectroscopy. *Review of Scientific Instruments*, 76(3):033102–033102–5, 2005. ISSN 0034-6748. doi: 10.1063/1.1863399.

[38] Thomas L. Fare, Ernest M. Coffey, Hongyue Dai, Yudong D. He, Deborah A. Kessler, Kristopher A. Kilian, John E. Koch, Eric Leproust, Matthew J. Marton, Michael R. Meyer, Roland B. Stoughton, George Y. Tokiwa, and Yanqun Wang. Effects of atmospheric ozone on microarray data quality. *Analytical Chemistry*, 75:4672–4675, 2003.

[39] Emil Fischer. Einfluss der configuration auf die wirkung der enzyme. *Berichte der Deutschen chemischen Gesellschaft zu Berlin*, 27(3):2985–93, 1894.

[40] P. J. Flory. *Statistical mechanics of chains molecules*. Carl Hanser Verlag, Munich, 1969.

[41] William G. Flynne. *Biotechnology and Bioengineering*. Nova Science Pub Inc, 2008.

[42] Theodor Förster. Zwischenmolekulare energiewanderung und fluoreszenz. *Annalen der Physik*, 437(1-2):55–75, 1948. ISSN 1521-3889. doi: 10.1002/andp.19484370105. URL http://dx.doi.org/10.1002/andp.19484370105.

[43] Tsuneo Fujii, Hiromasa Nishikiori, and Takuma Tamura. Absorption spectra of rhodamine b dimers in dip-coated thin films prepared by the sol-gel method. *Chemical Physics Letters*, 233(4):424 – 429, 1995. ISSN 0009-2614. doi: 10.1016/0009-2614(94)01477-D. URL http://www.sciencedirect.com/science/article/pii/000926149401477D.

[44] K F Geoghegan, P J Rosner, and L R Hoth. Dye-pair reporter systems for protein-peptide molecular interactions. *Bioconjug Chem*, 11(1):71–77, Jan-Feb 2000. ISSN 1043-1802 (Print); 1043-1802 (Linking).

[45] A. Göhler, S. André, H. Kaltner, M. Sauer, H.-J. Gabius, and S. Doose. Hydrodynamic properties of human adhesion/growth-regulatory galectins studied by fluorescence correlation spectroscopy. *Biophysical Journal*, 98:3044–3053, 2010.

[46] Markus Grabolle, Robert Brehm, Jutta Pauli, Franziska M. Dees, Ingrid Hilger, and Ute Resch-Genger. Determination of the labeling density of fluorophore-biomolecule conjugates with absorption spectroscopy. *BIOCONJUGATE CHEMISTRY*, 23(2):287–292, Feb 2012. ISSN 1043-1802. doi: 10.1021/bc2003428.

[47] M Griffith and K V Ewart. Antifreeze proteins and their potential use in frozen foods. *Biotechnol Adv*, 13(3):375–402, 1995. ISSN 0734-9750 (Print); 0734-9750 (Linking).

[48] H. Gutfreund. *Kinetics for the Life Sciences*. Cambridge Univ. Press, 1995. ISBN 052148586.

[49] Taekjip Ha. Single-molecule fluorescence resonance energy transfer. *Methods*, 25(1):78 – 86, 2001. ISSN 1046-2023. doi: 10.1006/meth.2001.1217. URL http://www.sciencedirect.com/science/article/pii/S1046202301912174.

[50] Hagen. Solvent viscosity and friction in protein folding dynamics. *Current Protein and Peptide Science*, 11(5):385–395. ISSN 1389-2037. doi: 10.2174/138920310791330596. URL http://dx.doi.org/10.2174/138920310791330596.

[51] Hermann Haken and Hans Christoph Wolf, editors. *Molekülphysik und Quantenchemie : Einführung in die experimentellen und theo-*

retischen Grundlagen ; mit 43 Tabellen und 133 Aufgaben. Springer-Lehrbuch. Springer, Berlin [u.a.], 5., völlig neubearb. und erw. aufl. edition, 2006. ISBN 3-540-30314-6 - 978-3-540-30314-5 - 978-3-540-30315-2. Vollständige Lösungen im Internet unter www.springer.de.

[52] G. M. Hale and M. R. Querry. Optical constants of water in the 200 nm to 200 µm wavelength region. *Appl. Opt.*, 12:555–563, 1973.

[53] Mike Heilemann, Sebastian van de Linde, Mark Schüttpelz, Robert Kasper, Britta Seefeldt, Anindita Mukherjee, Philip Tinnefeld, and Markus Sauer. Subdiffraction-resolution fluorescence imaging with conventional fluorescent probes. *Angew Chem Int Ed Engl*, 47(33): 6172–6176, 2008. ISSN 1521-3773 (Electronic); 1433-7851 (Linking). doi: 10.1002/anie.200802376.

[54] Stefan W. Hell and Jan Wichmann. Breaking the diffraction resolution limit by stimulated emission: stimulated-emission-depletion fluorescence microscopy. *Opt. Lett.*, 19(11):780–782, Jun 1994. doi: 10.1364/OL.19.000780. URL `http://ol.osa.org/abstract.cfm?URI=ol-19-11-780`.

[55] Greg T. Hermanson. *Bioconjugate techniques*. 2008. ISBN 978-0-12-370501-3.

[56] Jordi Hernando, Martijn van der Schaaf, Erik M. H. P. van Dijk, Markus Sauer, María F. García-Parajó, and Niek F. van Hulst. Excitonic behavior of rhodamine dimers: A single-molecule study. *The Journal of Physical Chemistry A*, 107(1):43–52, 2003. doi: 10.1021/jp0218995. URL `http://pubs.acs.org/doi/abs/10.1021/jp0218995`.

[57] John David Jackson. *Classical electrodynamics*. Wiley, New York [u.a.], 3. ed. edition, 1999. ISBN 0-471-30932-X.

[58] E. E. Jelley. Spectral absorption and fluorescence of dyes in the molecular state. *Nature*, 138:1009–1010, 1936.

[59] Katalin, A et al. Stereospecific reaction of muscle fiber proteins with the 5' or 6' isomer of (iodoacetamido)tetramethylrhodamine. *Biochemistry*, 31:12431–12440, 1992.

[60] Oleg Krichevsky and Gregoire Bonnet. Fluorescence correlation spectroscopy: the technique and its applications. *Reports on Progress in Physics*, 65(2):251–297, 2002. doi: 10.1088/0034-4885/65/2/203. URL `http://dx.doi.org/10.1088/0034-4885/65/2/203`.

[61] Florian Krieger, Beat Fierz, Oliver Bieri, Mario Drewello, and Thomas Kiefhaber. Dynamics of unfolded polypeptide chains as model for the earliest steps in protein folding. *Journal of Molecular Biology*, 332(1):265 – 274, 2003.

ISSN 0022-2836. doi: DOI:10.1016/S0022-2836(03)00892-1. URL http://www.sciencedirect.com/science/article/B6WK7-49C4SW0-W/2/709ab720fccf97f5072df29fc96c344d.

[62] H. Kuhn. A quantum-mechanical theory of light absorption of organic dyes and similar compounds. *Journal of Chemical Physics*, 17:1198, 1949.

[63] Elza V Kuzmenkina, Colin D Heyes, and G Ulrich Nienhaus. Single-molecule förster resonance energy transfer study of protein dynamics under denaturing conditions. *Proc Natl Acad Sci U S A*, 102(43):15471–15476, Oct 2005. ISSN 0027-8424 (Print); 0027-8424 (Linking). doi: 10.1073/pnas.0507728102.

[64] Lakowicz. *Principles of Fluorescence Spectroscopy*. Springer, 3 edition, 2006.

[65] Marc Löllmann. *Conformational Dynamics of Polypeptides and the Folding of Miniproteins studied by Fluorescence Spectroscopy*. PhD thesis, Bielefeld University, 2010.

[66] Anastasia Loman, Ingo Gregor, Christina Stutz, Markus Mund, and Jörg Enderlein. Measuring rotational diffusion of macromolecules by fluorescence correlation spectroscopy. *Photochemical & Photobiological Sciences*, 9:627–636, 2010.

[67] R. A. Marcus. On the theory of oxidation-reduction reactions involving electron transfer. i. *The Journal of Chemical Physics*, 24 (5):966–978, 1956. doi: 10.1063/1.1742723. URL http://link.aip.org/link/?JCP/24/966/1.

[68] N. Marmé, G. Habl, and J-P. Knemeyer. Aggregation behavior of the red-absorbing oxazine derivative mr 121: A new method for determination of pure dimer spectra. *Chemical Physics Letters*, (408):221–225, 2005.

[69] Chelsea R. Martinez and Brent L. Iverson. Rethinking the term "pi-stacking". *Chemical Science*, 3:2191ff, 2012. doi: 10.1039/c2sc20045g.

[70] Volkhard May and Oliver Kühn. *Charge and energy transfer dynamics in molecular systems*. Wiley-VCH, Weinheim, 3., rev. and enl. ed. edition, 2011. ISBN 978-3-527-40732-3. Literaturangaben.

[71] Xavier Michalet, Achillefs N Kapanidis, Ted Laurence, Fabien Pinaud, Sören Doose, Malte Pflughoefft, and Shimon Weiss. The power and prospects of fluorescence microscopies and spectroscopies. *Annu Rev Biophys Biomol Struct*, 32:161–182, 2003. ISSN 1056-8700 (Print); 1056-8700 (Linking). doi: 10.1146/annurev.biophys.32.110601.142525.

[72] Nivedita Mitra, Sharmistha Sinha, Thirumalai N.C. Ramya, and Avadhesha Surolia. N-linked oligosaccharides as outfitters for glycoprotein folding, form and function. *Trends in Biochemical Sciences*, 31(3):156 – 163, 2006. ISSN 0968-0004. doi: 10.1016/j.tibs.2006.01.003. URL http://www.sciencedirect.com/science/article/pii/S0968000406000247.

[73] Andreas Möglich, Florian Krieger, and Thomas Kiefhaber. Molecular basis for the effect of urea and guanidinium chloride on the dynamics of unfolded polypeptide chains. *J. Mol. Biol.*, 345:153–162, 2005.

[74] Andreas Möglich, Karin Joder, and Thomas Kiefhaber. End-to-end distance distributions and intrachain diffusion constants in unfolded polypeptide chains indicate intramolecular hydrogen bond formation. *Proceedings of the National Academy of Sciences USA*, 103(33):12394–12399, 2006. URL http://www.pnas.org/content/103/33/12394.abstract.

[75] Natalia N. Nalivaeva and Anthony J. Turner. Post-translational modifications of proteins: Acetylcholinesterase as a model system. *Proteomics*, 1(6):735–747, 2001. ISSN 1615-9861. doi: 10.1002/1615-9861(200106)1:6<735::AID-PROT735>3.0.CO;2-8. URL http://dx.doi.org/10.1002/1615-9861(200106)1:6<735::AID-PROT735>3.0.CO;2-8.

[76] Hannes Neuweiler, Marc Löllmann, Sören Doose, and Markus Sauer. Dynamics of unfolded polypeptide chains in crowded environment studied by fluorescence correlation spectroscopy. *Journal of Molecular Biology*, 365(3):856 – 869, 2007. ISSN 0022-2836. doi: DOI:10.1016/j.jmb.2006.10.021. URL http://www.sciencedirect.com/science/article/B6WK7-4M3R2CS-9/2/1062ac0f7ce435f9c8456ff88c6b237b.

[77] F. Noé, S. Doose, I. Daidone, M. Löllmann, M. Sauer, J. D. Chodera, and J. C. Smith. Dynamical fingerprints for probing individual relaxation processes in biomolecular dynamics with simulations and kinetic experiment. *Proceedings of the National Academy of Sciences USA*, 108(12):4822–4827, March 2011.

[78] B. Z. Packard, D. D. Toptygin, A. Komoriya, and L. Brand. Profluorescent protease substrates: Intramolecular dimers described by the exciton model. *Proceedings of the National Academy of Sciences USA*, 93(21):11640–11645, Oct 1996. ISSN 0027-8424.

[79] Beverly Z. Packard, Akira Komoriya, Dmitri D. Toptygin, and Ludwig Brand. Structural characteristics of fluorophores that form intramolecular h-type dimers in a protease substrate. *The Journal of Physical Chemistry B*, 101(25):5070–5074, 1997. doi: 10.

1021/jp9702210. URL http://pubs.acs.org/doi/abs/10.1021/jp9702210.

[80] Dieter Perl, Maik Jacob, Mikulás Bánó, Marek Stupák, Marián Antalík, and Franz X. Schmid. Thermodynamics of a diffusional protein folding reaction. *Biophysical Chemistry*, 96(2-3):173 – 190, 2002. ISSN 0301-4622. doi: DOI:10.1016/S0301-4622(02)00024-8. URL http://www.sciencedirect.com/science/article/B6TFB-454TR8R-3/2/21cfccdde0571051dc3da04ca44fca07.

[81] personal communication Phillip Kroehn (Group of Jörg Enderlein), 2013.

[82] personal communication T. Hagai (group of Yaakov Levy).

[83] Alexandros Pertsinidis, Yunxiang Zhang, and Steven Chu. Subnanometre single-molecule localization, registration and distance measurements. *Nature*, 466(7306):647–651, 07 2010. URL http://dx.doi.org/10.1038/nature09163.

[84] R. Poprawe. *Laser Fundamentals*. Springer, 2005.

[85] Eugene Rabinowitch and Leo F. Epstein. Polymerization of dyestuffs in solution. thionine and methylene blue1. *Journal of the American Chemical Society*, 63(1):69–78, 1941. doi: 10.1021/ja01846a011. URL http://pubs.acs.org/doi/abs/10.1021/ja01846a011.

[86] Suman Ranjit and Marcia Levitus. Probing the interaction between fluorophores and dna nucleotides by fluorescence correlation spectroscopy and fluorescence quenching. *Photochemistry and Photobiology*, 2012. doi: 10.1111/j.1751-1097.2012.01121.x.

[87] Andreas Reiner. Triplet-triplet energy transfer studies on conformational dynamics in peptides and a protein. *J Pept Sci*, 17(6):413–419, Jun 2011. ISSN 1099-1387 (Electronic); 1075-2617 (Linking). doi: 10.1002/psc.1353.

[88] Jan Roden, Alexander Eisfeld, Matthieu Dvorák, Oliver Bünermann, and Frank Stienkemeier. Vibronic line shapes of ptcda oligomers in helium nanodroplets. *The Journal of Chemical Physics*, 134, 2011.

[89] U. Rösch, Sh. Yao, R. Wortmann, and F. Würthner. Fluorescent h-aggregates of merocyanine dyes. *Angewandte Chemie*, 118(42):7184–7188, 2006. URL http://dx.doi.org/10.1002/ange.200602286.

[90] M. Sauer, J. Hofkens, and J. Enderlein. *Handbook of Fluorescence Spectroscopy and Imaging: From Ensemble to Single Molecules*. John Wiley & Sons, 2011. ISBN 9783527633524.

[91] G. Scheibe. Über die veränderlichkeit des absorptionsspektrums einiger sensibilisierungsfarbstoffe und deren ursache. *Angewandte Chemie*, 49(31):563, 1936.

[92] G. Scheibe. Über die veränderlichkeit der absorptionsspektren in lösungen und die nebenvalenzen als ihre ursache. *Angewandte Chemie*, 50(11):212–219, 1937. URL http://dx.doi.org/10.1002/ange.19370501103.

[93] Benjamin Schuler. Single-molecule fluorescence spectroscopy of protein folding. *Chemphyschem*, 6(7):1206–1220, Jul 2005. ISSN 1439-4235 (Print); 1439-4235 (Linking). doi: 10.1002/cphc.200400609.

[94] Franz Schwabl. *Schwabl, Franz.* Springer, 2006.

[95] Britta Seefeldt, Robert Kasper, Mirco Beining, Jochen Mattay, Jutta Arden-Jacob, Norbert Kemnitzer, Karl Heinz Drexhage, Mike Heilemann, and Markus Sauer. Spiropyrans as molecular optical switches. *Photochem. Photobiol. Sci.*, 9:213–220, 2010. doi: 10.1039/B9PP00118B. URL http://dx.doi.org/10.1039/B9PP00118B.

[96] M. Septinus, W. Seiffert, and H. W. Zimmermann. Über hydrophobe acridinfarbstoffe zur fluorochromierung von mitochondrien in lebenden zellen. *Histochemistry and Cell Biology*, 79:443–456, 1983. ISSN 0948-6143. URL http://dx.doi.org/10.1007/BF00491779. 10.1007/BF00491779.

[97] Dalit Shental-Bechor and Yaakov Levy. Folding of glycoproteins: toward understanding the biophysics of the glycosylation code. *Current Opinion in Structural Biology*, 19(5):524 – 533, 2009. ISSN 0959-440X. doi: 10.1016/j.sbi.2009.07.002. URL http://www.sciencedirect.com/science/article/pii/S0959440X09000980. <ce:title>Carbohydradtes and glycoconjugates / Biophysical methods</ce:title>.

[98] Bristol Naturalists' Society. *Proceedings of the Bristol Naturalists' Society.* Number Bd. 1. The Society, 1876. URL http://books.google.de/books?id=TC8UAAAAYAAJ.

[99] Sergey Solomatin and Daniel Herschlag. Chapter 3 - methods of site-specific labeling of {RNA} with fluorescent dyes. In Daniel Herschlag, editor, *Biophysical, Chemical, and Functional Probes of RNA Structure, Interactions and Folding: Part B*, volume 469 of *Methods in Enzymology*, pages 47 – 68. Academic Press, 2009. doi: 10.1016/S0076-6879(09)69003-0. URL http://www.sciencedirect.com/science/article/pii/S0076687909690030.

[100] Justin Spiriti, Federica Bogani, Arjan van der Vaart, and Giovanna Ghirlanda. Modulation of protein stability by o-glycosylation in a designed gc-maf analog. *Biophysical Chemistry*, 134(3): 157 – 167, 2008. ISSN 0301-4622. doi: 10.1016/j.bpc.2008.02.005. URL `http://www.sciencedirect.com/science/article/pii/S0301462208000264`.

[101] L. Stryer and R. P. Haugland. Energy transfer: a spectroscopic ruler. *Proc Natl Acad Sci U S A*, 58(2):719–726, August 1967. ISSN 0027-8424. URL `http://www.pnas.org/content/58/2/719.abstract`.

[102] Richard S. Swanwick, Alison M. Daines, Lai-Hock Tey, Sabine L. Flitsch, and Rudolf K. Allemann. Increased thermal stability of site-selectively glycosylated dihydrofolate reductase. *ChemBioChem*, 6 (8):1338–1340, 2005. ISSN 1439-7633. doi: 10.1002/cbic.200500103. URL `http://dx.doi.org/10.1002/cbic.200500103`.

[103] Charles Tanford and K. C. Aune. Thermodynamics of the denaturation of lysozyme by guanidine hydrochloride. iii. dependence on temperature. *Biochemistry*, 1970.

[104] Iwao Teraoka. *Polymer Solutions: An Introduction to Physical Properties*. John Wiley & Sons, 2002. ISBN 0-471-22451-0.

[105] Nikolaj Tjutjulkov, editor. *Polymethine dyes : structure and properties*. St. Kliment Ohridski Univ. Press, Sofia, 1991.

[106] Peter Tompa. *Structure and function of intrinsically disordered proteins*. Taylor & Francis, 2010.

[107] Erdal Toprak, Ahmet Yildiz, Melinda Tonks Hoffman, Steven S. Rosenfeld, and Paul R. Selvin. Why kinesin is so processive. *Proceedings of the National Academy of Sciences USA*, 106(31): 12717–12722, 2009. doi: 10.1073/pnas.0808396106. URL `http://www.pnas.org/content/106/31/12717.abstract`.

[108] V. N. Uversky. Intrinsically disordered proteins from a to z. *The International Journal of Biochemistry and Cell Biology*, 43:1090–1103, 2011.

[109] M. Sauer V. Buschmann, K. D. Weston. Spectroscopic study and evaluation of red absorbing fluorescent dyes. *Bioconjugate Chem.*, (14):195–204, 2003.

[110] Andrea C. Vaiana, Hannes Neuweiler, Andreas Schulz, Jürgen Wolfrum, Markus Sauer, and Jeremy C. Smith. Fluorescence quenching of dyes by tryptophan: Interactions at atomic detail from combination of experiment and computer simulation. *Journal of the American Chemical Society*, 125(47):14564–14572, 2003.

doi: 10.1021/ja036082j. URL http://pubs.acs.org/doi/abs/10.1021/ja036082j. PMID: 14624606.

[111] Bernard Valeur. *Molecular Fluorescence Principles and Applications*. WILEY-VCH Verlag GmbH, 2001.

[112] Sebastian van de Linde. *Photoswitching of organic dyes and single molecule based super resolution imaging*. 2011.

[113] S. Venketesh and C. Dayananda. Properties, potentials, and prospects of antifreeze proteins. *Critical Reviews in Biotechnology*, 28(1):57–82, 2008. doi: 10.1080/07388550801891152. URL http://informahealthcare.com/doi/abs/10.1080/07388550801891152. PMID: 18322856.

[114] Jan Vogelsang, Christian Steinhauer, Carsten Forthmann, Ingo H. Stein, Britta Person-Skegro, Thorben Cordes, and Philip Tinnefeld. Make them blink: Probes for super-resolution microscopy. *ChemPhysChem*, 11(12):2475–2490, 2010. ISSN 1439-7641. doi: 10.1002/cphc.201000189. URL http://dx.doi.org/10.1002/cphc.201000189.

[115] Hans-Achim Wagenknecht, Eric D. A. Stemp, and Jacqueline K. Barton. Evidence of electron transfer from peptides to dna: Oxidation of dna-bound tryptophan using the flash-quench technique. *Journal of the American Chemical Society*, 122(1):1–7, 2000. doi: 10.1021/ja991855i. URL http://pubs.acs.org/doi/abs/10.1021/ja991855i.

[116] William West and Sandra Pearce. The dimeric state of cyanine dyes. *The Journal of Physical Chemistry*, 69(6):1894–1903, June 1965.

[117] Jerker Widengren and Petra Schwille. Characterization of photoinduced isomerization and back-isomerization of the cyanine dye cy5 by fluorescence correlation spectroscopy. *The Journal of Physical Chemistry A*, 104(27):6416–6428, 2000. doi: 10.1021/jp000059s. URL http://pubs.acs.org/doi/abs/10.1021/jp000059s.

[118] Thorsten Wohland, Rudolf Rigler, and Horst Vogel. The standard deviation in fluorescence correlation spectroscopy. *Biophysical Journal*, 80, June 2001.

[119] Steve Wolter, Ulrike Endesfelder, Sebastian van de Linde, Mike Heilemann, and Markus Sauer. Measuring localization performance of super-resolution algorithms on very active samples. *Opt. Express*, 19(8):7020–7033, Apr 2011. doi: 10.1364/OE.19.007020. URL http://www.opticsexpress.org/abstract.cfm?URI=oe-19-8-7020.

[120] F. Würthner, Sh Yao, T. Debaerdemaeker, and R. Wortmann. Dimerization of merocyanine dyes. structural and energetic characterization of dipolar dye aggregates and implications for nonlinear optical materials. *J. Am. Chem. Soc.*, 124(32):9431–9447, July 2002.

[121] Frank Würthner, Theo E. Kaiser, and Chantu R. Saha-Möller. J-aggregates: From serendipitous discovery to supramolecular engineering of functional dye materials. *Angewandte Chemie International Edition*, 50(15):3376–3410, 2011. ISSN 1521-3773. doi: 10.1002/anie.201002307. URL `http://dx.doi.org/10.1002/anie.201002307`.

[122] Kejin Zhou, Haoming Liu, Shanrong Zhang, Xiaonan Huang, Yiguang Wang, Gang Huang, Baran D. Sumer, and Jinming Gao. Multicolored ph-tunable and activatable fluorescence nanoplatform responsive to physiologic ph stimuli. *Journal of the American Chemical Society*, 134(18):7803–7811, May 2012. ISSN 0002-7863. doi: 10.1021/ja300176w.

[123] Ruobo Zhou, Simone Kunzelmann, Martin R. Webb, and Taekjip Ha. Detecting intramolecular conformational dynamics of single molecules in short distance range with subnanometer sensitivity. *Nano Letters*, 0(0):null, 2011. doi: 10.1021/nl2032876. URL `http://pubs.acs.org/doi/abs/10.1021/nl2032876`.

[124] Peizhi Zhu, Jean-Pierre Clamme, and Ashok A Deniz. Fluorescence quenching by tempo: a sub-30 a single-molecule ruler. *Biophys J*, 89(5):L37–9, Nov 2005. ISSN 0006-3495 (Print); 0006-3495 (Linking). doi: 10.1529/biophysj.105.071027.

[125] Ruixue Zhu, Xun Li, Xin Sheng Zhao, and Anchi Yu. Photophysical properties of atto655 dye in the presence of guanosine and tryptophan in aqueous solution. *The Journal of Physical Chemistry B*, 115(17):5001–5007, 2011. doi: 10.1021/jp200876d. URL `http://pubs.acs.org/doi/abs/10.1021/jp200876d`.

[126] X Zhuang. Nano-imaging with storm. *Nat Photonics*, 3(7):365–367, 2009. ISSN 1749-4893 (Electronic); 1749-4885 (Linking). doi: 10.1038/nphoton.2009.101.

[127] Heinrich Zollinger. *Color chemistry*. 2003. ISBN 3-906390-23-3.